Chapter 1

Introduction

The aim of sound reproduction systems in cinemas is to provide a high quality listening experience, accurately reproducing the recording for any listener in the audience. The horn loaded loudspeaker is a component often used in cinema sound systems, and in related live sound reinforcement systems. This device is used because it is an efficient audio transducer, with some control over the spatial distribution of sound away from the horn mouth. The sound distribution, or beamwidth, is related to the shape of the horn and it is critical for listening quality that the sound be distributed evenly onto the audience at all frequencies. The beamwidth is not predicted adequately by existing analytical horn models, and the aim of the work described in this thesis is to develop a method to optimise the shape of the horn to give a smooth frequency independent beamwidth.

1.1 Background

Horn loaded loudspeakers consist of two main components: a compression driver; and a horn flare. The compression driver, a special kind of moving coil loudspeaker, produces the sound. The horn flare, with its gradual change in cross sectional area from throat

to mouth, increases the efficiency of the sound radiation by changing the acoustic impedance seen by the compression driver diaphragm. This means that less amplifier power is required for a given acoustic output, and is the traditional reason for the use of horns in audio.

Horn flares are also used to control the spatial distribution of the sound radiated from the horn mouth (the beamwidth). In the case of cinema audio, it is critical to the listening experience that the sound can be distributed evenly onto the audience at all frequencies (frequency independent beamwidth) with no variation in volume with frequency (smooth frequency response). Horn design methods published in the last 30 years have often emphasised control of beamwidth rather than frequency response. This is because the former can be gained at the expense of the latter by a shape which introduces internal reflections in the horn, and the resulting poor frequency response can be compensated by using a larger amplifier and level equalisation. Thus modern horn design is often a compromise, and beamwidth control achieved at the expense of sound quality (See Holland, 2003, for a discussion of the issues of horns in live sound as many of the issues raised there are similar to those of the cinema industry). It is intended that this thesis will contribute to the understanding of the physical mechanisms of sound propagation that occur in horns, with the aim of producing horn designs that achieve beamwidth control without compromising sound quality.

In summary the aim of horn design for cinemas is twofold: to produce an easily specified frequency independent beamwidth; and to provide a smooth frequency response over as large a bandwidth as possible. The overall aim of this thesis is to develop fast and reliable optimisation techniques for horn loaded loudspeakers with the intention of developing a better horn design method for cinema loudspeakers.

1.2 Motivation for this research

A review of the horn literature reveals that Webster's[1] horn equation is most often used to estimate the performance characteristics of horns provided there is a smooth variation in cross sectional area with distance along the horn axis. Models that use this equation generally tend to estimate acoustic impedance to a reasonable degree of accuracy, at least for low frequencies, but most acoustic horn models do not accurately estimate far field acoustic pressure either on or off axis. This leads to the conclusion that while these simple models may be suitable for optimisation to produce a smooth frequency response within the limits of validity of the Webster equation, they would not be suitable for optimisation of the beamwidth.

There is evidence in the literature (Holland et al., 1991, Di Cola et al., 2000, 2001) that variations in pressure and acoustic particle velocity across the mouth of the horn (higher order modes) can be significant at some frequencies. Although all of the models based on Webster's approach assume that this variation is negligible both inside and outside the horn, a simple measurement of the sound field at the mouth of the horn would confirm this. This measurement, along with the measurement of the far field pressure, would allow an examination of the validity of numerical models of horn loaded loudspeakers. Thus, the need exists for experiments that measure both the near and far sound radiation field of horn loaded loudspeakers.

Alternative approaches to modelling acoustic horns such as Finite Element Analysis (FEA) or the Boundary Element Method (BEM) have been found in the literature. However, while these methods can eliminate problems associated with the approximate equation of Webster, it has been found that 3-D FEA is intractable for large horn models and high frequencies, and unsuitable for application to optimisation techniques (Morgans et al., 2000). There is also evidence that 3-D BEM is similarly unsuitable at the mid to high

[1]The origin of this equation is commonly attributed to Webster (1919) in the horn literature. However Daniel Bernoulli, Lagrange and Euler first derived it in the 18th century (Eisner, 1967).

frequencies needed for cinema applications (von Estorff, 2000). Thus the need exists for efficient and accurate numerical models of acoustic horns.

The optimisation of horn loaded loudspeakers to produce a desired outcome has been attempted previously. Examples include an optimisation of the beamwidth of a horn loaded woofer using a 3-D BEM (Miccoli, 1999), the optimisation of the frequency response of a horn loaded tweeter using axisymmetric BEM (Henwood, 1993, Geaves and Henwood, 1996), and most recently FEA to optimise the frequency response of a planar horn (Bängtsson et al., 2003). None of these methods have been applied to both beamwidth and frequency response of the type of horns used in cinema loudspeaker systems. Thus the need exists for the development of fast and robust optimisation techniques that will produce a horn geometry with a specified frequency independent beamwidth and a smooth frequency response over as large a bandwidth as possible.

In response to the issues raised above, the specific aims of the current study are as follows;

- **To examine experimentally the nature of the sound field at the horn mouth (near field) and the horn beamwidth (far field).**

  These experiments, whilst obtaining data for the validation of subsequent numerical models, will look at the validity of currently used numerical horn models and the existence of higher order modes at the horn mouth.

- **To develop fast and accurate numerical models of horn loaded loudspeakers.**

  These models should be able to predict the beamwidth to a level of accuracy suitable for optimisation, given the horn geometry. The technique should be suitable for both axisymmetric and 3-D simulations, and should be as fast as possible because many different geometries will typically be evaluated during an optimisation procedure.

- **To develop fast and reliable optimisation techniques for horn loaded loudspeakers.**

  These optimisation techniques should reliably find a horn shape that satisfies the

given horn design aims, provided these aims are physically realisable. Initially the technique would be developed for axisymmetric horns, but the method should be general and applicable to 3-D horns.

1.3 Overview of the Thesis

This thesis begins in Chapter 2 with a thorough review of the literature relevant to modelling and optimising horn loaded loudspeakers. It gives an introduction to horn loaded loudspeakers, and describes traditional modelling approaches and their limitations. The applications of alternative modelling techniques for horn loaded loudspeakers found in the literature are critiqued, as are horn optimisation techniques.

Chapter 3 presents experimental results examining the nature of the sound field at the mouth of two small axisymmetric horns. An automated traverse system has been used to measure the pressure across the mouth of each horn, and the results decomposed into cylindrical modes. The circumferential variation of the sound field is examined, and existence of plane waves above a certain limiting frequency tested. These experiments are needed to examine the validity of currently used numerical horn models and test the hypothesis that higher order modes exist at the horn mouth.

Numerical models able to accurately and quickly calculate the far field pressure from arbitrary structures are investigated in Chapter 4. Results obtained from the analytical solution of a vibrating cap mounted on the surface of a sphere are compared with two alternative boundary element based numerical methods. The accuracy and speed of the far field pressure solution for both methods is examined. Techniques that speed up solution time without compromising accuracy are investigated.

Chapter 5 compares results from experiments with two representative horn loaded loudspeakers with the numerical methods described in the Chapter 4. The capability and

range of validity of the source superposition technique (Koopmann and Fahnline, 1997) in modelling horn loaded loudspeakers is investigated, as is its applicability for use as a component in optimisation techniques.

In chapter 6, the concept used in the development of a Constant Beamwidth Transducer (CBT) (Rogers and Van Buren, 1978) is explored in relation to horn design. Specifically the nature of the frequency independent beamwidth is investigated, giving cues as to how to design a horn loaded loudspeaker to achieve a frequency independent beamwidth. Further, robust optimisation techniques are introduced to investigate their applicability to horn shape optimisation in future chapters.

Chapter 7 draws together the work of previous chapters to develop a method to optimise the geometry of a horn to give a specified smooth beamwidth. The geometry of the horn is parameterised, and the source superposition technique used to calculate the beamwidth. An investigation is made of a geometrically simple horn profile consisting of an essentially conical horn with a radiused entry at the horn throat and a radiused flare at the horn mouth. The ability of this geometry to achieve the desired nominal beamwidth is investigated, as is the the effect of throat radius on the performance of the system.

More complicated geometry parameterisations are investigated, and a Bézier spline based geometry is found to be flexible enough to define a shape that approaches constant beamwidth behaviour, although it may not be able to find a desired nominal beamwidth. This geometry parameterisation is then solved repeatedly for a wide range of lengths and throat dimensions, and a method developed to enable an optimum design to be quickly found.

Finally, in Chapter 8 a summary of the work completed in this thesis is given. It clearly states the contributions to current knowledge in the optimisation of horn loaded loudspeakers, and gives recommendations for future work.

Chapter 2

Literature review

This chapter provides a thorough review of the literature relevant to modelling and optimising horn loaded loudspeakers. It gives an introduction to horn loaded loudspeakers, and describes traditional modelling approaches and their limitations. The applications of alternative modelling techniques for horn loaded loudspeakers found in the literature are critiqued, as are horn optimisation techniques.

2.1 Background

Acoustic horns have been used for over 100 years to provide sound in consumer equipment, theatres and public address systems (Hilliard, 1976). Probably the most famous image of an acoustic horn is that in the painting "His Master's Voice" (see Figure 2.1) where a small dog is seen staring attentively at the mouth of an acoustic horn, waiting for his master's voice to speak. Acoustic horns are also used as components of musical instruments, for example the flared ends of brass or woodwind instruments Keefe (1990). Geddes (1989) describes the difference between these two uses as horns designed for sound *reproduction* and sound *production,* and suggests that characteristics desirable for

sound production may not be compatible with the performance of audio reproduction devices, and vice versa. The purpose of the work described here is to model and optimise sound reproduction devices, and specifically horn loaded loudspeakers.

Figure 2.1: The famous oil painting "His Master's Voice" by Francis Barraud (1895) of the dog Nipper and an Edison-Bell cylinder phonograph, using a horn to load the mechanical transducer to provide the "amplification" necessary to hear the recording.

Horn loaded loudspeakers are used as components in cinema sound systems (Figure 2.2) because of their ability to produce high sound pressure levels efficiently, and their ability to control the direction in which the sound is distributed over the audience. Hilliard (1976) gives compelling evidence for the use of these speaker systems;

> "*The overall electrical to acoustic efficiency on horn-type systems approaches 20%. This is a very high efficiency when one considers that a typical modern home entertainment speaker system is only 0.1% - 1% efficient. Utilising a horn-type system, less amplifier power is required for theatres of 1000 seats to generate the same loudness as would be produced in an average living room with conventional cone-type speaker systems.*"

2.1.1 Loudspeaker components

A horn loaded loudspeaker consists of two main components, a compression driver and a horn flare (see Figure 2.3). From here on, the term *horn* will generally refer to the horn

Figure 2.2: Commercially available cinema loudspeaker system. The horn loaded loudspeaker is mounted on top of a low frequency direct radiator loudspeaker, and the system is located behind the cinema screen.

flare, and the term *horn loaded loudspeaker* will refer to the combination of compression driver and horn flare.

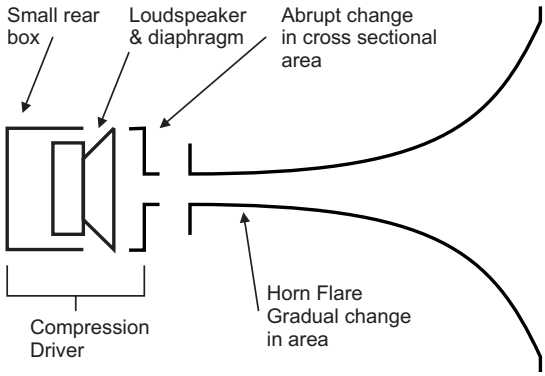

Figure 2.3: Schematic of a horn loaded loudspeaker system. The source of the sound, the compression driver, consists of a small (usually titanium) diaphragm driven by a conventional electromagnetic drive (voice-coil and magnet) positioned in front of an abrupt change in cross sectional area. The flare changes the cross sectional area gradually from the throat through to the mouth of the horn.

Compression drivers

The compression driver, as shown in Figure 2.4, converts electrical inputs into mechanical motion of a diaphragm (typically titanium) through an electro-mechanical drive (voice coil and magnet). The movement of the diaphragm produces fluctuations in pressure, which act through a small cavity, a change in cross sectional area (a compression ratio), and a series of small channels (a phase plug) to enter the horn at the throat of the flare. There is then a further change in cross sectional area through to the mouth of the horn.

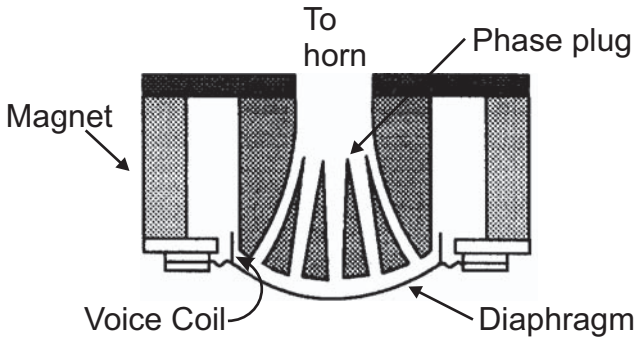

Figure 2.4: Schematic diagram of a compression driver. Reproduced from Colloms (1997).

Most manufacturers of horn loaded loudspeakers purchase compression drivers from suppliers as pre-fabricated components, and generally have little influence over their design. The modelling and design of compression drivers, and similar devices such as direct radiator loudspeakers have been covered previously in the literature (Geddes, 1987, Leach, 1979). Thus, consideration of compression driver modelling is not included in this thesis. However, loudspeaker system manufacturers are concerned about the performance in conjunction with a particular horn flare design. Although not considered in this study, such design issues can be solved by the experimental characterisation of compression drivers, adapting techniques used by other researchers (McLean et al., 1992, Abom, 1989, De Blok and Van Den Brink, 1993, Behler and Makarski, 2003).

Horn flares

The horn flare component, with its gradual change in cross sectional area from throat to mouth, increases the efficiency of sound radiation by matching the acoustic load driven at the horn throat. Horn flares are also used to control the spatial distribution of sound radiating from the horn mouth.

For horns used in large scale public address systems, the control of the sound distribution can be used to advantage by arranging a series of horns together in an array to achieve maximum overall sound coverage with minimal destructive interference at the fringes of an individual horn's coverage (Brown, 1995).

An approximate equation (Webster, 1919) can be used to estimate the performance characteristics of horns, provided the function that governs the change in cross sectional area is simple. These types of horns are usually named by the function governing the increase in area, (exponential, catenoidal or hyperbolic horns), or their shape (conical horn).

2.1.2 Sound quality metrics

In the case of cinema audio, it is critical to the listening experience that the sound be distributed evenly onto the audience at all frequencies (frequency independent beamwidth) with no variation in volume with frequency (smooth frequency response) (THX, 1996). It is also desirable that distortion of the signal by the horn itself is minimised. In order to assess the sound quality of existing speakers and compare new designs it is important to have well defined measures of sound quality.

Beamwidth

The general characteristics of sound radiation from the mouth of a circular horn can be described by considering a simplified physical model of a horn loaded loudspeaker; a

spherical cap mounted on the surface of a sphere (Morse and Ingard, 1986). A rigid, massless spherical cap of the same radius, a, as the mouth of the horn vibrates with a prescribed radial velocity, and is set flush on the surface of a sphere. Figure 2.5 shows a schematic of this simplified representation.

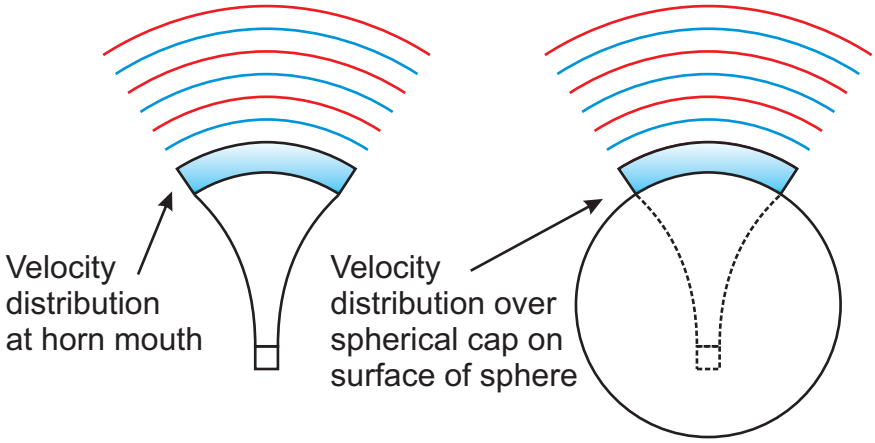

Figure 2.5: Simplified physical model of horn loaded loudspeaker. The velocity at the horn mouth can be approximated by a velocity distribution over a spherical cap on the surface a sphere.

The distribution of the sound field in front of the sphere varies with the frequency of excitation. A suitable non-dimensional measure of frequency is ka, the ratio of cap circumference to wavelength of sound, λ, where $k = 2\pi/\lambda$ is the wavenumber. Figure 2.6 shows a polar plot of the magnitude of the measured pressure, normalised by the maximum pressure, for a 45° vibrating spherical cap, for three different non-dimensional frequencies, $ka = \{3, 10, 20\}$.

It also plots the beamwidth, or coverage angle in a plane, defined as the "angle formed by the -6dB points (referred to the on-axis reading) and the source center" (Davis and Davis, 1997). The beamwidth is a measure of the distribution of sound in the specified plane. At low frequencies ($ka = 3$) the sound is almost omni-directional and the beamwidth is large. At higher frequencies ($ka = 10$) the sound converges toward the axis and the beamwidth becomes narrower . At some frequencies ($ka = 20$), the sound pressure on the axis is less than the pressure off axis (on axis null), and the beamwidth becomes artificially widened.

The variation of beamwidth with frequency for a 45° vibrating spherical cap on the surface

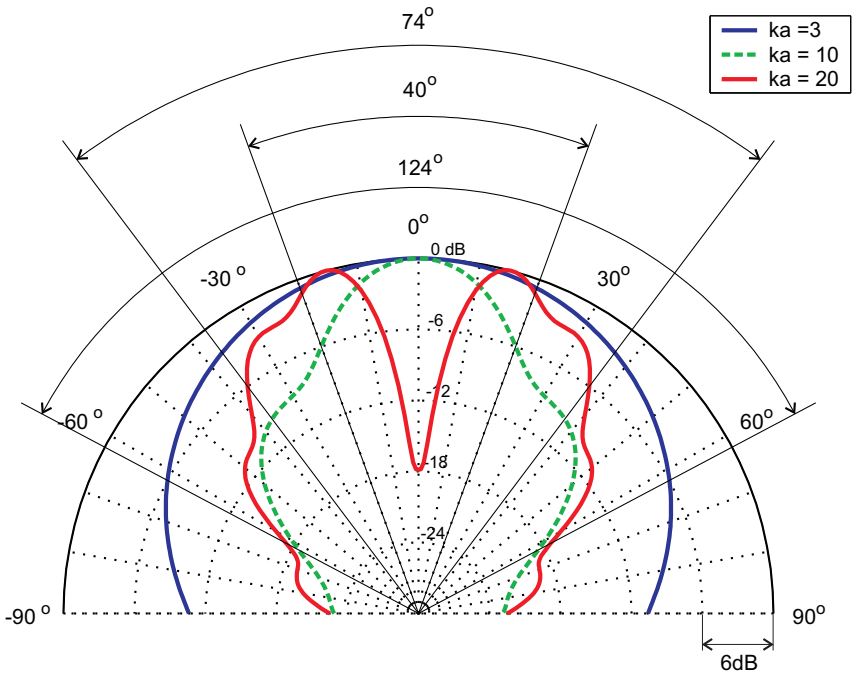

Figure 2.6: Far field polar plot of the magnitude of the measured pressure, normalised by the maximum pressure, for a 45° *vibrating spherical cap on the surface of a sphere. Beamwidth is also shown for each frequency.*

of a sphere is shown in Figure 2.7. This shows the omni-directional coverage at low frequencies and the narrowing at mid to high frequencies.

Chamness (1994) discusses deficiencies associated with the measurement of beamwidth and that of directivity, another measure of sound distribution related to the relative amount of on-axis to off-axis energy, and proposes methods to overcome them. Specification of the beamwidth variation with frequency for both the horizontal and vertical planes has long been industry practice (Davis and Davis, 1997) and more recently and importantly has been used by Lucasfilm, an important industry body, in the THX (1996) specification of sound quality requirements for cinema loudspeaker systems.

The characterisation of loudspeaker coverage in a single plane, or in two orthogonal planes, does not account for off-plane (e.g. non vertical or horizontal) variations in the sound field. Various studies have tried to develop more rigorous representations (Baird and Meyer, 1999, Angus and Evans, 1998).

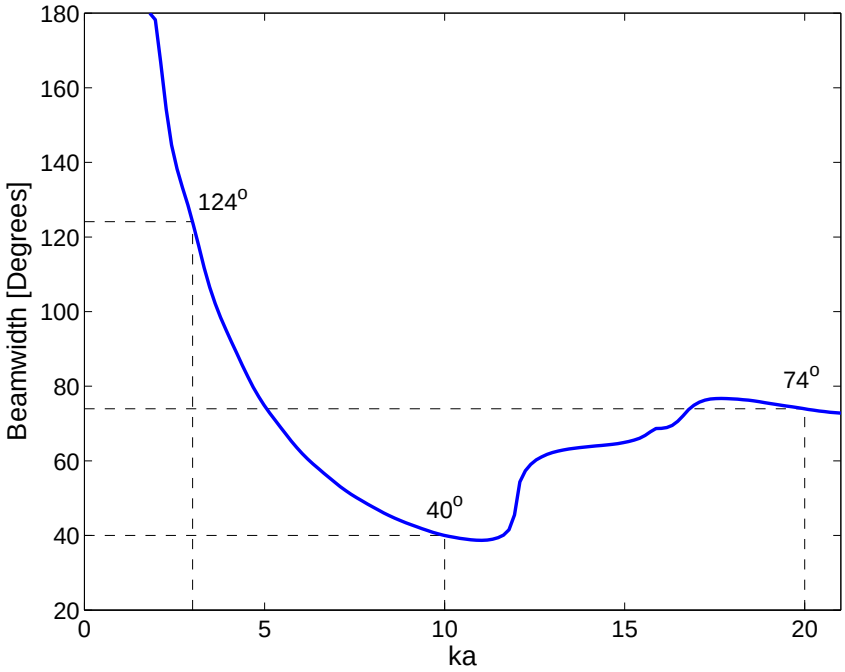

Figure 2.7: The variation of beamwidth with frequency for a 45° *vibrating spherical cap on the surface of a sphere.*

Frequency response

A smooth frequency response is critical to the listening experience, and the reproduced sound should not exhibit large variations in volume at different frequencies. A theoretical analysis of "infinite" horns (Beranek, 1986, Pierce, 1994) shows that below a certain frequency horns cannot transmit power, and the corresponding sound volume will be low. Real horns exhibit this behaviour as well (Molloy, 1950), and this phenomena is considered an inherent characteristic of horns. Low frequency horns of necessity are large, and the horns considered in this thesis are the relatively small high frequency components of the cinema loudspeaker system.

Fahy (2001, Section 8.11) describes the rationale behind using horn loaded loudspeakers to increase transducer efficiency without introducing large variations in frequency response. He suggests that there is considerable advantage in using a "stiff, lightweight diaphragm of small diameter, provided that appropriately high radiation resistance can be offered to it", and that this radiation resistance should be frequency independent. The

stiff, lightweight diaphragm of a compression driver, attached to an anechoic termination at the end of a tube would offer the highest frequency independent radiation resistance, but this device is impractical for sound reproduction. Truncating the tube at a fixed length would lead to reflections from the tube mouth, and large variations in the frequency response (see Fahy, 2001, Figure 8.7). A mode ideal situation is a horn which increases its cross section gradually from the compression driver exit until the mouth is large enough to radiate sound efficiently, minimising reflections and providing a smooth frequency response. Keele (1973) describes a method to match the impedance of an exponential horn section with the radiation impedance of a piston, giving an "optimum horn mouth size" that produces an optimal frequency response.

Sometimes the frequency response is not the primary design criterion (e.g. beamwidth or horn size may be more important), and equalisation of the input signal is required. Yashima et al. (1995) describe the use of digital signal processing to improve the frequency response of horn loaded loudspeakers.

Distortion

Distortion in horns is still a key sound quality metric, and there have been a number of attempts to model and compensate for various types of distortion (Czerwinski et al., 1999, Schurer et al., 1995). As distortion is a non-linear phenomenon, it is usually examined in the time domain, whereas most linear acoustic modelling occurs in the frequency domain. Most distortion in horns is generated by non-linear behaviour of air in the compression driver, and is thus considered an input to the horn itself. Distortion modelling is beyond the scope of the current work, which will be constrained to modelling the linear behaviour of horn loaded loudspeakers.

Some types of horn loaded loudspeakers have been reported in the literature to have a characteristic sound (Holland et al., 1996). Holland (1992) attributed this to reflections from the horn mouth, an inherently linear phenomenon, rather than non-linear distortion.

2.1.3 Existing design approaches

There are many approaches used in designing horn flares, and these have changed over time to reflect the changing technology and requirements of the audio reproduction industry. Geddes (1989) covers some aspects of changing design emphasis in his review of horn theory and Hilliard (1976) provides a historical review. Holland (2003) gives an excellent overview of horn loaded loudspeakers for live sound, which is very similar in requirements to the cinema industry. A brief overview of design approaches is given here.

Initially, horn shapes were axisymmetric, or mostly so with a few gradual bends (as shown in Figure 2.1), and the horn was viewed as primarily a loading device to improve efficiency. Indeed, for phonographs needing purely mechanical gain (i.e. no electronic amplifier) the horn was an essential part of the system.

Improvements in amplifier technology have reduced the importance of efficiency as a horn design criteria. It was found that the degradation in beamwidth of axisymmetric horns with increasing frequency, and their equivalent beamwidth in both horizontal and vertical planes was too limiting. Some control over the beamwidth was provided by multicellular and radial/sectorial horns (see Hilliard (1976), and Figure 2.8), but their frequency response suffered from significant peaks and troughs. It is possible to "equalise out", to some extent, the peaks and troughs in the frequency response by attenuating certain frequency bands until the overall response is flat. This results in the overall gain of the system being lower, counteracting one of the advantages of horns over direct radiator loudspeakers, and care must also be taken to avoid introducing distortion. Bauman et al. (1993) suggest that a *flat frequency response, control of directivity* and *reduction of distortion* are key components in designing modern horns.

Keele (1975) also finds several problems associated with the beamwidth of radial / sectorial horns, but developed "the foundations of current horn design philosophy" (Geddes, 1989) with the constant directivity horn. Figure 2.9, adapted from Murray (2000), shows

NOTE: This figure is included on page 17 in the print copy of the thesis held in the University of Adelaide Library.

Figure 2.8: Horn designs for greater control of beamwidth, reproduced from Holland et al. (1991).

a constant directivity horn. Keele suggested a design where a small exponential horn section, here called the flute, provided loading to the device, and a conical horn, here called the flare, could be attached to this to provide beamwidth control. The interface between the flute and the flare is called the "diffraction slot". He discovered that an outer flange could be attached to stop "mid-range polar narrowing", where the beamwidth narrows in the mid-frequency region before returning to the design beamwidth. Modelling of the effects of flanges on horn radiation performance are discussed by Geddes (1993, 2002) and also by Johansen (1994). The culmination of Keele's work led to a Patent (Keele, 1982) and a horn design that still competes in the market today.

NOTE: This figure is included on page 17 in the print copy of the thesis held in the University of Adelaide Library.

Figure 2.9: *Constant directivity* horn of Keele (1975) , adapted from Murray (2000).

The "Manta-Ray" horn of Henricksen and Ureda (1978) is another constant directivity de-

sign approach that provides good control of beamwidth. It was "designed from the mouth inward", and the authors admit that this control is possibly at the expense of frequency response, because the horn was designed with smooth frequency response as a "secondary consideration". Figure 2.10, adapted from Murray (2000) shows a Manta-Ray horn. The horn shown in Figure (2.2) is also a derivative of the "Manta-Ray" design.

NOTE: This figures is included on page 18 in the print copy of the thesis held in the University of Adelaide Library.

Figure 2.10: Manta Ray horn of Henricksen and Ureda (1978), adapted from Murray (2000).

In both the constant directivity and "Manta-Ray" horns, reflections from discontinuities and the horn mouth are detrimental to the frequency response. Holland et al. (1996) suggests that mouth reflections are a contributing factor to the sound quality of horns. Murray (2000) also discusses a problem that occurs when the sound from a number of horns is combined in an array. The "apparent apex" is the apparent centre of the sound when the far field is extrapolated back into the near field. In constant directivity and

.

"Manta-Ray" horns, the vertical apparent apex and the and horizontal apparent apex are in different positions, rendering the performance of arrays of horns ineffective.

Geddes has used an innovative approach to the design of horns, that he calls the "acoustic waveguide" design, but his work (Geddes, 1989, 1993, 2002) has found little acceptance in the industry, possibly due to the daunting mathematical nature of the analytical modelling approach, although Bauman et al. (1993) use the design for stadium sound systems.

The aim of the work detailed in this thesis is to provide a design approach, and ultimately a design method to calculate the required shape of a horn to give both a flat frequency response and adequate control of beamwidth without compromising overall output.

2.2 Simple horn models

Webster (1919) is often cited as the major work in the field of horn theory, and the equation derived to describe the propagation of sound in tubes that vary in cross section along their length is called the Webster horn equation. However Eisner (1967) (see also Campos, 1984), in a review and bibliography of horn theory, credits Daniel Bernoulli, Lagrange and Euler in the 18th century with discovering the horn equation. He suggests that Webster should instead be credited with introducing the concept of "acoustic impedance", the ratio of average acoustic pressure to volume velocity at a plane, to a wide audience.

For a very thorough review of the derivation and applicability of the horn equation, see Putland (1994, Chapter 3), and Putland (1993). He expands on the concept of a one-parameter acoustic field, introduced by Morse (1976), defined as "a solution to the wave equation depending on only one of three spatial coordinates". Putland proves that the only coordinate systems that can sustain an exact one parameter solution are "those whose level surfaces are parallel planes, coaxial cylinders, or concentric spheres", or in terms of geometry: rectangular ducts; cylindrical tubes or cylindrical sectorial horns; and conical horns. This work has implications for horn modelling, as the commonly used exponential horn is not *exactly* described by Webster's horn equation, but Putland (1993, Section 5.5) describes in detail criteria under which the wave is *approximately* one-parameter. These criteria generalise to a "cross section that varies only gradually" assumption and exponential horns with low flare rates fit this criteria.

Webster (1919) solves his equation for the degenerate case of a straight tube, and a conical, hyperbolic and exponential horn, and Salmon (1946) introduces a more general series of approximately one-parameter horns ranging from a catenoidal horn, through exponential to conical in shape. (Molloy, 1950) found these models useful for the design of axisymmetric horns of the given shapes at low frequencies, below $ka = 1.2$. Mawardi (1949) solves the general case by using both an electrical analogy and the singularities of the differential equation, and states that "the horn contours that have been studied are very few

in number" and that "this is due to the difficulty of solving Webster's equation exactly when the horn contours are of arbitrary shape". Mawardi's work is not widely referenced.

The approaches outlined by Webster (1919) and Salmon (1946) have been the most accessible to the audio engineering community and have been used extensively for horn design for calculating the cut-on frequency (Section 2.1.2) and size of these horns. These approaches have been used even when the *approximately* one-parameter criteria are not strictly applicable, such as in the constant directivity design of Keele (1975). In these cases, although the analysis is useful for preliminary design and general concepts, there is a need for analysis methods that overcome the limitations inherent in Webster's equation: the accuracy of the analysis under conditions where the one parameter approximation breaks down; and the ability to solve the equation easily for more general shapes.

Most modern approaches to modelling acoustic horns overcome the difficulties in solving Webster's equation in complicated geometries by the use of a transmission matrix approach (Lampton, 1978, Patrick, 1979). This numerical method is useful in modelling complicated electro-acoustic systems by breaking the system down into smaller component parts. Each acoustic component can be described by a 2×2 matrix that relates the average pressure p and the volume velocity U at the input to the same quantities at the output, and similar relations can be found to describe mechanical and electronic components. The entire system can then represented by a cascade of such matrices. Lampton (1978) summarised the use of transmission matrices in electro-acoustics and Patrick (1979) gives a useful overview in the context of duct acoustics.

The wide adoption of the transmission matrix method (Keefe, 1984, 1990, McLean et al., 1992, Mapes-Riordan, 1993), and other similar methods based on cascaded components, such as the use of the electronics analysis package SPICE to simulate acoustic horns by Leach (1996), and the stepped exponential horn method of Holland et al. (1991), is probably due to their ease of implementation and numerical stability. Such models also allow the modelling of the acoustic path back to the compression driver diaphragm, through the

mechanical and electromagnetic components to give the electrical input impedance of the horn loaded loudspeaker, a quantity that is easily measured by the loudspeaker designer and can be used to verify the design.

Care must be taken when using the transmission matrix approach. The method is able to easily obtain solutions to complex horn shapes with sections of rapid change in cross sectional area, such as the constant directivity design (McLean et al., 1992). However, these designs stray from the approximately one parameter criteria of Putland (1993), that the "cross-section varies only gradually and remains small compared to the wavelength", and the validity of the result obtained is in question. McLean et al. (1992) mention this deficiency and suggest improvements related to incorporating higher order modes into their model (see Section 2.3.2).

In modern literature there are an abundance of approaches, other than the transmission matrix method, used to solve Webster's equation: Holland et al. (1991) applied numerical integration to a transformed version of the Webster equation, a first order differential equation describing the harmonic time dependence of the complex pressure reflection coefficient; Kergomard (1998) applied continued fraction expansions to the problem; and Arenas and Crocker (1999) used the Wentzel-Kramers-Brinoulin (WKB) approximation to solve Webster's equation for a cosine shaped horn. There are also time domain approaches for modelling musical instruments (Berners, 1999). A simple extension to the Webster equation by Benade and Jansson (1974) (see also Jansson and Benade, 1974) allows for the existance of both plane and spherical waves within a horn, and the conversion of energy between these modes.

Methods of solving Websters equation are still very much an area of active research, see for example Rienstra (2002), Hélie (2003) and Martin (2004). Again, these methods only look to solve Webster's equation more rigorously, or in more complex shapes, and do not address the inherent deficiencies in the underlying equation.

2.2.1 Modern simple horn models

The work of Holland et al. (1991), McLean et al. (1992) and Mapes-Riordan (1993) are the most prominent in the horn literature and deserve further review.

Holland et al. (1991) applied modelling techniques using a stepped exponential horn to simulate the throat impedance of horn geometries that vary from a simple shape. After initially solving the Webster equation numerically, and noting that in this formulation the approximation to the flare rate was constant over an "element", which was exactly equivalent to a short exponential horn section, they found that a more stable solution was achievable, and that the number of elements in the model was related to the "degree of departure of the horn shape from exponential". After giving a physical explanation of horn behaviour and measuring the amplitude and phase distribution of pressure across the mouth of a large axisymmetric horn, they applied an extension to the stepped exponential horn model to account for wavefront curvature, which increased the ability of the model to accurately represent a wide variety of horns. They reported that predictions of transfer impedance, the ratio of the pressure at the mouth of the horn to the volume velocity at the throat, were 2 or 3 dB lower than those measured. They surmised that this effect was due to "beaming", which is a non-uniform acoustic particle velocity profile across the mouth of the horn with bias toward the axis of the horn, and that their "plots clearly indicate the limitations of the one-parameter model for the prediction of the performance of a horn".

McLean et al. (1992) applied transmission matrix modelling using many short straight duct sections of increasing diameter joined together to approximate a constant directivity horn, and compared the results to measured data. Their results for acoustic impedance show reasonable agreement with experiment, except for an unexplained resonant peak. The model over predicts slightly the magnitude of the acoustic impedance at high frequencies, possibly due to "radiative and viscous damping", and shows that most of the reflected energy occurs at the flute-flare interface (the diffraction slot, see Figure 2.9). They ascribe the unexplained resonant peak to a mechanical resonance in the structure

of the horn (presumably in the large flat surface on the side of the constant directivity horn) coupling with the acoustic field inside the horn. This phenomenon has implications for commercial manufacture of horns in terms of sound quality and the design of horn structure, and has been seen in other horns (Murphy, 2002), but is beyond the scope of the current work and will not be considered further. The work also shows the utility of the transmission matrix approach in calculating acoustic impedance for horns of arbitrary profile for frequencies up to $ka \approx 30$, where the dimension a is the radius of a circular mouth of equivalent area to the rectangular horn. However, no comparison is made between experimental data and the prediction of acoustic pressures either within the horn mouth or external to it.

By using the transmission matrix method, and taking the limit of an infinite number of duct sections, McLean et al. (1992) show the transmission matrix method is equivalent to Webster's horn equation (although with a possible non-constant flare rate). This work draws the discrete transmission matrix approach and the continuous Webster equation approach together theoretically, and this is a significant contribution to horn theory.

Mapes-Riordan (1993) modelled acoustic horns using a transmission approach, with both stepped cylindrical and conical element models with the idea that a series of short, connected conical horns can model a varying horn shape with less elements than a cylindrical approximation. He also included both loss-free and dissipative elements (Keefe, 1984). It was found that for "typical audio applications, the difference between a dissipative and loss free conical element is negligible". There is no comparison of the horn model results with experiment, but instead there is a comparison with numerical simulations of a dissipative conical element with "an asymptotically large number of elements (100 000 elements)" because this element "possesses the most detailed structure of the four models". While an infinite conical horn satisfies Webster's horn equation exactly, the use of concatenated conical horn sections to model horns of varying cross sectional area is not necessarily strictly valid, and comparison to at least analytical solutions of these horns

would have been useful.

2.2.2 Radiation boundary conditions

Models of realistic, finite length horns require the modelling of acoustic radiation from the mouth of the horn. Some models predict the far field pressure using various approximations, whereas other models are only concerned with the acoustic impedance presented to the compression driver.

Most modellers assume a constant velocity across the mouth of the horn, and use the impedance of a piston in an infinite baffle to represent the resistance that the air presents to the horn. Before the use of computers to accurately calculate the frequency dependent impedance of a piston in an infinite baffle, Bauer (1944) provided a widely used approximation of a resistor and inductor in parallel with approximately constant coefficients. He warns that this "Approximate treatment yields impedance errors of the order of 20 percent or more in the important frequency range", but describes this error as "tolerable" given other approximations generally made when modelling horns.

The model of Mapes-Riordan (1993) assumed implicitly that the horn was mounted in the middle of a large wall, and used the piston in an infinite baffle as an approximation to the actual impedance. He states that "More research is needed to develop better approximations of the radiation impedance of horns, particularly with large mouth flares". Mapes-Riordan applied a model of the far field pressure and directivity to the radiation from a resonant tube loudspeaker, but did not use this explicitly to model horns.

Molloy (1950) applied the boundary conditions of a circular tube, with no flange, with the same radius as the horn mouth. This boundary condition, based on the work of Levine and Schwinger (1948), is a more realistic approach when modelling horns with finite flanges than the effectively "infinite" flange boundary condition with piston in an infinite baffle, provided any horn flange is much smaller than the wavelength. Moreover Molloy

calculates the acoustic pressure at a distance on the axis of the horn, and comparison with experiment over a relatively narrow bandwidth shows good agreement, apart from a discrepancy at the first resonant peak, attributed to “minor differences between the actual parameters of the system and those assumed for the purposes of calculation”.

Holland et al. (1991) applied the solution for radiation from a spherical surface to a special “external” element in their modelling of various horn shapes, and state that with their model it is “impossible to predict the far field radiated by this horn”, because their “hemispherical shape of the mouth element would lead to every horn being omnidirectional”. The authors claim that this approach allows the accurate modelling of the acoustic impedance at the throat of the horn, a quantity found to be important in listening tests of acoustic horns (Holland et al., 1996). However, the far field acoustic pressure pattern, which is of great importance to cinema horn designers, is not modelled.

Radiation from spherical surfaces was also used by Geddes (1987), who modelled the whole horn mounted in a spherical surface. He used the radiation from a spherical cap at the mouth of the horn to calculate the acoustic radiation load, as well as the external pressure field. This is the only work in the simple horn modelling literature found to report both on axis and off axis pressure distributions. The choice of a spherical cap radiating in a spherical surface as a radiation boundary condition representing a real, unflanged horn is at least as valid as the standard choice of a piston in an infinite baffle, and would be an excellent choice for higher order models (Section 2.3.2) in spherical coordinates. Geddes approach does not allow for variation in acoustic particle velocity over the spherical cap at the horn mouth, and hence does not allow for variations in radiation patterns away from the underlying model. This work does report experimental results for off axis response, but unfortunately does not plot direct comparisons with model results.

McLean et al. (1992), when modelling the rectangular mouth of a constant directivity horn (Figure 2.9), used a rectangular piston in an infinite baffle model for acoustic radiation. They noted that for nearly square mouths, the rectangular impedance function

gives similar results to the impedance function for a circular piston in an infinite baffle. This implies that a circular approximation to a square mouth should accurately model the acoustic impedance at the throat of the horn. McLean et al. (1992) were only interested in modelling horn throat acoustic impedance, and did not attempt to model the pressure outside the horn. A simple extension to the rectangular piston radiation model to include the far field directivity would produce a horn model that allowed for variation between the vertical and horizontal pressure patterns, albeit one that assumed constant acoustic particle velocity across the rectangular mouth and hence the beamwidths would be related to the mouth dimensions and frequency, not the horn shape.

An interesting use of simple models of horns and acoustic radiation is that of Keele (1973), who presented an analysis of the optimum horn mouth size for round horns. He matched both the real (resistive) and imaginary (reactive) parts of the acoustic impedance at the end of the horn with the acoustic radiation impedance, and showed that this produced the smoothest frequency response. Keele stated that the accuracy "depends on how well the assumed radiation load model agrees with the actual physical conditions at the mouth of the horn". The approach used is entirely theoretical, and no comparison to experiment is made and hence the actual physical conditions are unknown. To overcome uncertainty, he applied the matching technique to three different models of radiation: a piston in an infinite baffle, a piston at the end of a long tube, and a piston radiating into fractional space. Results show that the optimum mouth size for minimising the reflections from the horn mouth varies slightly with the choice of radiation boundary condition. Again, this model is only strictly valid at low frequencies.

Most of the horn models mentioned so far are concerned with modelling acoustic radiation with sufficient accuracy to calculate the horn throat acoustic impedance. Some of these horn models calculate the on axis pressure response. These models do not take into account variations in velocity profile seen across the mouth of horns in practice (Holland et al., 1991, Di Cola et al., 2000, 2001), and the beamwidth calculate by these models

will be the same as the assumed underlying model for mouth radiation: a round (Mapes-Riordan, 1993) or rectangular (McLean et al., 1992) piston in an infinite baffle; a round piston at the end of a long tube (Molloy, 1950); or a spherical cap mounted in a sphere (Geddes, 1987). Hence there is a need for models of horn loaded loudspeakers that include the effect of varying acoustic particle velocity across the mouth of the horn.

2.2.3 Propagating higher order modes

Above a certain frequency, called the cut-on frequency, higher order modes of sound can propagate in ducts (Pierce, 1994, Morse and Ingard, 1986). These modes propagate at different speeds in the duct, but all oscillate at the same frequency, are linear in nature and are not related to non-linear phenomena such as distortion. Below the cut-on frequency, these modes decay exponentially with distance from their creation (evanescent modes). Both propagating and evanescent modes result in variations in sound pressure level across any duct cross section, and the pressure at any point in the duct can be considered to be made up of the orthogonal contribution of all modes. Section 3.4 describes the theory of circular modes and Figures 3.13 to 3.16 show a graphical representation of some mode shapes in a rigid walled circular duct.

The cut-on frequency, f_c, for higher order modes circular cross-sectioned ducts is (Fahy, 2001, Page 220),

$$f_c = \frac{1.84c}{2\pi a} \tag{2.1}$$

where c is the speed of sound and a is the duct radius. Table 2.1 shows the cut on frequencies for typical horn throat and mouth dimensions used in this thesis with $c = 343$ m/s.

Typical frequencies of interest are between 400 and 12000 Hz, and these calculations

	Radius	Cut on frequency
	(m)	(Hz)
Throat	0.025	4020
Mouth	0.165	610

Table 2.1: Cut of frequencies for higher order modes

show that is is possible for higher order modes to propagate in circular ducts at these frequencies, and it is probable that higher order modes exist in horns.

There is much evidence for the need to include higher order modes in calculations involving acoustic horns. Geddes (1993) concludes that departure of experimental data from predictions made with an idealised view of wave propagation in horns, the one-parameter behaviour encapsulated in Webster's horn equation, "is mostly due to the presence of higher order modes".

Hudde (1989) compared solutions obtained using a higher order mode modelling technique, applied to arbitrary shaped transitions between round ducts, to a low frequency approximate method based on Webster's equation, and stated that "higher order modes have to be taken into account even when they cannot propagate". McLean et al. (1992) state that their simple model of a constant directivity horn "yielded reasonably accurate results" but that they could improve accuracy by incorporating a model for mode conversion at the flute-flare interface (the "diffraction slot"). They point out that "while no higher order modes propagate in this region, energy is stored in evanescent modes near the discontinuity". These comments are applicable to horns of non smooth profile below the cut-on frequency of a duct the size of a horn mouth. As the frequency increases ($>$ 4000 Hz in the analysis of McLean et al. (1992)) these evanescent modes become propagating modes and change the variation in acoustic particle velocity across the mouth of the horn.

2.2.4 Summary

From the many models of acoustic horns mentioned here, which use a simple one-parameter (Webster) approach, the most important limitations are concerned with:

- accurately representing acoustic propagation, even at low frequencies, in horn shapes that have non-ideal profiles; and
- calculating the sound field external to the horn mouth.

Therefore any models that are developed in this thesis must be able to account for variations in the sound field through the horn cross section, and the sound field external to it.

2.3 Alternative horn models

There are many approaches that can be taken in developing accurate models of horn loaded loudspeakers. One approach is an extension of the one-parameter equation to include the effect of higher order modes, either by applying a stepped approximation to the horn cross section or using a technique such as asymptotic analysis. Another approach is to use a general numerical technique for solving the Helmholtz equation and apply it to the given horn geometry. Some of the techniques found in the literature are outlined below.

2.3.1 The “acoustic waveguide” approach of Geddes

The approach of Geddes (1989) to the design of what he called “acoustic waveguide” horns is innovative and thought provoking. In his original paper Geddes, after a short

review of horn theory, discussed the merits of constructing a horn by considering surfaces defined by constant coordinate values in various coordinate systems, and asking the question "what horn contour is *required* to yield the desired performance?" rather than "what loading properties will an arbitrary horn contour exhibit?".

After examination of the 11 possible separable co-ordinate systems, he chose to use an "Oblate Spheroid" co-ordinate system. He analysed the horn by considering the pressure variation along the horn to be a function of one co-ordinate only, which is effectively the one-parameter approach. This raised considerable objection from Putland (1993) and was the partial topic of his PhD Thesis (Putland, 1994).

In addressing errors in the original work, Geddes (1993) produced a model of sound propagating in an infinitely long oblate spheroid waveguide, and showed that for narrow horn beamwidths and low frequencies, the horn acted in a one-parameter manner. He discussed the advantages of modal cut-on in the design of horns in terms of the evanescent nature of the (oblate spheroid) higher order modes produced by a source (the compression driver) as they travel down the horn, specifically for the case of oblate spheroid horns. Presumably for shapes other than oblate spheroid horns a similar process may occur. Geddes (1993) also proposed a method to extend the operating range of horns by designing the velocity distribution of the source to reduce the modal contribution of higher order modes.

By considering an infinite waveguide, Geddes (1993) assumed that there are no reflections from the mouth of the horn. Real horns have reflective terminations, and it has also been shown that there can be significant coupling between incident and reflected modes (Zorumski, 1973, Muehleisen, 1996), which may be important in developing accurate models of oblate spheroid horns.

One aspect of Geddes' (1989) work that deserves further mention is the design of non-axisymmetric horns by "squashing" the horn from a round to an elliptical shape, so that different design beamwidths can be specified for different directions, although his model can only consider these horns approximately. Experiments conducted by Bauman et al.

(1993) on one of these horns show an improved stability of directivity control over rectangular horns, which often show a degraded performance in their diagonal plane directivity.

2.3.2 Higher order mode horn modelling

Alfredson (1972) developed a method of analysing a circular acoustic horn with arbitrary flare rate. He approximated the shape of the horn by dividing it into a series of small straight ducts joined by stepped discontinuities. When modelling horns, this "stepped approximation" allows the inclusion of higher order modes in the calculation, and allows for a more accurate representation of the physics of horns at high frequencies. An iterative solution technique was used, and the radiation boundary conditions were an extension by Lansing (1970) of the classic work of Levine and Schwinger (1948), on radiation from an unflanged circular duct from a single mode to many modes. The use of an unflanged termination is most unusual in the horn modelling literature, but probably reflects a more realistic modelling approach than the use of infinite flanged terminations, at least for frequencies with wavelength much greater than the characteristic flange width. The simulations and experiments at $ka = 5.5$ and $ka = 10.9$ were reported for directivity, radial pressure at the horn mouth and axial pressure in the horn, and the agreement was very good.

Oie et al. (1980) modelled a round horn loudspeaker using a stepped approximation and an infinite baffle. They did not compare their results to experiment. Their study shows that there is a significant difference between the results for the on axis pressure containing only a single propagating mode, and the multi-modal solution above $ka \approx 3$. This is shown in their directivity plots at $ka = 3$ and $ka = 4$, and is evidence that higher order modes are important in the modelling of horn loaded loudspeakers at high frequencies ($ka > 3$).

Shindo et al. (1990) use the stepped approximation approach to reduce the size of the dense matrix produced by Boundary Element Analysis (BEA) calculations of rectangular

horns. They calculated the sound field in the first section of the interior of a horn using the stepped approximation technique and calculated the rest of the sound field using a boundary element technique. The results appear to be quite accurate when compared to experimental data, and polar plots of both the vertical and horizontal sound fields for different horns show excellent agreement with experiment. The maximum frequency considered was $ka = 3.75$, where the dimension a is the radius of a circular mouth of equivalent area to the rectangular horn. They suggest that numerical problems related to the dynamic range of representation of floating point numbers (overflow or underflow), can occur with the stepped approximation technique for some horn geometries. Schuhmacher and Rasmussen (1999) produced a model of a rectangular horn using the stepped approximation and refute the claim of Shindo et al. (1990) that a coupled BEA approach is required to provide a stable numerical model.

For simulations of a high frequency rectangular horn, Schuhmacher and Rasmussen (1999) found "good agreement" between their model and experimental results, provided that the number of modes included in the simulation was "sufficient". Their model uses 4 rectangular acoustic modes of even order (symmetric), as only symmetric excitation was assumed. This assumption is valid, as Muehleisen (1996) reported that for a symmetric stepped duct, there is "no coupling between even and odd numbered modes". They modelled a number of rectangular horns exiting into an infinite baffle and performed Monte-Carlo (statistically sampled) numerical integration to provide radiation boundary conditions, because there are no known analytical solutions for this case. Their results for a high frequency horn show excellent agreement with experimental measurement of on axis far-field pressure to $ka \approx 2$, with general trends predicted to $ka \approx 8$, and poor predictions to the limits of calculations of $ka \approx 12$, where the dimension a is the radius of a circular mouth of equivalent area to the rectangular horn. For the high frequency horn, no comparisons of off axis performance are given. A low frequency horn shows similar trends, with off axis performance also reported. Increasing the number of included modes would show the effect of truncation on the infinite series for velocity potential,

and may improve predictions at high frequencies. The accuracy of the radiation boundary condition can be tested by using other numerical methods (Muehleisen, 1996) as Monte-Carlo techniques are traditionally used when accuracy is of secondary importance (Press et al., 1992, Section 7.6). Schuhmacher and Rasmussen (1999) also suggest future use of their model in calculating multiple arrays of horns. If mutual interaction between the horn mouths were ignored, this would be a simple extension to their model. However the suggestion that their linear model may be extended to include distortion would involve considerable effort given the non-linear nature of the governing equations and the vastly different numerical methods required to solve them.

Kemp et al. (2001) model round horns used in musical instruments. They are mainly interested in the effects of higher order modes on the input impedance of the horn. They use the discrete section method of Pagneux et al. (1996) and the radiation boundary condition of Zorumski (1973) and find excellent agreement with experimental measurement of the input impedance to an estimated $ka \approx 3$. They show that the inclusion of higher order modes is necessary for the high flare rate horns used as terminations of musical instruments such as trumpets and trombones. There is no comparison with experimental results in the far field, although this is not a limitation inherent in the method used.

All of the horn models reported in this section are limited to round or rectangular cross sectional shapes by the requirement of an analytical description of the cross sectional modes. The cross sectional shapes of most modern horns are neither round nor rectangular, with the best designs being found by a combination of approximate simple modelling and experimental verification (Keele, 1975). Rienstra (2003) has developed an approach that is valid for the more complicated problem of a slowly varying lined duct of arbitrary cross section with flow (used in simulations of jet engines), of which horns of arbitrary cross section are a subset. He has not presented any results as modelling arbitrary cross sectional shapes requires a numerical approach, and this is a significant disadvantage of these methods. On the other hand, these methods have potential to be more efficient than

alternate techniques such as finite or boundary element techniques, although no comparisons have been made in the horn literature.

2.3.3 Finite Element Analysis

The finite element technique (Kohnke, 2001), or Finite Element Analysis (FEA) is a general numerical method that can be used to solve a partial differential equation with appropriate boundary conditions. It has been used to solve problems in a wide variety of areas such as heat transfer, linear and non-linear solid mechanics, and fluid flow. The Helmholtz harmonic wave equation, that governs the propagation of linear sound waves, can be solved in arbitrary domains by this method. FEA involves discretising or "breaking up" a domain of interest into smaller "finite" elements, and the underlying differential equation is approximated over these elements. This leads to a system of linear equations, which are solved after the application of boundary conditions, to provide a solution for the whole domain.

For these techniques to give accurate results for acoustic problems, the elements need to be a small fraction of an acoustic wavelength in size. As the frequency considered in the analysis increases, the acoustic wavelength decreases, and the corresponding number of elements required to accurately model a certain size component increases approximately as the cube of frequency, with a corresponding increase in computational time. For a discussion of element size, the "dispersion error" problem and an introduction to the current state of the art in FEA formulations of the Helmholtz equation, see Oberai and Pinsky (2000). Another problem arises in unbounded domains, such as at the mouth of the horn. There is a requirement to truncate the domain at some point, and appropriate boundary conditions are required (Gerdes, 2000, Dreyer and von Estorff, 2003). However, none of the limitations inherent in simple horn models are present when calculating horn solutions using FEA.

Morita et al. (1980) and Beltran (1998) used linear acoustic FEA to model horns. Both used axisymmetric analyses, but the Morita et al. analysis used a radiation boundary condition calculated using an analytical integral equation at the mouth of the horn, implicitly assuming the mouth of the horn is mounted in an infinite baffle. This approach reduced the numerical complexity of the problem, and still allowed the effects of the variation in acoustic particle velocity across the mouth of the horn to be modelled. They report on and off axis far field acoustic pressures, and both models show reasonable agreement with experiment up to $ka \approx 4.6$. Importantly, they show that the directivity of a circular piston differs from the directivity of real horns at high frequencies. This implies that the circular piston model used in simple horn models is inadequate at high frequencies, and alternative models that can take into account variations in acoustic particle velocity across the horn mouth are needed.

The Beltran (1998) analysis used a commercial code (Kohnke, 2001) with the radiation boundary condition being non-reflective on a spherical surface, requiring the mesh to extend outside the horn mouth. The model included a representation of the compression driver, with the "complicated mechano-acoustic" interaction of the compression driver diaphragm with the horn, and indeed this interaction seems to be the major thrust of this work. The throat pressure is compared to experimental measurements, and "the general shape and major features of the calculated response is very close to the actual response". The computational model accurately predicts the location and direction of "9 of the 12 peaks" in the measured response, however there is a "decrease in accuracy above 12 kHz", attributed to material property inaccuracies in the diaphragm material. It is more likely to be due to inaccuracies in representing the geometry of the diaphragm, and the coarse element size compared to the wavelength in this region. Further efforts by Beltran (1998) to investigate the coupling between the compression driver and horn show the utility of a FEA approach to the design of compression drivers. This thesis is not concerned with compression driver design.

Beltran (1998) does not report far field pressures and beamwidths, probably because the FEA model extends only to the near field, and some form of near to far field transformation would be necessary (Morgans et al., 2000). A comparison between the horn mouth model and experimental pressure would have been useful in verifying the accuracy of an FEA approach to modelling horn flares. No mention is made in the article of the horn throat dimension used. An approximate scaling from the given figure and known throat dimension (1" diameter) imply a mouth diameter of 0.5 m. At 12 kHz, this implies $ka \approx 54$, a very high frequency in comparison to other results presented in the literature.

The analyses of Morita et al. (1980) and Beltran (1998) are both axisymmetric, and there have been no reports of fully three dimensional horn FEA found in the literature. It has been found (Morgans et al., 2000) that fully three dimensional FEA of large horns is limited in scope, that "the analysis is constrained by the size of the problem at high frequencies" and that the model "cannot simulate to the highest frequency required by the design standards of industry; thus a need exists for more computationally efficient analysis techniques." These issues will be addressed within the scope of this thesis.

2.3.4 Boundary element method

The boundary integral equation method, or Boundary Element Method (BEM) (Wu, 2000, von Estorff, 2000) is a general numerical method for solving the Helmholtz harmonic wave equation that governs the linear acoustic field in arbitrary domains. It solves a surface integral equation that only requires the bounding surface to be discretised into elements, rather than the whole volume. It also deals implicitly with radiation boundary conditions. These are significant advantages over a technique such as FEA.

The traditional approach to boundary element analysis (the direct method) is based on numerically approximating the Kirchoff-Helmholtz (K-H) integral equation (See Section 4.2.3) which is derived from the inhomogeneous Helmholtz equation. The variation of

pressure on the exterior surface of a volume is discretised with shape functions similar to those used in FEA and a numerical technique called “collocation” is generally used to solve for the pressure. The method produces dense, non-symmetric, frequency dependent matrices, which can be badly conditioned if the frequency is close to an eigenfrequency of the related interior problem (Copley, 1968). This is called the irregular frequency problem and can be solved by techniques such as CHIEF (Schenek, 1968). The direct BEM approach requires care when applied to thin bodies such as plates or disks. To represent a thin body with a finite volume, the distance between opposing surfaces must be small, which can cause numerical problems. This “thin shape breakdown” is a well documented (Martinez, 1991) and can produce spurious results. Figure 2.11 shows a representation of a horn loaded loudspeaker volume with finite thickness walls. If the finite thickness becomes too small, then “thin shape breakdown” will occur.

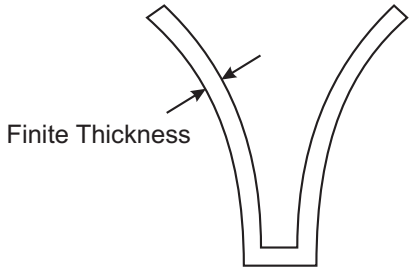

Figure 2.11: Schematic of a BEM representation of a horn loaded loudspeaker with a finite thickness.

An alternative approach to direct BEM is the indirect method (Hamdi and Ville, 1986, Vlahopoulos and Raveendra, 1998, Gardner et al., 1996), which discretises the normal derivative of the K-H integral equation. Instead of solving for the variation in pressure, the variation in the jump in pressure across a thin surface is solved. Theoretically this eliminates the non-uniqueness problem for closed volumes as both the interior and exterior of the volume are solved for simultaneously. In practice numerical limitations at the eigenfrequencies of the interior problem require treatment (Wu, 2000, Chapter 6). The indirect BEM is usually solved with a variational technique leading to increased matrix formulation time, but symmetric matrices. Edge conditions and multiple connections

must be dealt with in special ways making the indirect boundary element method less popular than the direct method with CHIEF.

There have been a number of attempts in the literature to model horn loaded loudspeakers with either direct or indirect BEM. Kristiansen and Johansen (1989) use a collocation matrix assembly technique like direct BEM, with a double layer potential formulation like indirect BEM, with approximate integration to calculate the sound field from horns. It can be considered a hybrid, lying somewhere between the two methods (see also Wu 1995). They report good agreement with far field results at frequencies up to $ka = 13.7$ for axisymmetric horns. Calculations are also reported for rectangular horns in Johansen (1994), although they could easily be extended to include non-rectangular shapes.

Shindo et al. (1990) use a direct BEM approach, combined with an embedded stepped approximation (Section 2.3.2) model to reduce the problem size, to model rectangular horns. This analysis appears to be the first in the literature to analyse non-axisymmetric horns. The comparisons between predicted and experimental far field pressure patterns are excellent, and it appears as though BEM is at least as capable as FEA in the modelling of acoustic horns. No problems with irregular frequencies are reported, which has been shown to be an issue with the direct BEM method. This may be because the maximum frequency considered was $ka = 3.75$, where the dimension a is the radius of a circular mouth of equivalent area to the rectangular horn, and the irregular frequencies occur at the eigenvalues of the associated interior problem, related to the volume of the horn. The maximum frequency may be close to an upper limit, because the first eigenmode of a sphere with equivalent volume would occur at $ka = \pi$.

Both Henwood (1993) and Geaves and Henwood (1996) use direct BEM to model a short horn attached to a dome tweeter. Their model is axisymmetric, and again their results for far field pressure show excellent agreement with experiment over all frequency ranges reported (up to $ka \approx 12.8$). They are able to use the direct method because they model the horn embedded in a spherical volume. Because the distance between the inner surface

of the horn and the outer surface of the spherical volume is large, problems with thin shape breakdown of direct BEM are avoided. CHIEF (Schenek, 1968) is used to avoid the irregular frequency problem.

Hodgson and Underwood (1997) calculate the throat impedance and on-axis far field pressure of a quarter-symmetric rectangular horn using indirect BEM. They report results to $ka \approx 9$, where the dimension a is the radius of a circular mouth of equivalent area to the rectangular horn. They do not report any results for off-axis far-field pressure, but show that indirect BEM is a good potential choice for modelling horn loaded loudspeakers. Other studies have looked at the low frequency response of a horn using indirect BEM (Miccoli, 1999, Bright et al., 2004).

2.3.5 Other horn models

Other novel horn modelling techniques appear in the literature, and should be mentioned here. The Huygens-Fresnel wave model of Backman (1993) has not been compared to experiment, has not been widely adopted, and is not suitable for general horn shapes. Noreland (2002) considers a hybrid model including a lumped parameter model where the flare rate of the horn is small, and an axisymmetric finite-difference model for large flare rates. This model is used in the simulation of musical horns. Neither of these methods are suitable for the current study and are not considered any further.

2.3.6 Summary

There are many choices for modelling horn loaded loudspeakers at frequencies for which a simple one-parameter approach is not valid. For the current application, which is optimisation of the horn geometry, it is imperative that the method be as computationally efficient as possible. In the horn modelling literature, no comparison has been made between

higher order mode models, FEA or BEM in terms of solution resource requirements, so no comment can be made here about their relative efficiency. The review also finds little difference between the accuracies achieved by the best implementation of each method, and the applicable frequency range. The high frequency limit of the Beltran (1998) FEA analysis may be considered an outlier because of uncertainty of the size of the horn mouth, and the study was mainly concerned with the compression driver response.

The higher order mode modelling technique has disadvantages when modelling horns with cross sectional areas that are not circular nor rectangular, and previous experience with FEA modelling (Morgans et al., 2000) suggests that some form of BEM would be appropriate. Direct BEM has problems with modelling the thin surfaces found in horns, and indirect BEM, while able to model thin surfaces, requires more time for matrix assembly than direct BEM. The method of Kristiansen and Johansen (1989) is a good candidate for the modelling work undertaken in this thesis, as it combines the better aspects of each traditional BEM method. Looking to the general acoustic modelling literature, a promising numerical technique called the source superposition technique (Koopmann and Fahnline, 1997) has been identified as a potential candidate for modelling horn loaded loudspeakers. This technique, like that of Kristiansen and Johansen (1989) is able to model thin structures like indirect BEM and uses a collocation like assembly technique similar to direct BEM. It has been validated extensively for the calculation of acoustic power radiated from structures, and one method it uses to calculate power is to integrate the far-field intensity over a spherical surface covering the structure. It is hypothesised that this method will calculate accurate values of far field pressure more efficiently that standard BEM, and it is investigated as a potential candidate for developing fast numerical models of horn loaded loudspeakers in this thesis.

2.4 Horn optimisation

The ability to compute the required shape of a horn, given a specified beamwidth and frequency response, is greatly desired by horn designers and is the overall aim of the current work.

The earliest reference to optimisation of horn beamwidths is Alfredson (1972), who suggests that his method of modelling acoustic horns could be extended to "predict the rate of flare required to produce (if possible) particular radiation directivity pattern". A review of the literature referencing this paper has not found any work on this technique applied to the optimisation of horn geometries. Because the higher order mode modelling technique used by Alfredson has disadvantages when modelling horns with cross sectional areas that are not circular nor rectangular, this method will not be further considered.

It is interesting to note the "if possible" caveat that Alfredson places on his statement, and Morse (1976) touches on this subject saying that "the limits of possible variation of the beam distribution are stringent" when a desired radiation pattern is produced by controlling the modal velocity distribution of various radiating cylindrical modes, and that it may not be possible to generate certain radiation patterns. One restriction Morse mentions is that the main lobe or the radiation pattern "can never be made narrower", but can be made wider by "juggling the velocity distribution of the piston". One question that should be answered by this thesis is "what is physically possible" when it comes to the design of optimal horns.

2.4.1 Objective functions

Shape optimisation routine for horn loaded loudspeakers requires the definition of a set of parameters that control the geometry of the horn. The geometry is then used as an input to a numerical model of the horn, with the beamwidth and frequency response calculated outputs. An objective function then uses the outputs and returns a measure of

the effectiveness of these input parameters in achieving the desired goals. The iterative optimisation procedure, such as Sequential Quadratic Programming (SQP, see B.2), then drives the inputs to achieve the desired goals.

An ideal objective function for use in designing acoustic horns would measure many parameters; the smoothness of the frequency response; the difference between target and actual beamwidth; the smoothness of the beamwidth; and possibly the amount of gain required over a certain bandwidth. In the optimisation of a horn loaded woofer by Miccoli (1999), the single objective cost function incorporated a 90° beamwidth as a 6dB difference in sound pressure level between an on-axis measurement and a 45° off axis measurement. No measure of smoothness of frequency response was mentioned in this work.

Bängtsson et al. (2003), when optimising a planar (2D) horn using FEA, were not concerned with the sound field outside the horn. They required that the shape of the horn minimise reflections and thus match the impedance of the horn with the surrounding air. The objective function used was equal to the sum of the square of the reflection coefficient at each frequency considered (their objective function also contains a term that can be considered to be part of the optimisation technique used, not the fundamental aim of the minimisation). A horn with no reflections would have an "ideal" one parameter response, and would hopefully have a smooth frequency response.

To ensure a smooth frequency response, Henwood (1993) used the weighted average of the squared difference between the pressure at a single frequency and the pressure averaged over all frequencies of interest as a single objective cost function. Geaves and Henwood (1996) used a more complicated cost function that has "exponentially increasing penalties" for designs that do not meet the required design criteria. They measured both the flatness of the frequency response and the gain increase seen by adding a short horn to a dome tweeter, and suggest that further work will deal with beamwidth requirements. Their cost function involves multiple unrelated objectives but combines them in

an arbitrarily weighted single cost function, albeit one that is exactly zero if all objectives are met. There may be difficulty in selecting weights if other criteria are added. Deb (2001) describes the problems with this weighted average approach and suggests that a true multi-objective approach be used, where the cost function is a vector rather than a scalar, and (for 2 objectives) there is "line" of optimal solutions, rather than one single optimum. Ideally a true multi-objective approach would be used for a multi-objective problem, but the solution techniques require an enormous number of function evaluations, and this approach may not be feasible.

2.4.2 Optimisation methods

The optimisation technique used by Miccoli (1999) to minimise the cost function was a non-linear programming approach, and used a commercial optimisation package. Geaves and Henwood (1996) used a method called the Weighted Random Search Method (WRSM), where after starting with an initial state, "random changes are made to the design in such a way that the probability of making a small change is greater than that of making a large change", and the objective function is calculated. The new solution is kept if it is superior to the old solution, otherwise the old solution survives, and the method is iterated until convergence or the maximum number of iterations is reached. They use this method in preference to traditional deterministic methods based on the calculation of the gradient of the cost function because they found a large number of local minima in a sample calculation of their cost function. The traditional methods are not very robust with these types of problems, as they tend to get "stuck" on these local minima. They also suggest that robust optimisation techniques such as Genetic Algorithms (Goldberg, 1989, Deb, 2001) and Simulated Annealing (Ingber, 1993, p444) would be suitable for this kind of optimisation.

Both Henwood (1993) and Geaves and Henwood (1996) use an axisymmetric BEM model of a horn loaded tweeter, and the computational requirements for this approach are small

compared to a fully three dimensional model. It was found in Howard et al. (2004) that optimisation techniques such as Genetic Algorithms (and presumably the WRSM) require a large number of cost function evaluations, and efficient numerical methods are required to make the technique feasible.

Bängtsson et al. (2003) used FEA to model their 2D planar horn, and there may be issues extending this technique to 3D (Morgans et al., 2000). They do, however, use a novel approach to finding the optimum shape of the horn to minimise reflections. They use an adjoint technique to find the gradient (Jameson, 1995, 2003) used in a quasi-Newton minimisation algorithm. The adjoint technique finds the gradient of any number of parameters at the same cost as solving the original model. In contrast, a forward difference approximation to the gradient would require as many additional solves as there are variables, and may not be robust (See B.2). The parameters in Bängtsson et al. are the position of each finite element mesh point defining the shape of the horn, and some form of mesh smoothing or filtering is required to eliminate local minima and "wiggly" solutions.

The use of the adjoint method is attractive when a large number of parameters is used in the optimisation. The method has been applied to efficient implementations of FEA (Feijóo et al., 2001) for the solution of inverse scattering problems, and to BEM (Ghayour and Baysal, 2000) for the minimisation of sound transmission over a barrier. This interesting approach has not been applied to the source superposition method before, and will not be considered further in this thesis.

2.5 Summary and gaps in the current knowledge

The aim of the current work is to develop a design method to calculate the required shape of a horn to give both a flat frequency response and the desired beamwidth over a specified frequency range.

In an extensive review of the literature, it was found that most acoustic horn models are based on a simple, one parameter (Webster), model of sound propagation within the horn and do not accurately model far field acoustic pressure, either on or off axis. They generally tend to model acoustic impedance to a reasonable degree of accuracy, provided there are no sharp changes in the horn cross sectional area. There is evidence in the literature (Holland et al., 1991, Di Cola et al., 2000, 2001) that variations in pressure and acoustic particle velocity across the width of the horn (higher order modes) can be significant at some frequencies, and measurement of the sound field at the mouth of the horn would confirm this. These measurements, along with the measurement of the far field pressure, would allow an examination of the validity of numerical models of horn loaded loudspeakers. Thus, the need exists for experiments that measure both the near and far field of horn loaded loudspeakers.

Alternative approaches to the simple horn models, such as higher order mode models, Finite Element Analysis (FEA) or the Boundary Element Method (BEM) have been found in the literature. However, while these methods can eliminate problems associated with the approximate equation of Webster, it has been found that higher order mode models are limited in cross sectional geometry, and that 3D FEA is intractable for large horn models and high frequencies, and unsuitable for application to optimisation techniques (Morgans et al., 2000). There is also evidence that 3D BEM is similarly unsuitable at the mid to high frequencies needed for cinema applications (von Estorff, 2000). As such, there exists a need to develop models of acoustic horns that can include the effects of higher order modes. The source superposition technique (Koopmann and Fahnline, 1997) has been identified as a potential candidate for efficient modelling of horn loaded loudspeakers, but no evidence has been found in the literature of this technique applied to modelling far-field acoustic pressure. To evaluate this technique effectively, a rigorous comparison to both known analytical solutions and other numerical methods is required.

The ability to compute the shape of a horn, given a specified beamwidth and frequency

response, is greatly desired by horn designers. The optimisation of horn loaded loudspeakers to produce a desired outcome has been attempted previously. Examples include an optimisation of the beamwidth of a horn loaded woofer using a 3D BEM (Miccoli, 1999), the optimisation of the frequency response of a horn loaded tweeter using axisymmetric BEM (Henwood, 1993, Geaves and Henwood, 1996), and most recently FEA to optimise the frequency response of a planar horn (Bängtsson et al., 2003). None of these methods have been applied to optimising both beamwidth and frequency response for the type of horns used in cinema loudspeaker systems. Thus the need exists for the development of fast and robust optimisation techniques that will produce a horn geometry with a specified frequency independent beamwidth and a smooth frequency response over as large a bandwidth as possible.

Chapter 3

The sound field at the horn mouth

The nature of the sound field at the mouth of two small axisymmetric horns is investigated experimentally. An automated traverse system was used to measure the pressure across the mouth of each horn, and the results were decomposed into amplitudes and phases of cylindrical modes, solutions to the Helmholtz equation in cylindrical coordinates.

The circumferential variation of the sound field was examined, and existence of plane waves above a certain limiting frequency was tested.

3.1 Introduction

Typically acoustic horns are modelled using the assumption that the radiation from the mouth can be adequately described by radiation from a piston in an infinite baffle. Many simple numerical models of horns assume that the mouth of the horn is placed in an infinite baffle[1], however most commercially produced horns are not used or tested in this configuration. The baffled piston assumption, which is equivalent to assuming only plane waves exist at the mouth of the horn, appears to give reasonable results for the acoustic

[1] A common alternative to a piston in an infinite baffle is to assume that the horn mouth is a spherical cap mounted on the surface of a sphere (Geddes, 1987, Holland et al., 1991).

impedance at low frequencies (McLean et al., 1992). There is also experimental evidence, such as nulls in the on-axis frequency response of the horn (Chamness, 1994) and a non-uniform pressure profile across the mouth of the horn (Holland et al., 1991, Di Cola et al., 2000, 2001), suggesting that at higher frequencies the piston radiator assumption may be inaccurate, and alternate approaches such as the consideration of higher order modes are needed.

In the work described in this thesis the sound field in the mouth of small axisymmetric horns is experimentally measured, for both exponential and two step conical horns, with an unbaffled exit plane condition. The assumption that only plane waves exist at the mouth of the horn is tested by a modal decomposition. This assumption has implications regarding the choice of numerical method needed to model the horns.

First, the experimental equipment used to measure the sound field is described in detail. Then the experiments are described and the pressure field results for a number of frequencies presented, giving an indication of the complexity of the sound field. The theory of cylindrical modes is presented, and a modal decomposition of the measured results calculated. Finally, conclusions as to the nature of the sound field and requirements for numerical methods are presented.

3.2 Experimental equipment

The sound field at the exit plane of the horn was measured for an unbaffled condition in a semi anechoic facility. Transfer functions between the input to the horn compression driver and the pressure (the sensitivity) at the horn exit plane were measured at a series of points that map the horn mouth. The MLSSA measurement system (Rife, 2001) and an automated two axis traverse were used. The experimental arrangement is shown in Figure 3.1.

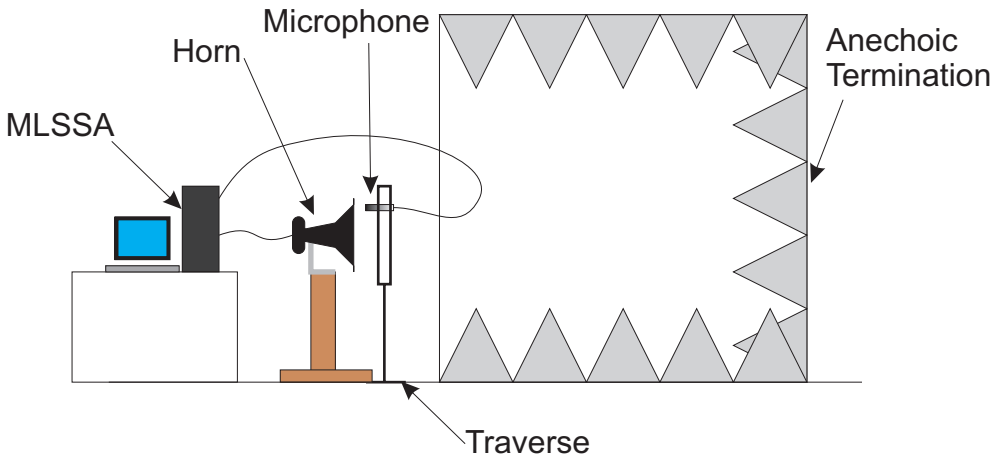

Figure 3.1: Experimental arrangement showing MLSSA measurement system driving (through an amplifier) the horn loaded loudspeaker under test. The pressure at the horn mouth is measured by the microphone, which is positioned by the traverse. Reflections from the walls are reduced by an anechoic termination on the walls.

3.2.1 Experimental facility

The experiments were undertaken using a semi-anechoic facility, as shown in Figure 3.2. In this room, the surfaces on one end have been covered with wedges of sound absorbent material, and the other half is a measurement and testing laboratory. The sound absorbent wedges are not totally anechoic, especially at low frequencies, but the absorption in the frequency range of interest is large, and the ability of MLSSA to gate the impulse response of measurements before reflections return (Rife and Vanderkooy, 1989) mean that accurate measurements in the near field of acoustic horns can be made.

3.2.2 Acoustic horns

Two simple axisymmetric horns have been manufactured to allow experimental validation of any models developed. These horns, shown in Figure 3.3, both have a 2 inch (50 mm) diameter throat; an 11 inch (280 mm) diameter mouth with a 1 inch (25 mm) flange; and they are 9.25 inches (235 mm) in length. One horn has an exponential variation in area between the throat and the mouth, and the other is a two step conical horn. These

Figure 3.2: Semi-anechoic facility showing wedges of acoustic absorptive material.

sample horns have been designed to operate from above 400 Hz to 20,000 Hz (the upper limit of human hearing), enabling validation of the models developed in this project to be examined over a wide frequency range, although the performance at high frequencies will be compromised due to bandwidth limitations of the driver.

(a) Exponential horn

(b) Two step conical horn

Figure 3.3: Axisymmetric horns used in experimental measurements.

3.2.3 Traverse system

An automated traverse system, developed by the School of Mechanical Engineering, was used to move the sensor automatically across the face of the horn in a repeatable controlled manner. The traverse allows three axis positioning via stepper motor control, although the current setup uses only two axes. Figure 3.4 shows the traverse used in these experiments.

Figure 3.4: Automated traverse used to position the microphone during experiments.

Low level step control is provided by a custom controller box, which is connected to a computer via a parallel port. A C language library (Morgans, 2004) has been written to control the traverse as well as programs to interactively move the sensor, and to automate the measurement by external calls from the MLSSA measurement system.

The positions that the traverse moves to during a measurement run are determined by the centroids of a triangular finite element mesh, generated by the finite element program ANSYS (Kohnke, 2001). The use of a finite element mesh generalises the use of the traverse to almost any shape, and allows an even spacing between measurements. Figure 3.5 shows the mesh used to capture the sound field over the mouth of the horn. It also shows a close up of the mesh, with the red dots showing the centroid of the elements, indicating the coordinates over which the microphone is positioned. For the mesh used in these experiments, 3434 positions were used. This should allow resolution up to a frequency of 12 kHz (Based on a mean element spacing of 0.0047 m and 6 elements per wavelength), provided the microphone used is small enough.

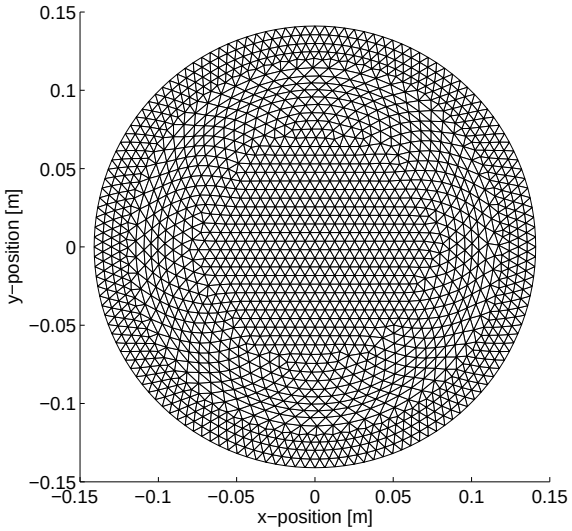

(a) Positional mesh

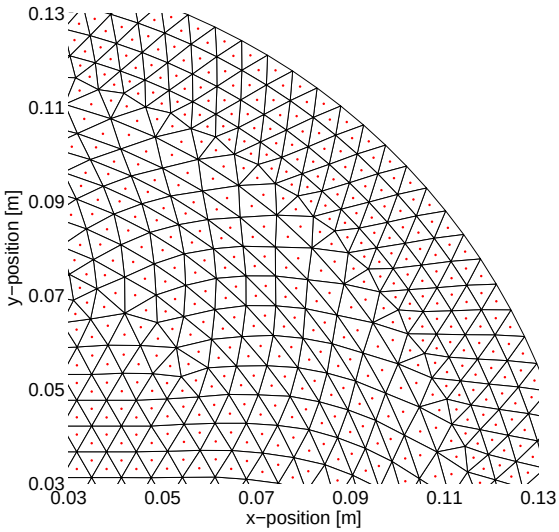

(b) Close up of mesh

Figure 3.5: Mesh used to position the microphone traverse over the mouth of the horn.

3.2.4 Measurement system

The Maximum Length Sequence (MLS) technique measures the impulse response of a system in the time domain, rather than applying an inverse Fast Fourier Transform (FFT) to the measured transfer function. By directly measuring the impulse response, any required FFT can be performed as a post processing operation, reducing computation complexity. This advantage may have been significant in 1989 (Rife and Vanderkooy, 1989) with the speed of personal computers available at that time, but is not as relevant now. The MLSSA measurement system does however have other advantages, including noise immunity, high signal-to-noise ratios, and the ability to truncate the impulse response before reflections return (for example from the rear wall of the semi-anechoic facility).

The MLSSA measurement system (Rife, 2001), a commercially available signal processing card and software, was used to measure the acoustic pressure. The software provides a reasonably complete measurement and analysis system and has a macro processing facility with the ability to run external programs between automated measurements.

The signal from the MLSSA card was amplified by a BJR 100W amplifier and connected to a Beyma model CP800/Ti compression driver (Beyma, 1999).

3.2.5 Pressure sensor

Pressure measurements were taken using a $1/8$" Brüel & Kjær microphone Type 4138 connected to a Brüel & Kjær Nexus preamplifier. Measurements were made to confirm that the output level used was well above the noise floor. Figure 3.6 shows the on-axis sensitivity, the Sound Pressure Level (SPL) produced by 1 Volt of input, measured using MLSSA at the mouth of the horn. Four different stimulus levels were applied with an almost 20 dB difference between the highest and lowest levels. Only minor differences between the measured sensitivities are seen, confirming the noise rejection capability of the MLSSA system and its utility in measuring audio equipment.

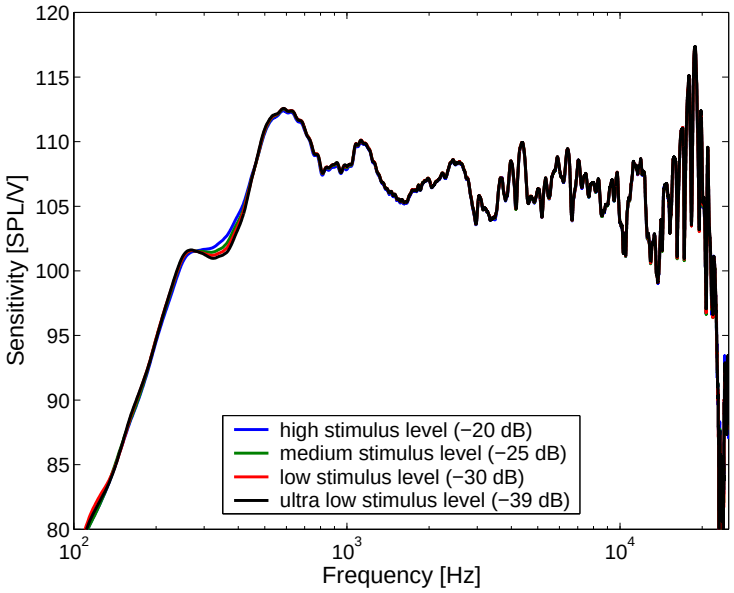

Figure 3.6: On-axis sensitivity measured in the plane of the horn mouth for varying stimulus levels.

3.2.6 Experimental method

The particular horn under test was placed on a suitable stand facing into the semi-anechoic room. The traverse was secured in front of the horn, after suitable alignment. The program `interact` (Morgans, 2004) contains an option to find the centre of a circle by interactively moving to three points on the circumference of the circle. This option was used to find the centre of the horn, and a suitable offset saved and written to disk.

The microphone was attached to the preamplifier and MLSSA measurement system and calibrated using a Brüel & Kjær Type 4231 acoustical calibrator. The macro option in MLSSA was used to automate the measurements. After each measurement was made and written to disk, the program `movetrav` (Morgans, 2004) was called to move the traverse to the next position. To avoid backlash in the system, and to speed up the measurements, an algorithm was developed that only allowed the stepper motors to drive forward. When the motor needs to move backward to go to the next position, the system zeros itself and then drives forward again.

3.3 Results

The results were processed using MATLAB at 50 frequencies varying linearly between 100 and 15000 Hz. At a subset of these frequencies,

$$f = \{410,\ 710,\ 1320,\ 2840,\ 4360,\ 7400,\ 10440,\ 12260\}\,\text{Hz} \tag{3.1}$$

results were plotted for both magnitude and phase, relative to the on-axis result. These appear in full in Appendix A. Some results are given below for the acoustic pressure magnitude response only for the exponential and two step conical horns at low (710 Hz, Figure 3.7), medium (4360 Hz, Figure 3.8) and high (10440 Hz, Figure 3.9) frequencies.

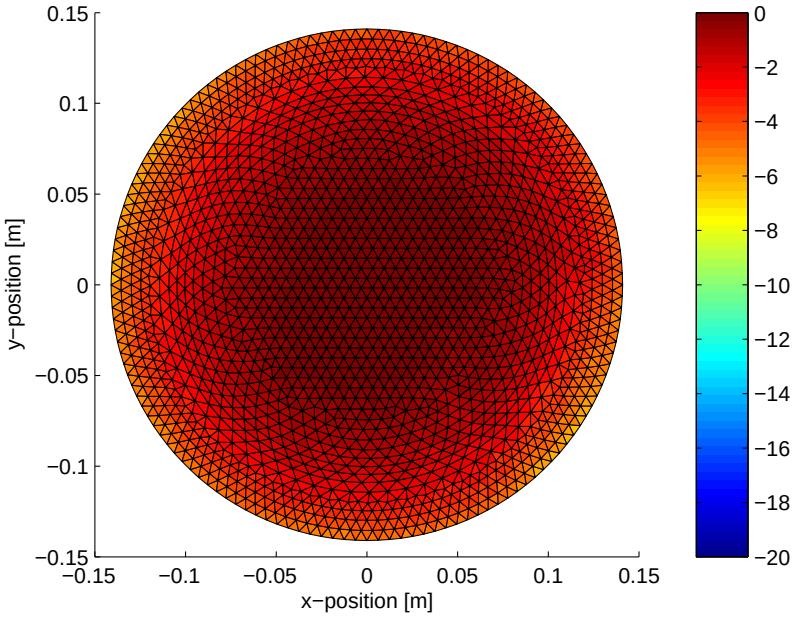

(a) Exponential horn

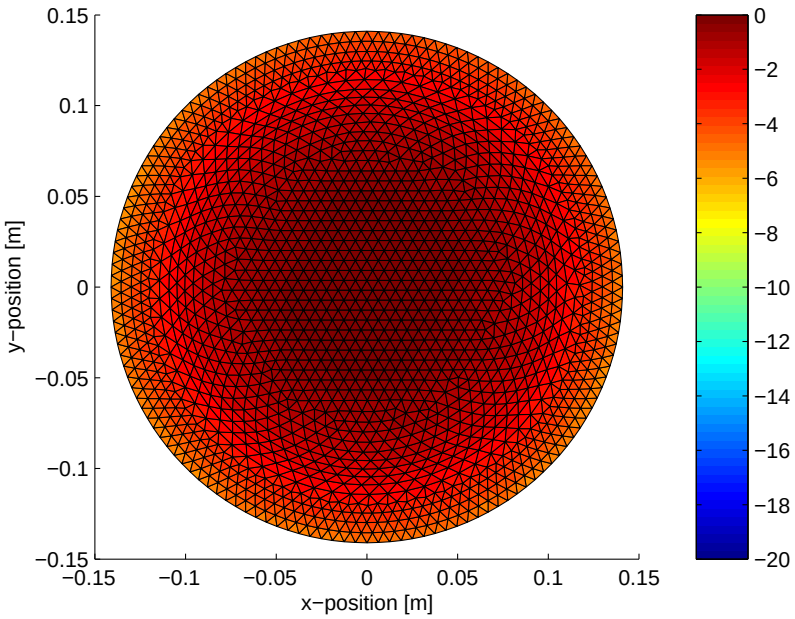

(b) Two step conical horn

Figure 3.7: Acoustic pressure magnitude response, dB reference is on-axis pressure, at 710 *Hz.*

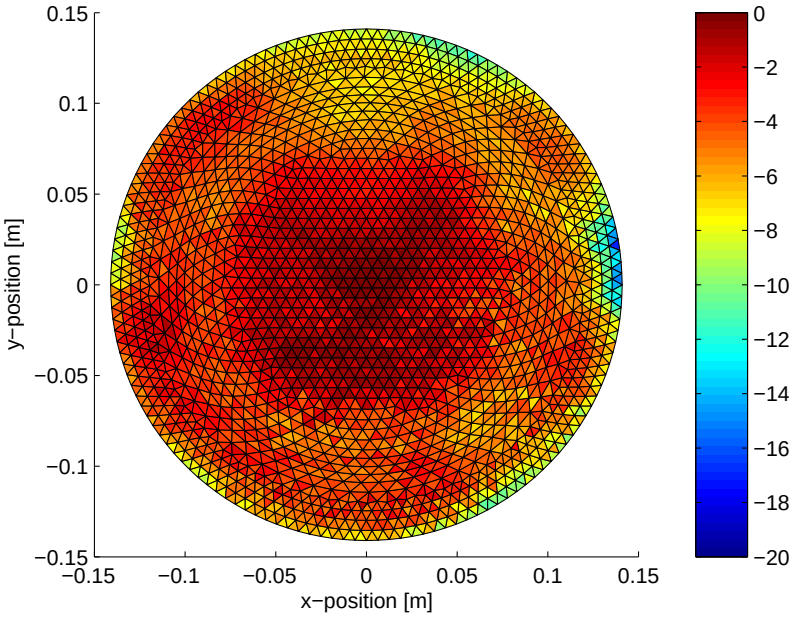

(a) Exponential horn

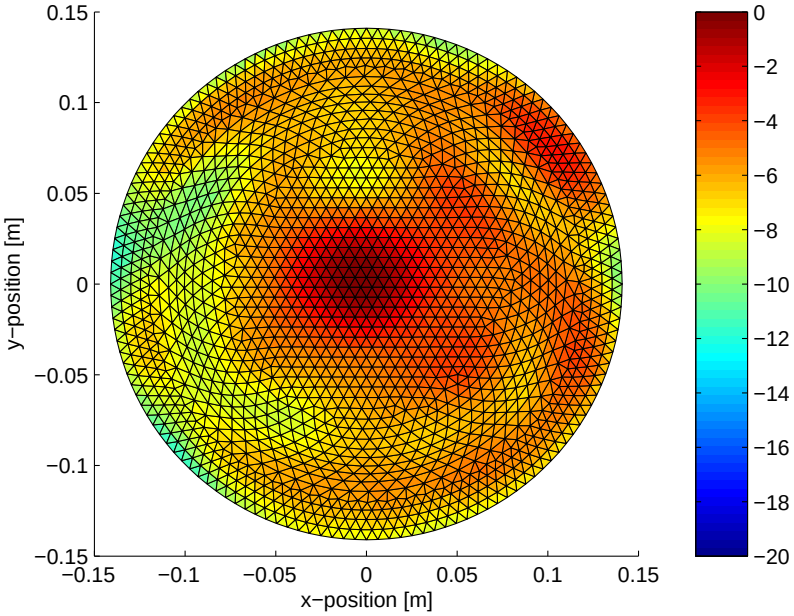

(b) Two step conical horn

Figure 3.8: Acoustic pressure magnitude response, dB reference is on-axis pressure, at 4360 *Hz.*

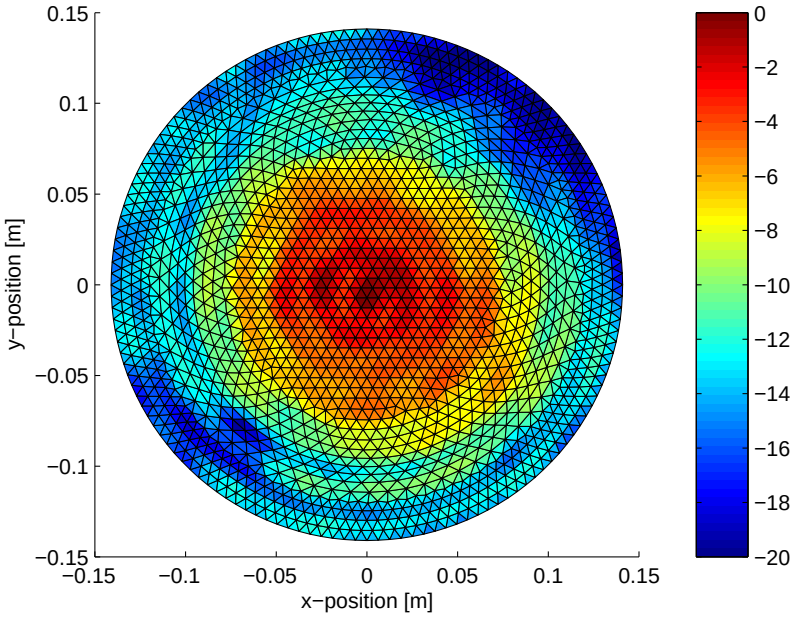

(a) Exponential horn

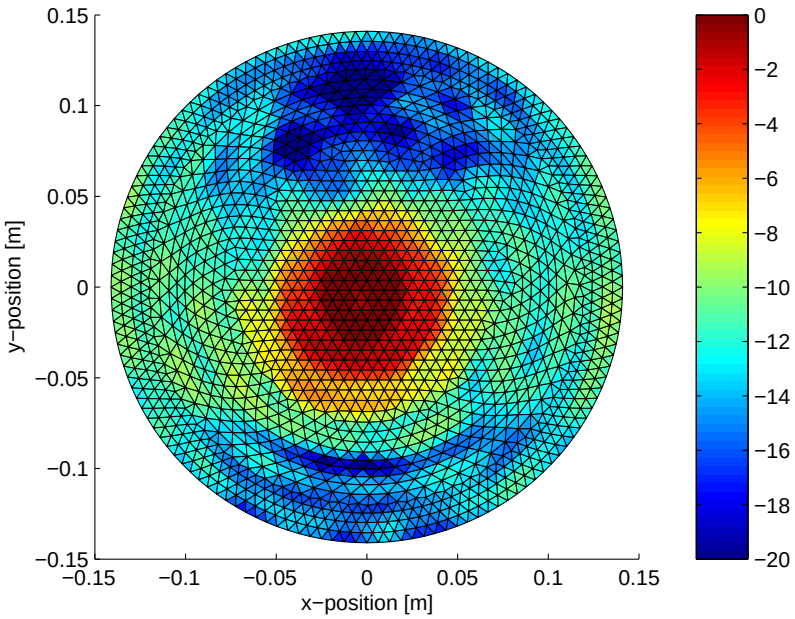

(b) Two step conical horn

Figure 3.9: Acoustic pressure magnitude response, dB reference is on-axis pressure, at 10440 *Hz.*

These results show a strong degree of similarity between the two horn types at low frequencies, and the sound field produced by these horns in the far field should be similar. This can be seen by reference to Figure 3.10, a plot of the beamwidth (Section 2.1.2) of the two horns. At low frequencies the beamwidth produced by the two horns is identical. At the mid frequencies, the pressure field at the mouth of the exponential horn is somewhat uneven. It is, however, quite different to the pressure field of the two step conical horn, which has a high pressure region at the centre. The beamwidth of each horn at these mid frequencies is dramatically different. At high frequencies both horns have a high pressure region at the centre, and appear to have radial waves developing over the horn cross section.

This is experimental evidence that the sound field at the mouth of horns of the type used in cinema loudspeaker applications is quite complicated above a certain limiting frequency. Figure 3.10 shows a divergence in the beamwidth at approximately 2400 Hz. Examining the sound field below (2230 Hz, Figure 3.11) and above (2840 Hz, Figure 3.12) this frequency shows some differences. Below 2400 Hz, both sound fields appear similar. Above this frequency the exponential horn appears to generate a sound field which is broadly similar to the low frequency one, however the two step conical horn generates a very different field, with 5 “lobes” of intensity equal to the centre, appearing radially around the horn. The exponential horn shows some evidence of this “lobing”; however the intensity is not as great.

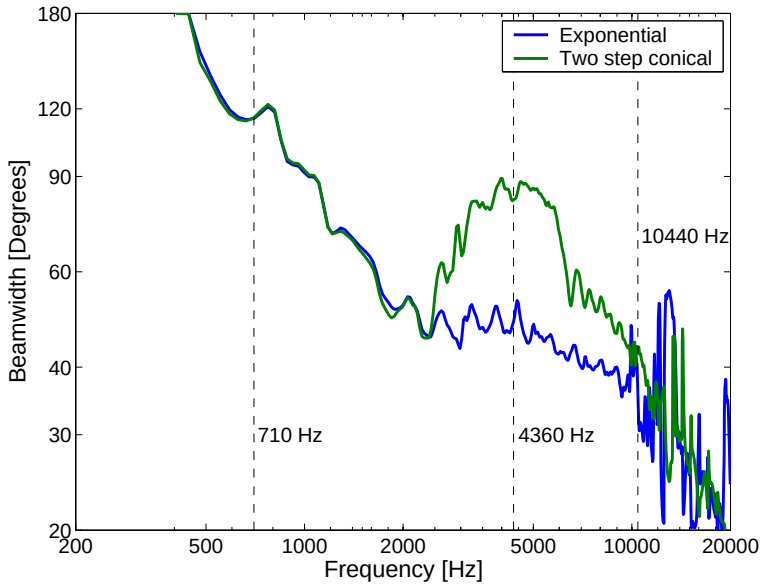

Figure 3.10: Beamwidth of exponential and conical horn.

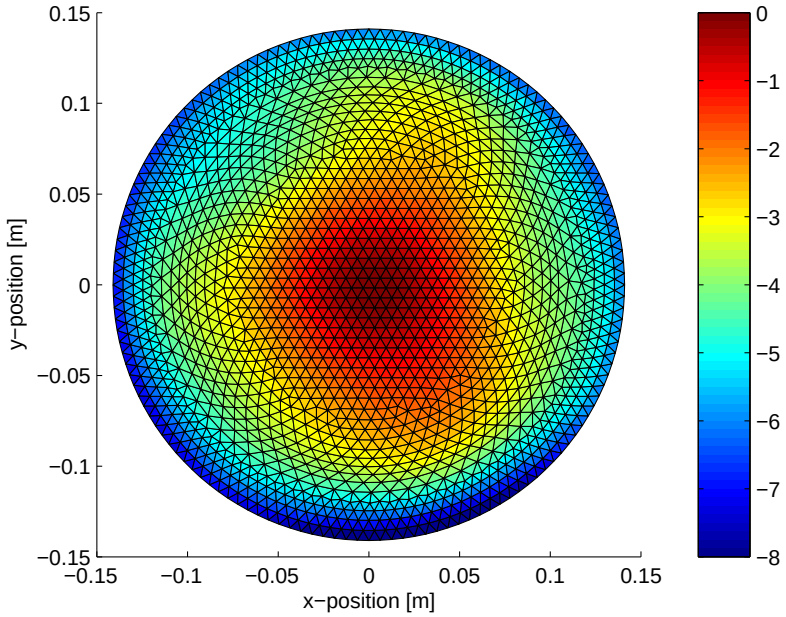

(a) Exponential horn

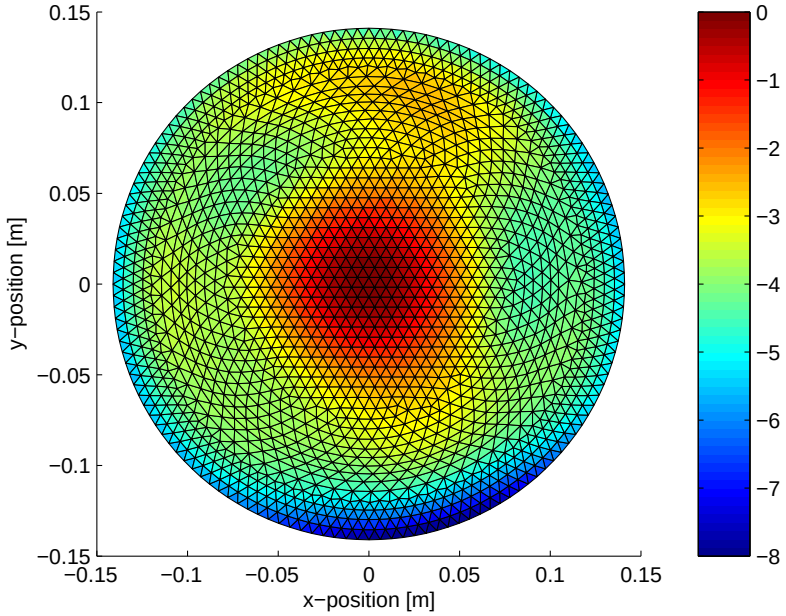

(b) Two step conical horn

Figure 3.11: Acoustic pressure magnitude response, dB reference is on-axis pressure, at 2230 *Hz.*

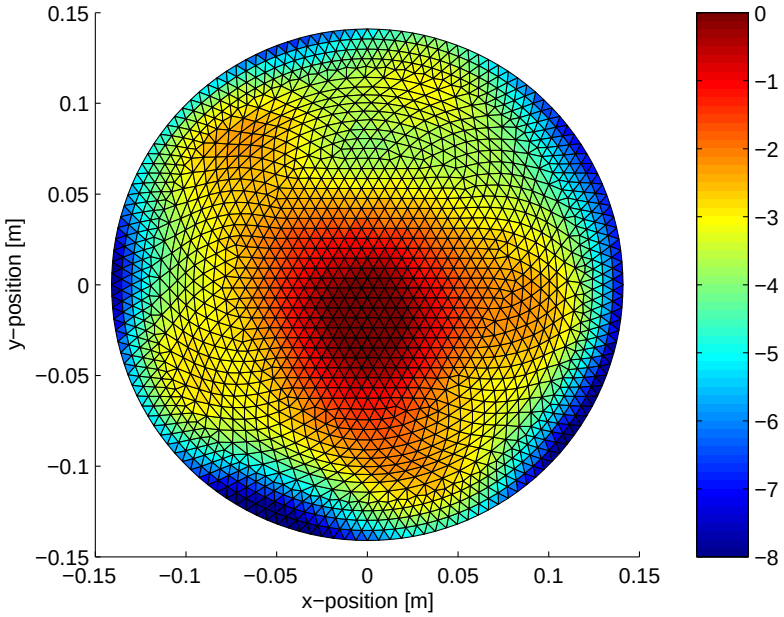

(a) Exponential horn

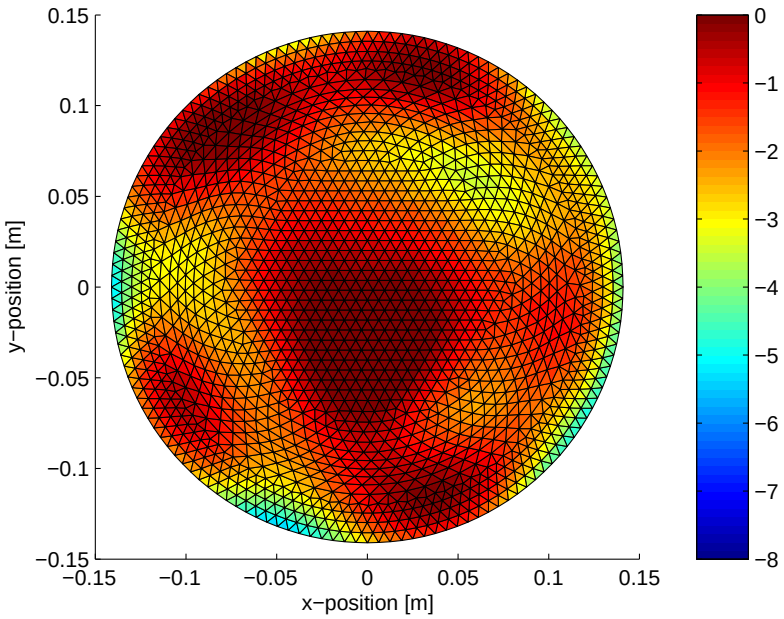

(b) Two step conical horn

Figure 3.12: Acoustic pressure magnitude response, dB reference is on-axis pressure, at 2840 *Hz.*

3.4 Theory

The above analysis of the results is entirely qualitative. A quantitative analysis can be carried out by decomposing the sound field at the mouth of the horn into a series of orthogonal modes, such as those used in duct acoustics (see Pierce (1994) Chapter 7). In this case, the modes chosen are cylindrical duct modes of the same diameter as the mouth of the horn (280 mm).

The acoustic pressure $p(r,\theta)$ at radius r, angle θ in the mouth of the horn, can be written in terms of the fundamental solutions to the Helmholtz equation. This gives,

$$p(r,\theta) = \sum_{m=0}^{\infty}\sum_{n=0}^{\infty} A_{mn} J_m(\alpha_{mn} r) \left\{ \begin{array}{c} \cos m\theta \\ \sin m\theta \end{array} \right\} \tag{3.2}$$

where J_m is a Bessel function of the first kind, A_{mn} is the modal amplitude of radial mode m and circumferential mode n, $\alpha_{mn} = \eta_{mn}/a$, where a is the radius of the duct and η_{mn} is the n^{th} zero of the derivative of J_m, for a hard walled duct. The term α_{mn} is the wavenumber related to the cut-on frequency for propagation of mode (m,n) in a duct. For each radial mode $m > 0$, two degenerate modes exist, a cosine mode and a sine mode.

Equation 3.2 can be rewritten by replacing the double summation with a single index running from 1 to M, the number of retained modes. The modes can be sorted by wavenumber, giving,

$$p_i = \sum_{j=1}^{M} A_j \phi_{ij} \tag{3.3}$$

Where p_i is the acoustic pressure at position i, j is the mode summation index (related to both n and m), A_j is the modal amplitude for mode j and

$$\phi_{ij} = J_m(\alpha_{mn} r_i) \left\{ \begin{array}{c} \cos m\theta_i \\ \sin m\theta_i \end{array} \right\}$$

is the mode shape for the single index j. The equation can be written in vector form,

$$p_i = \Phi_i A_i \tag{3.4}$$

where Φ_i is a row vector of mode shapes at position i and A is a column vector of modal amplitudes.

For N points in space, the matrix relationship

$$P = \Phi A \tag{3.5}$$

can be written, where P is a column vector of pressures at the N points, A is a column vector containing the M retained modal amplitudes and Φ is the $N \times M$ modal shape matrix.

The individual mode shapes can be plotted for each position in space. These are the columns of Φ. The first $(0,0)$, or plane wave, mode has no spatial variation, as shown in Figure 3.13. This mode will propagate in a duct at all frequencies.

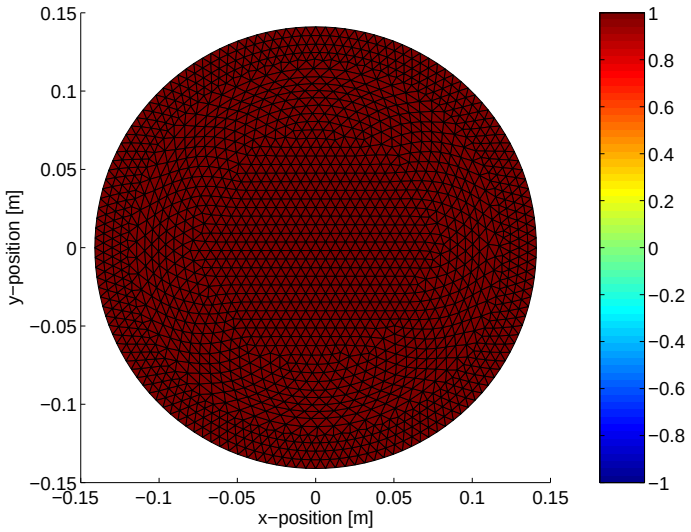

Figure 3.13: Mode $(0,0)$, cut-on at 0 Hz.

The second pair of degenerate modes $(1,0)$, shown in Figure 3.14 have a single radial

node (a single variation around the circumference) and no circumferential nodes (no radial variation), and will propagate in a duct above the cut-on frequency of 710 Hz.

The third pair of degenerate modes $(2,0)$, shown in Figure 3.15, have two radial nodes (two complete loops around the circumference) no circumferential nodes (no radial variation). These modes will propagate in a duct above 1180 Hz.

The final example of a mode shape is shown in Figure 3.16. This is the $(0,1)$ mode, with no radial nodes (circumferential variation) and a single circumferential node (radial variation). It will propagate in a duct at frequencies above 1480 Hz.

The vector P in Equation 3.5 is the measured pressure at each point on the grid, and the mode shape Φ is known. Using a pseudo inverse (MATLAB function `pinv`) it is possible to find the modal amplitudes at each frequency using,

$$A = \texttt{pinv}\,(\Phi)\,P \tag{3.6}$$

This will give the modal amplitude of each mode at each frequency. This quantity is complex valued, and a more appropriate measure of mode strength is the absolute modal amplitude squared, $\left|A^2\right|$.

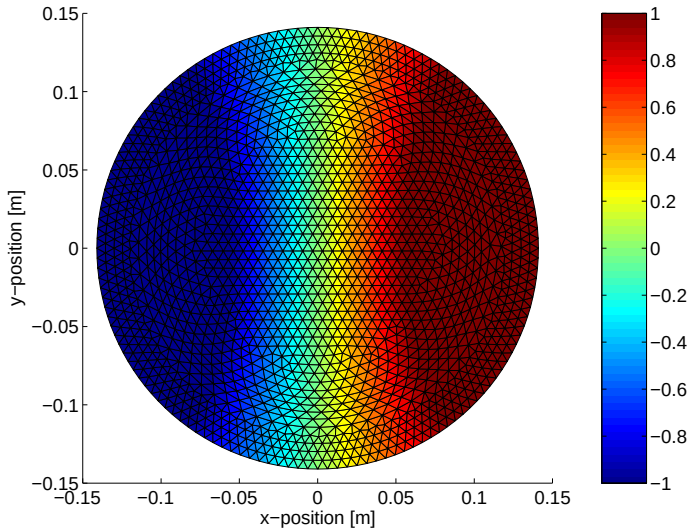

(a) Cos mode

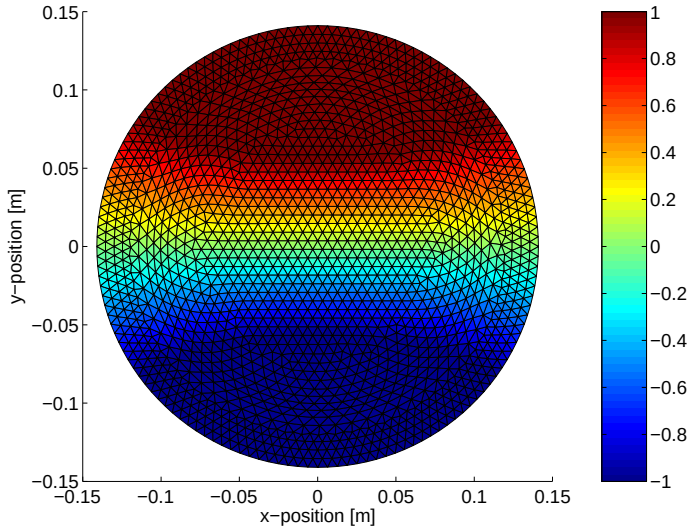

(b) Sin mode

Figure 3.14: Mode $(1,0)$*, cut-on at* 710 *Hz*

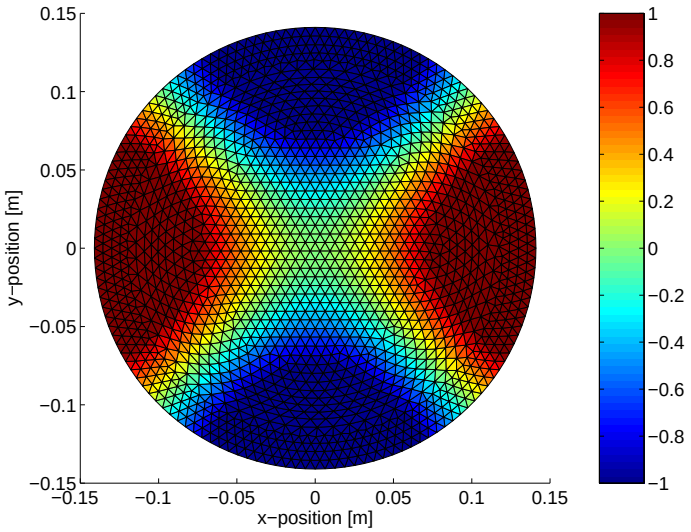

(a) Cos mode

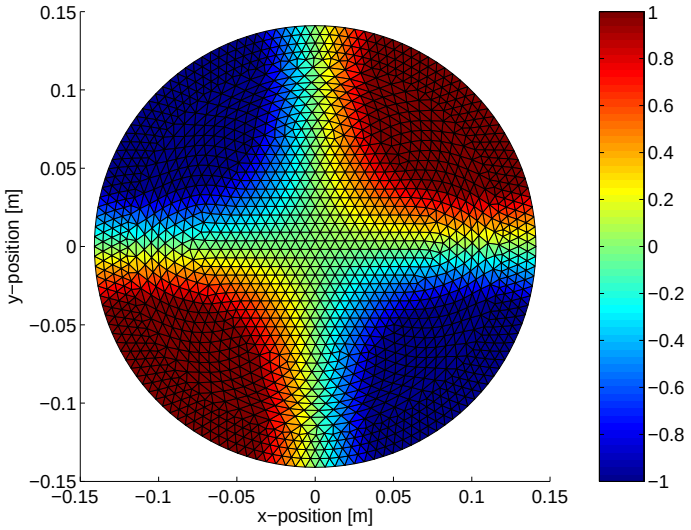

(b) Sin mode

Figure 3.15: Mode $(2,0)$*, cut on at* 1180 *Hz*

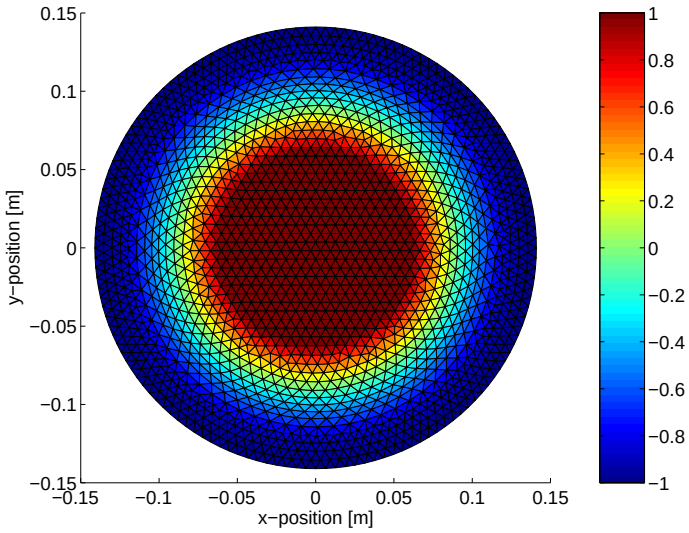

Figure 3.16: Mode $(0,1)$*, cut on at* 1480 *Hz.*

3.5 Analysis

The modal decomposition described in the previous section was performed. The results for the absolute modal amplitude squared, $|A^2|$, normalised by the maximum value of $|A^2|$ at each frequency, are plotted as an image (in dB) in Figure 3.17 for both the exponential and two step conical horns. The abscissa is frequency and the ordinate is mode number ordered from top to bottom by increasing cut-on frequency.

Re-ordering the mode index to have increasing circumferential (n), then radial (m) order gives the results shown in Figure 3.18 for both the exponential and two step conical horns.

What is immediately evident from both these sets of graphs is that the energy at the mouth of the horn is contained almost exclusively in a small number of modes, as indicate by the bands of colour in the figures. If the absolute modal amplitude squared is summed over each radial mode (i.e. starting with $m = 0$, for all n), then the fraction of energy in each radial mode can be calculated. For the two step conical horn 99.7% of total acoustic power is retained in the $m = 0$ modes. Similarly for the exponential horn 99.6% of the total acoustic energy is retained in the $m = 0$ modes. There is almost no energy in the higher radial modes. This means that even though the pressure maps may look like they have a strong circumferential variation, for example Figure 3.12 (b), the contribution of this variation to the total field is small.

Considering only the $m = 0$ modes, Figure 3.19 shows the variation of the first 16 radial mode strengths with frequency. It can be clearly seen that above a certain limiting frequency, the plane wave mode does not contribute to the sound field at the horn mouth. This phenomenon does not appear to be limited to the two step conical horn, although the frequency of transition is slightly lower for the two step conical horn than for the exponential horn.

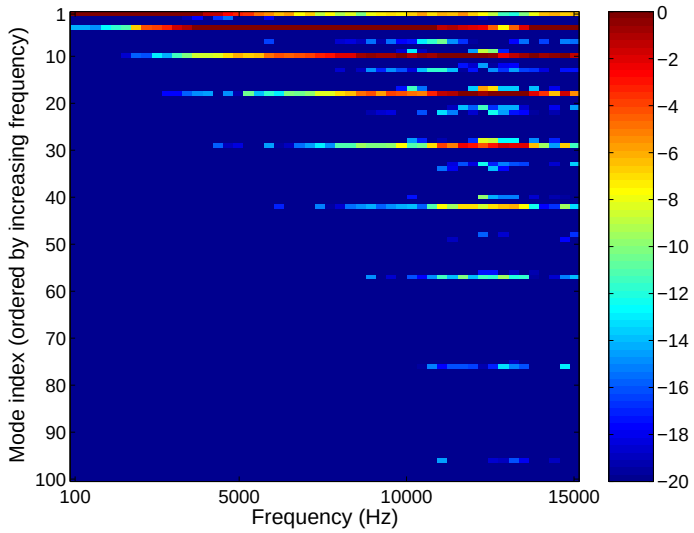

(a) Exponential horn

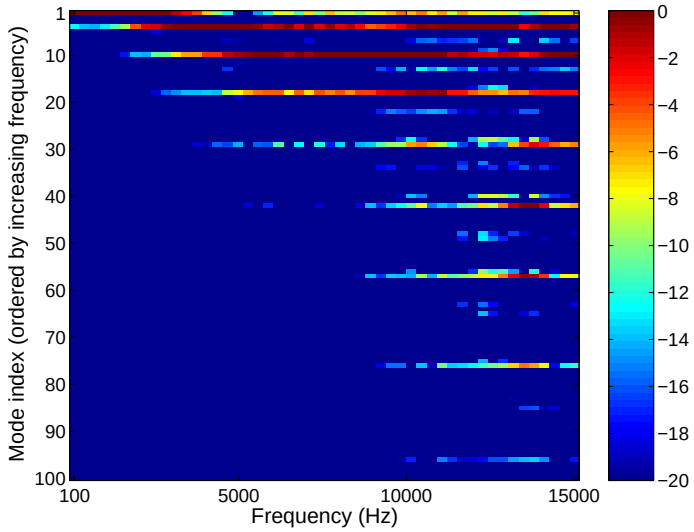

(b) Two step conical horn

Figure 3.17: Absolute modal amplitude squared, $\left|A^2\right|$, for mode index ordered by increasing cut-on frequency.

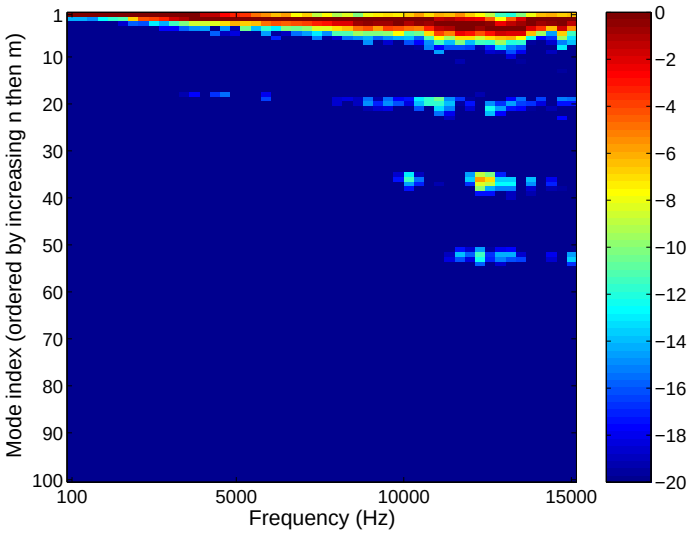

(a) Exponential horn

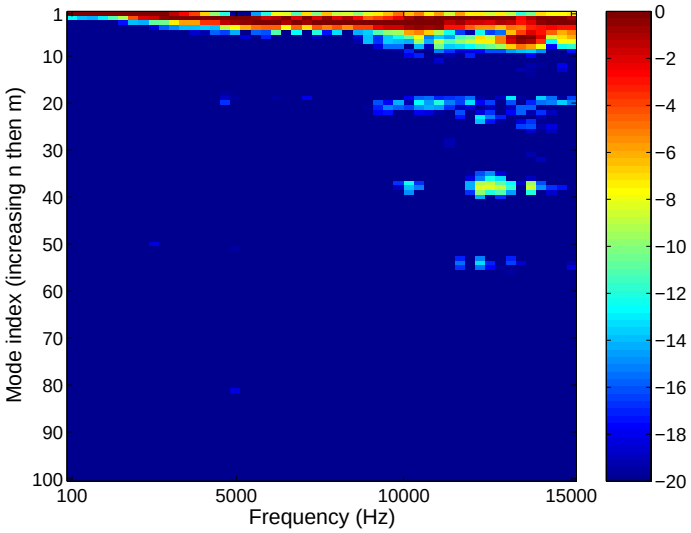

(b) Two step conical horn

Figure 3.18: Absolute modal amplitude squared, $|A^2|$, ordered by increasing circumferential (m) then radial (n) order.

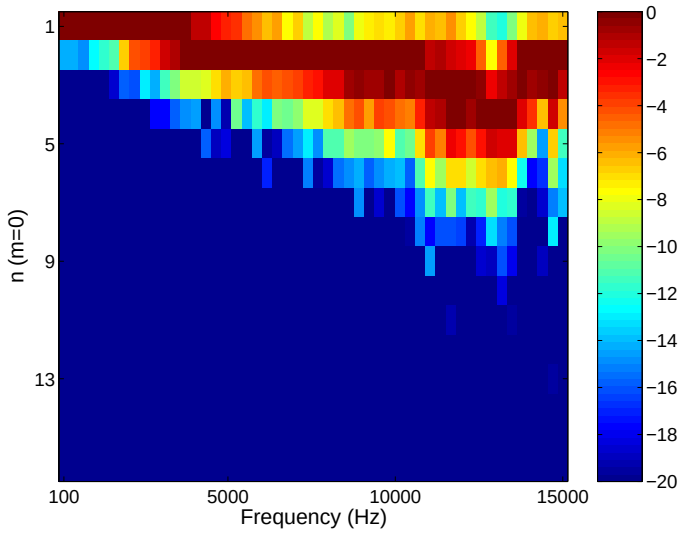

(a) Exponential horn

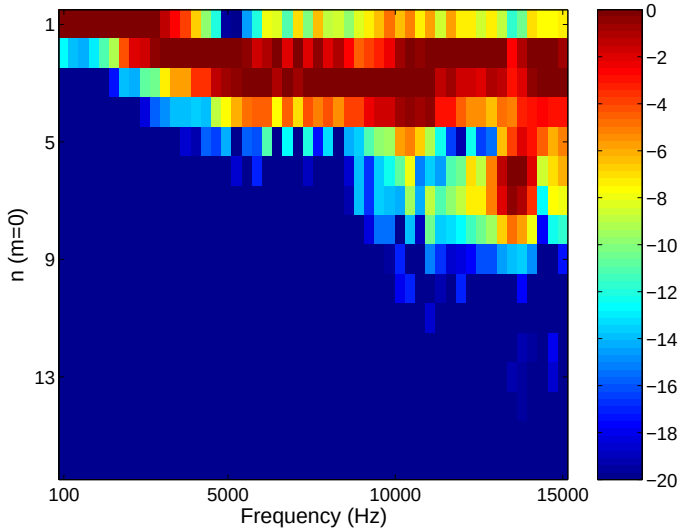

(b) Two step conical horn

Figure 3.19: Absolute modal amplitude squared, $|A^2|$, $m = 0$ modes only.

3.6 Conclusions

Experiments to measure the sound field at the mouth of two small horns have been undertaken to examine the validity of the plane wave radiation assumption made by a number of horn models. The horns are representative of the size and design required for cinema loudspeaker systems, but are axisymmetric. The experimental results demonstrate that this geometric simplicity does not mean that a simple sound field exists at the mouth.

The sound field was measured by an automated microphone traverse. Almost 3500 individual measurements were made across the face of each horn, providing a high spatial resolution. The results were presented as magnitude plots of sound pressure level relative to the on-axis sound pressure level. At low frequencies, the sound field from both the two step conical and exponential horns were similar, as expected. Above a certain frequency, the sound fields became more complex.

An analysis of the data using a modal decomposition with cylindrical duct modes of the same diameter as the exit plane of the horn revealed that almost all of the energy in the system existed in $m = 0$ modes, i.e. modes with no circumferential variation, and that indeed, above a certain limiting frequency, plane waves ceased to exist at the mouth of each horn.

This work sets the stage for the numerical models in future chapters. Any numerical model must be capable of efficiently modelling variations in the sound field across the mouth of the horn. Models based on plane wave approximations should not be used for modelling these experimental horns, at least above a certain critical frequency.

Chapter 4

Fast boundary element methods

Numerical models able to accurately and quickly calculate the far field pressure from arbitrary shapes are investigated. This chapter compares results obtained from the analytical solution of a vibrating cap mounted on the surface of a sphere with the results obtained using two alternative boundary element based numerical methods. The accuracy and speed of the far field pressure solution for both methods is examined. It has been found that a number of techniques can be used to speed up solution time without compromising accuracy.

4.1 Introduction

The experiments performed in Chapter 3 show that for small axisymmetric horn loaded loudspeakers, above a certain limiting frequency, a sound field with a complex radial variation in amplitude exists at the mouth of the horn. Simple theoretical models of horn loaded loudspeakers such as those of Holland et al. (1991), McLean et al. (1992) and Mapes-Riordan (1993) assume a smooth radial variation in sound field amplitude across the mouth of the horn, and cannot model the beamwidth of these acoustic horns in the frequency range of interest. Hence, there is a need for numerical methods capable of

modelling complex variations in sound field inside the horn, and more importantly, accurately modelling the acoustic pressure field away from the mouth of the horn, as required for estimation of the beamwidth (Section 2.1.2).

Traditional approaches to predicting radiation from structures have been limited to either analytical solutions of the governing equations, or to high or low frequency approximations to these equations (Junger and Feit, 1993, Morse and Ingard, 1986). The analytical solutions are limited to structures with surfaces that conform to constant coordinate values in a small number of separable co-ordinate systems (Morse and Feshbach, 1953), such as cylinders or spheres. As most horns are not of this form[1], and the frequencies of interest generally lie between the low and high frequency approximations, alternative approaches must be sought.

Numerical methods such as Finite Element Analysis (FEA) (Beltran, 1998) or the Boundary Element Method (BEM) (Hodgson and Underwood, 1997) have been used to predict sound fields from horn loaded loudspeakers. However, while these methods can eliminate problems associated with analytical techniques, it has been found that fully three-dimensional (3D) FEA can become intractable for large models and high frequencies, and unsuitable for application to optimisation techniques (Morgans et al., 2000). There is also evidence that fully 3D direct BEM is similarly unsuitable for the mid to high frequencies (von Estorff, 2000). A promising numerical technique, called the source superposition technique (Koopmann and Fahnline, 1997), was identified as a possible candidate to develop fast numerical models of horn loaded loudspeakers. To evaluate this technique effectively, a rigorous comparison to both known analytical solutions and other numerical methods was necessary. Both the accuracy of modelling the pressure in the far field and the speed of solution had to be investigated, as these numerical methods are applied to the optimisation of the horn geometry described in later chapters. No previous studies have been found that examine the trade-off between accuracy of solution in the far-field and

[1]The ”acoustic waveguide” approach of Geddes (2002) (see Section 2.3.1) uses this approach to design “Oblate Spheroid” horns.

speed of solution.

This chapter investigates the application of a fully 3D direct BEM (Wu, 2000), as well as the source superposition technique of Koopmann and Fahnline (1997), to the modelling of a vibrating cap mounted on the surface of a sphere. This geometry and loading condition were chosen because analytical solutions are readily available, and it is a good first step to developing fast and accurate models of horn loaded loudspeakers.

First, the theoretical backgrounds to the analytical solution and both the direct BEM and the source superposition method are given. The exact analytical results are compared with the results obtained using the numerical methods, and an analysis of the speed of solution is made. The accuracy of the far field pressure solution for both methods is examined when the mesh density is reduced to below 6 elements per wavelength. Further techniques to increase the speed of solution of the source superposition technique using fast matrix solvers, rotational symmetry and frequency interpolation are examined. Finally, a full model utilising all of the speedup techniques described in this chapter is developed and conclusions are drawn as to the utility of the source superposition technique for numerical modelling of horn loaded loudspeakers.

4.2 Theory

This section gives an introduction to the theory used in this thesis. Linear acoustic sound propagation from an arbitrarily shaped surface, such as a horn loaded loudspeaker, can be described by the wave equation. First, this equation is described and boundary conditions for a solid surface and infinite boundary given. The Helmholtz equation is then derived from the wave equation. This equation is the basis of all the analytical and numerical methods used in this thesis. The analytical solution of the Helmholtz equation in spherical coordinates is then used to derive an equation for the far field pressure from a velocity distribution over the surface of a sphere, a simple model of horn radiation (Figure 2.5).

This analytical solution is used to verify the numerical methods used in this chapter. The Kirchoff-Helmholtz integral equation, which can be derived from the Helmholtz equation, is then described. This equation is useful because it allows a description of any sound field in terms of simple fundamental solutions to the wave equation, monopoles and dipoles. The Kirchoff-Helmholtz equation is the theoretical basis for the traditional Boundary Element Method (BEM). The theory of BEM is described, and finally the theoretical basis of the source superposition method of Koopmann and Fahnline (1997) is described, along with potential advantages of this method when used to model horn loaded loudspeakers.

The wave equation (Morse and Ingard, 1986, Pierce, 1994) describes the time dependent propagation of acoustic waves in a fluid

$$\nabla^2 p(\mathbf{x},t) - \frac{1}{c^2}\frac{\partial^2 p(\mathbf{x},t)}{\partial t^2} = 0 \tag{4.1}$$

where p is the time dependent pressure, $\bigtriangledown = \left\{\frac{\partial}{\partial x}, \frac{\partial}{\partial y}, \frac{\partial}{\partial z}\right\}$ in Cartesian coordinates, c is the speed of sound in the medium, $\mathbf{x} = \{x, y, z\}$ is the position vector and t is time. The linear acoustic momentum equation describes the relationship between pressure gradient and velocity

$$\rho_0 \frac{\partial \mathbf{v}(\mathbf{x},t)}{\partial t} = -\nabla p \tag{4.2}$$

where $\mathbf{v} = \left\{v_x, v_y, v_z\right\}$ is the velocity vector and ρ_0 is the fluid density.

These equations have been derived by assuming the acoustic variables are in fact small perturbations around a mean value in the linearised equations of conservation of mass and momentum, and are related with an equation of state. This derivation has been performed many times (Morse and Ingard, 1986, Pierce, 1994, Koopmann and Fahnline, 1997) and will not be repeated here.

If the acoustic variables vary harmonically with time, i.e. for pressure $p(\mathbf{x},t) = \hat{p}(\mathbf{x})e^{j\omega t}$ where $j = \sqrt{-1}$, $\omega = 2\pi f$ is the circular frequency, f is the frequency and $\hat{p}$ is the complex

pressure amplitude, then Equation 4.1 becomes the homogeneous Helmholtz equation

$$\nabla^2 \hat{p}(\mathbf{x}) + k^2 \hat{p}(\mathbf{x}) = 0 \tag{4.3}$$

where $k = \omega/c$ is the wavenumber. Boundary conditions for a solid surface in contact with the fluid can be found using Equation 4.2, and relate the normal velocity on the surface of interest to the normal pressure gradient,

$$\hat{\mathbf{v}}(\mathbf{x}) \cdot \mathbf{n} = -\frac{1}{j\omega\rho_0} \nabla \hat{p}(\mathbf{x}) \cdot \mathbf{n} \tag{4.4}$$

where $\mathbf{n}$ is the normal vector. If the surfaces of interest are assumed to be surrounded by a fluid extending to infinity, which is a valid assumption if any other surfaces are a large distance away, a boundary condition called the Sommerfeld radiation condition (Sommerfeld, 1949, Page 189) is required

$$\lim_{r \to \infty} r\left(\hat{p}(\mathbf{x}) - \rho_0 c \hat{v_r}(\mathbf{x})\right) = 0 \tag{4.5}$$

where r a radial coordinate centred on the vibrating surfaces and $\hat{\mathrm{v}}_r$ is the radial velocity. Equation 4.5 uses conservation of energy to describe how the amplitudes of propagating waves decrease as the surface area of the waves get larger as they travel further from the source. Once a wave is far enough away from the source, the waves appear planar and are related through their characteristic impedance, $\rho_0 c$.

4.2.1 Sound radiation from a sphere

As described in Section 2.1.2, the far field pressure distribution of a spherical cap mounted on the surface of a sphere can be regarded as a simplified physical model of a horn loaded loudspeaker. In this section the pressure distribution produced by a velocity distribution over the surface of a sphere is derived by considering the Helmholtz equation in spherical

coordinates. The analytical equation thus derived for the pressure field generated by a vibrating spherical cap is used in this thesis to as a simple example to validate the numerical methods considered. The theory developed in this section is also used in Chapter 6 to investigate the generation of a frequency independent beamwidth with an arbitrary velocity distribution over the surface of a sphere.

Equation 4.3 is separable in spherical coordinates. This coordinate system is described in Figure 4.1. Ignoring variations in the ϕ direction, i.e. assuming axisymmetry, gives,

$$\frac{1}{r^2}\frac{\partial}{\partial r}\left(r^2\frac{\partial \hat{p}(r,\theta)}{\partial r}\right)+\frac{1}{r^2\sin\theta}\frac{\partial}{\partial \theta}\left(\sin\theta\frac{\partial \hat{p}(r,\theta)}{\partial \theta}\right)+k^2\hat{p}(r,\theta)=0 \tag{4.6}$$

where r and θ are the radial and angular coordinates respectively.

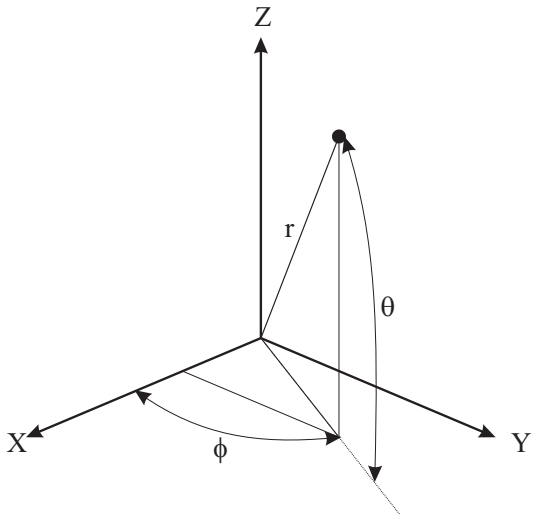

Figure 4.1: Co-ordinate system defining a vibrating spherical surface.

By assuming that the solution to the Equation 4.6 can be separated into components that vary in only a single coordinate system,

$$\hat{p}(r,\theta)=R(r)\Theta(\theta) \tag{4.7}$$

the Helmholtz equation (Equation 4.6) becomes

$$\left[\frac{1}{R(r)}\left(r^2\frac{d^2R(r)}{dr^2}+2r\frac{dR(r)}{dr}\right)+k^2r^2\right]+\left[\frac{1}{\Theta(\theta)}\sin\theta\frac{d}{d\theta}\left(\sin\theta\frac{d\Theta(\theta)}{d\theta}\right)\right]=0 \quad (4.8)$$

with two terms in square brackets each involving a single variable only. For this equation to hold, each term must be a constant, equal and opposite. Setting this constant to C we find,

$$r^2\frac{\partial^2R(r)}{\partial r^2}+2r\frac{\partial R(r)}{\partial r}+\left(k^2r^2-C\right)R(r)=0 \quad (4.9)$$

$$\frac{1}{\sin\theta}\frac{\partial}{\partial\theta}\left(\sin\theta\frac{\partial\Theta(\theta)}{\partial\theta}\right)+C\Theta(\theta)=0 \quad (4.10)$$

It can be shown (Morse and Ingard, 1986) that $C=n(n+1)$ if Equation 4.10 is to have finite solutions for all values of θ. This equation has a solution that can be written in terms of $P_n(x)$, the Legendre Polynomials. These functions form an orthogonal set, and represent waves travelling around the sphere. They are not orthonormal, and

$$\begin{aligned}\int_{-1}^{1}P_n(x)P_m(x)\,dx &= \int_0^{\pi}P_n(\cos\theta)P_m(\cos\theta)\sin\theta d\theta \\ &= \begin{cases}0 & n\neq m\\ \frac{2}{2n+1} & n=m\end{cases}\end{aligned} \quad (4.11)$$

The radial equation (Equation 4.9) has solutions for outgoing waves that satisfy the Sommerfeld radiation condition (Equation 4.5). These are given by spherical Hankel functions of the second kind of order n,

$$h_n^{(2)}(r)=\sqrt{\frac{\pi}{2r}}\left(J_{n+\frac{1}{2}}(r)-j\,N_{n+\frac{1}{2}}(r)\right) \quad (4.12)$$

where J_n and N_n are the Bessel functions of the first and second kind of order n. These

functions represent outgoing radial waves. For $n = 0$, the function is,

$$h_0^{(2)}(r) = j\,\frac{e^{-jr}}{r} \tag{4.13}$$

The pressure can be written as,

$$\hat{p}(r,\theta) = \sum_{n=0}^{\infty} A_n P_n(\cos\theta)\, h_n^{(2)}(kr) \tag{4.14}$$

where A_n are unknown coefficients. The relation between velocity and radial pressure gradient can be found by the linearised momentum equations (Equation 4.4) in spherical coordinates,

$$\frac{d\hat{p}(r,\theta)}{dr} = -j\omega\rho\hat{\mathrm{v}}_r(r,\theta) \tag{4.15}$$

where $\mathrm{v}_r(r,\theta,t) = \hat{\mathrm{v}}_r(r,\theta)\,e^{j\omega t}$ is the radial velocity. The radial derivative of the pressure (Equation 4.14) can be evaluated, giving the velocity

$$\hat{\mathrm{v}}_r(r,\theta) = \frac{1}{-j\rho c}\sum_{n=0}^{\infty} A_n P_n(\cos\theta)\, h_n'^{(2)}(kr) \tag{4.16}$$

where $h_n'^{(2)}(r)$ is the derivative of the spherical Hankel function of the second kind with respect to the radial co-ordinate r. This can be calculated easily (Morse and Ingard, 1986, Equation 7.2.13)

$$h_n'^{(2)}(r) = \frac{1}{2n+1}\left(n h_{n-1}^{(2)}(r) - (n+1)\, h_{n+1}^{(2)}(r)\right) \tag{4.17}$$

An arbitrary velocity profile, $U(r,\theta)|_{r=a}$, on the surface of a sphere of radius a can be written as an infinite sum of a series of Legendre functions,

$$U(r,\theta)|_{r=a} = \sum_{n=0}^{\infty} U_n P_n(\cos\theta) \tag{4.18}$$

where U_n is a velocity series coefficient. By multiplying both sides of Equation 4.16 by $P_m(\cos\theta)\sin\theta$, integrating from 0 to π, and using the orthogonality condition (Equation 4.11) we can find the velocity series coefficient, U_n, for any given velocity profile, $(U(r,\theta)|_{r=a})$

$$U_n = \left(n+\frac{1}{2}\right)\int_0^{\pi} U(r,\theta)|_{r=a}\, P_n(\cos\theta)\sin\theta d\theta \tag{4.19}$$

By equating Equation 4.16 evaluated at $r = a$ and Equation 4.18,

$$A_n = \frac{-j\rho c U_n}{h_n'^{(2)}(ka)} \tag{4.20}$$

,we can find values for the unknown coefficients in terms of the velocity coefficients. Substitution of Equation 4.20 into Equations 4.14 and 4.16 gives the value for the pressure at any point on or away from the sphere as

$$p = -j\rho c\sum_{n=0}^{\infty} U_n P_n(\cos\theta)\frac{h_n^{(2)}(kr)}{h_n'^{(2)}(ka)} \tag{4.21}$$

Equations 4.21 and 4.19 fully define the pressure field produced by an arbitrarily specified velocity profile. Once the frequency (k) of excitation, radius (a) of the sphere and the velocity profile ($U(r,\theta)|_{r=a}$) are known, Equation 4.19 can be used to calculate the velocity coefficients (U_n), and Equation 4.21 can then find the pressure at position (r,θ), provided the infinite series is truncated to a finite value of n.

Equation 4.19 does not have a general analytical solution for arbitrary velocity profiles. For some velocity profiles, such as a uniformly vibrating spherical cap on the surface of a sphere, an analytical solution is possible. This velocity profile is shown in Figure 4.2, with the cap covering angle θ_0 and vibrating with uniform radial velocity u_0.

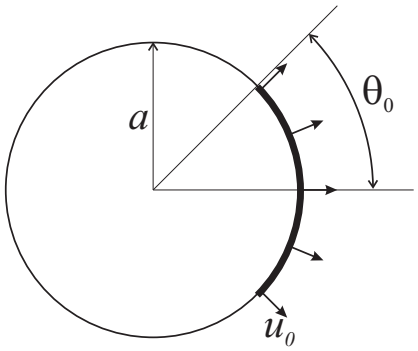

Figure 4.2: A cap covering angle θ_0 mounted on the surface of a sphere of radius a , vibrating with uniform velocity u_0.

The velocity distribution on the surface of the sphere is,

$$u_C = \begin{cases} u_0 & , \quad 0 < \theta < \theta_0 \\ 0 & , \quad \theta_0 < \theta < \pi \end{cases} \tag{4.22}$$

Substitution of Equation 4.22 into Equation 4.19 gives analytical solutions for velocity series coefficient (Morse and Ingard, 1986, Page 343),

$$\begin{aligned} U_n &= \left(n+\frac{1}{2}\right) u_0 \int_{\cos\theta_0}^{1} P_n(x)\,dx \\ &= \frac{1}{2} u_0 \left[P_{n-1}(\cos\theta_0) - P_{n+1}(\cos\theta_0)\right] \end{aligned} \tag{4.23}$$

This analytical solution can be easily calculated and provides an excellent reference for verification of the numerical models used in this thesis in Section 4.3.

4.2.2 Monopoles and dipoles

The analytical method of solving sound radiation described in Section 4.2.1 is only applicable to co-ordinate systems that are separable. Sound radiation from arbitrary shapes such as horn loaded loudspeakers require a different approach. They cannot be described by a surface of a constant coordinate value (such as $r = a$ in spherical coordinates for a

sphere), and require a more general numerical method. One such approach is the Boundary Element Method (BEM) (Wu, 2000). This method, along with the source superposition method of Koopmann and Fahnline (1997), uses fundamental solutions to the Helmholtz equation (Equation 4.3) to provide numerical methods that can solve sound radiation from arbitrary shapes. This section investigates the nature of these fundamental solutions as a precursor to introducing both the BEM in Section 4.2.3 and the source superposition method in Section 4.2.4.

The homogeneous Helmholtz equation (Equation 4.3) is derived assuming no additional sources of mass are introduced into the fluid, and that the waves are propagating unhindered in free space. If the injection (or removal) of a vanishingly small source of mass per unit volume, $\hat{m}_s$, is included in the derivation, then the inhomogeneous Helmholtz equation results,

$$\nabla^2 \hat{p}(\mathbf{x}) + k^2 \hat{p}(\mathbf{x}) = -j\omega\rho_0 \hat{q}_s \delta(\mathbf{x} - \mathbf{x_s}) \tag{4.24}$$

$$\hat{q}_s = \frac{j\omega\hat{m}_s}{\rho_0} \tag{4.25}$$

where $\hat{q}_s$ is the volume velocity per unit volume (Fahy, 2001). A Green's function $\hat{G}(\mathbf{x} \mid \mathbf{x_s})$ is defined as any solution of Equation 4.24 with

$$\hat{q}_s = \frac{1}{j\omega\rho_0} \tag{4.26}$$

The inhomogeneous partial differential equation for $\hat{G}(\mathbf{x} \mid \mathbf{x}_s)$ is

$$\nabla^2 \hat{G}(\mathbf{x} \mid \mathbf{x}_s) + k^2 \hat{G}(\mathbf{x} \mid \mathbf{x}_s) = -\delta(\mathbf{x} - \mathbf{x}_s) \tag{4.27}$$

One such solution for this equation (Koopmann and Fahnline, 1997) is the free-space Green's function,

$$\hat{g}(\mathbf{x} \mid \mathbf{x}_s) = \frac{e^{jkR}}{4\pi R} \tag{4.28}$$

where

$$R = |\mathbf{x} - \mathbf{x}_s| = \sqrt{(x - x_s)^2 + (y - y_s)^2 + (z - z_s)^2}$$

is the distance from the source point at a position defined by vector $\mathbf{x}_s = \{x_s, y_s, z_s\}$, to the field point $\mathbf{x} = \{x, y, z\}$. This solution to the free-space Green's function represents the sound field due to a point source. Note that Equation 4.28 is singular when the source and field point coincide.

A dipole is also a fundamental solution of Equation 4.27, derived from the linearised equations of conservation of momentum and mass with the addition of a localised force. It represents the sound field of two monopoles in close proximity operating 180° out of phase and is the directional derivative of Equation 4.28

$$\bigtriangledown \hat{g}(\mathbf{x} \mid \mathbf{x}_s) \cdot \mathbf{n}_s \tag{4.29}$$

where $\mathbf{n}_s$ is the unit vector describing the major axis of the dipole.

Conceptually, any solid surface, such as the surface of a horn loaded loudspeaker (see Figure 2.11), can be replaced by a distribution of monopoles and dipoles. Both these sources act at a point in free space, but because they are fundamental solutions to the differential equation, any combination, or even continuous distribution, of these sources positioned in space can be used to represent a sound field. The effect of the surface is replaced by the action of a distribution of forces aligned normal to the boundary, and can be represented by a distribution of dipoles. An imposed velocity can be replaced with the injection of volume velocity from a distribution of monopoles. Figure 4.3 shows a representation of this effect.

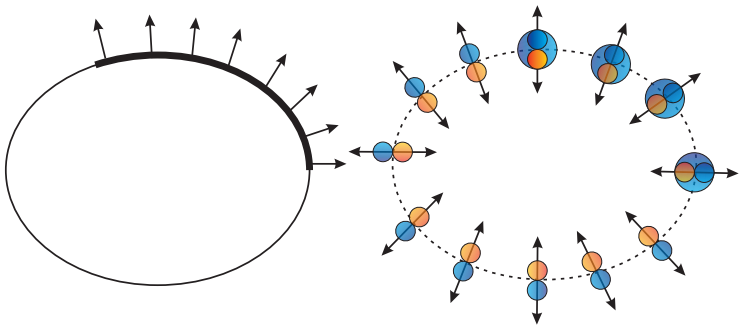

(a) (b)

Figure 4.3: A solid surface with an imposed velocity over part of the surface, (a), can be replaced by a suitable distribution of monopoles and dipoles, (b).

4.2.3 Boundary element method

The Boundary Element Method (BEM) is a numerical technique that is able to model the sound radiated by arbitrary shapes, such as horn loaded loudspeakers. It has been used extensively in horn modelling, and an overview of this application is given in Section 2.3.4. The BEM has many different implementations, however all of them involve the discretisation of the Kirchoff-Helmholtz (K-H) equation that describes a continuous distribution of monopoles and dipoles over a solid surface. This section describes the Kirchoff-Helmholtz (K-H) equation, and the advantages and disadvantages of an implementation of the BEM called "direct BEM". It also briefly describes the "indirect BEM", as well as different methods of modelling horn loaded loudspeakers with the BEM.

The Kirchoff-Helmholtz (K-H) equation describes the sound field radiated from a solid surface by a continuous distribution of monopoles and dipoles. Figure 4.4 shows a representation of the solid surface S, the exterior surface of closed volume V. The sound field of interest is that exterior to the closed volume V, and the vector n_s represents the outward normal of surface S.

The Kirchoff-Helmholtz (K-H) equation can be derived from the Helmholtz equation (Equation 4.3) by using a vector identity and Green's second theorem (Koopmann and

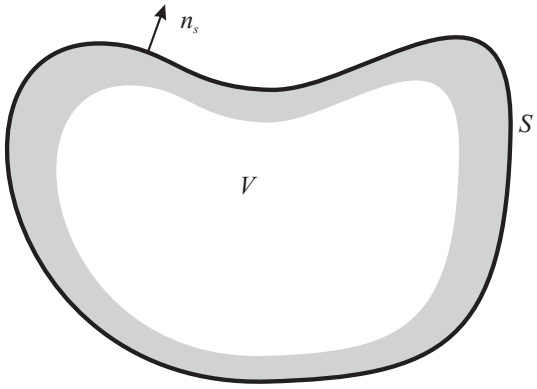

Figure 4.4: Representation of solid surface S, the exterior surface of closed volume V, used in the derivation of the Kirchoff-Helmholtz equation.

Fahnline, 1997). Fahy (2001) gives a more physical derivation, and Juhl (1993) gives an interpretation referencing Huygens's principle. The equation is,

$$c(\mathbf{x})\,\hat{p}(\mathbf{x}) = \int_s j\omega\rho_0\hat{v}_n(\mathbf{x}_s)\,\hat{g}(\mathbf{x}\mid\mathbf{x}_s) + \hat{p}(\mathbf{x}_s)\,\frac{\partial\hat{g}(\mathbf{x}\mid\mathbf{x}_s)}{\partial n_s}ds \tag{4.30}$$

where

$$c(\mathbf{x}) = \begin{cases} 1, & \text{for } \mathbf{x} \text{ outside the volume V} \\ \frac{1}{2}, & \text{for } \mathbf{x} \text{ on the surface S of the volume V} \\ 0, & \text{for } \mathbf{x} \text{ inside the volume V} \end{cases} \tag{4.31}$$

is a position dependent constant, and n_s is a normal vector pointing away from the volume of interest. Equation 4.31 is discontinuous across the surface of the volume, and results from the "treatment of the singular integral involving the derivative of the Green's function" (Raveendra, 1999). For a non-smooth surface (i.e. one that is discontinuous, or has sharp edges) values for this constant can be calculated numerically (Wu, 2000, Juhl, 1993).

Examination of the Kirchoff-Helmholtz (K-H) equation (Equation 4.30) shows that the pressure at any point on or away from the exterior surface, *S*, of the volume of interest can be represented by the surface integral of a combination of monopoles and dipoles. In this equation, the monopole source strength is weighted by the density times the surface

acceleration, and the dipole source strength is weighted by the surface pressure. The equation is important because it only requires a knowledge of the surface of the solid to calculate the sound field away from the solid. Given a distribution of surface normal velocity, once the surface pressure is found, the BEM can calculate any pressure field, and the dimension of the problem has been reduced by one. A numerical discretisation of Equation 4.30 only requires discretisation of the surface of interest, whereas alternative techniques, such as a finite element discretisation of Equation 4.3, require a discretisation of the whole domain.

Equation 4.30 cannot be solved directly, because the pressure on the exterior surface is not known *a priori*. Approximations to this equation exist in the form of the Rayleigh integral and High Frequency Boundary Element Method (HF-BEM), but these techniques have been shown to fail when representing curved surfaces (Herrin et al., 2003).

The direct BEM finds the surface pressure by discretising Equation 4.30 with nodes and elements similar to those used in FEA (Seybert et al., 1985, Wu, 2000). The geometry of the surface is now represented by local interpolation functions. If the surface variables are also represented by these same values (isoparametric elements, see Juhl (1993), 4.4.3), then the nodes represent the values of the surface variables at discrete locations, and shape functions are used to represent the variation in surface variables between the nodes. For each element, the local representation can be written as,

$$\hat{p}(\mathbf{x}) = \sum_{\alpha} N_{\alpha} p_{\alpha m} \tag{4.32}$$

$$\hat{\mathrm{v}}_n(\mathbf{x}) = \sum_{\alpha} N_{\alpha} \mathrm{v}_{\alpha m} \tag{4.33}$$

where N_α is a shape function, $p_{\alpha m}$ is the discrete pressure at node α on element m and $\mathrm{v}_{\alpha m}$ is the discrete normal velocity at node α on element m.

If field point $\mathbf{x}$ is positioned at each of the nodal points, and the discrete representations of the surface variables used, then the surface integral in Equation 4.30 now becomes a

summation of integrals across each element and can be re-written as

$$\sum_{i=1}^{N_n}\sum_{j=1}^{N_n}\left(c\left(\mathbf{x}_s\right)N_i-\int_{s_j}N_i\frac{\partial\hat{g}\left(\mathbf{x}_i\mid\mathbf{x}_j\right)}{\partial n_s}ds\right)p_i=\sum_{i=1}^{N_n}\sum_{j=1}^{N_n}\left(\int_{s_j}j\omega\rho_0N_i\hat{g}\left(\mathbf{x}_i\mid\mathbf{x}_j\right)ds\right)\mathrm{v}_i \tag{4.34}$$

The numerical integration technique used must be capable of dealing with the singularities found at the locations of the monopoles and dipoles, and there are many such techniques available (Wu, 2000, Juhl, 1993, Telles, 1987, Wang and Atalla, 1997).

Equation 4.34 can be written in matrix form,

$$[F]\{p\}=[G]\{\mathrm{v}\} \tag{4.35}$$

The application of boundary conditions, either a known pressure, normal velocity, or surface impedance, allows the formation of the problem,

$$[A]\{x\}=\{b\} \tag{4.36}$$

In this thesis, only a velocity boundary condition will be considered, and $[A]=[F]$, $\{x\}=\{p\}$ and $\{b\}=[G]\{\mathrm{v}\}$. This set of linear equations can be solved by standard solution techniques (Matlab, 2002, LAPACK, 2004) and the surface pressures found. The field pressures can then be easily calculated from a numerical implementation of Equation 4.30.

There are a number of disadvantages to the direct BEM approach. The K-H integral equation represents the sound field on the exterior of a finite volume. At the natural frequencies of the interior of the finite volume, the exterior problem breaks down and the matrix becomes ill-conditioned. This is well documented (Copley, 1968) and many solutions have been attempted (Schenek, 1968, Burton and Miller, 1971, Cunefare et al., 1989, Juhl, 1993). The CHIEF technique of Schenek (1968) has proved to be a very popular technique due to its simplicity. This technique solves an overdetermined system

of equations formed placing extra points inside the volume of interest, where the pressure is zero (Equation 4.31). Provided the points are not placed at a nodal line of the interior solution, this will improve the matrix condition number and allow the matrix to be solved in a least squared sense.

The direct BEM code used in this research is HELM 3D (Wu, 2000), a Fortran 77 implementation using linear elements. The CHIEF method is used to overcome the interior natural frequency problem. For this application the code was modified to accept quarter symmetric models, a change necessary to reduce overall run time.

Another problem with the direct BEM occurs when the volume, needed in the derivation of the K-H equation, is required to represent a so called "thin shape". Figure 4.5 shows a "thin shape", where two sides of the same surface are brought together in close proximity due to a thin dimension, resulting in spurious solutions called "thin-shape breakdown" (Martinez, 1991).

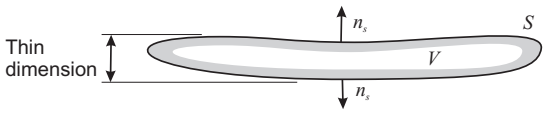

Figure 4.5: Representation of a "thin shape", where volume (V) has two sides of the same surface (S) that are brought together in close proximity due to a thin dimension.

This "thin-shape breakdown" problem means that the direct BEM has difficulty in modelling geometries that are best represented with a thin surface. Figure 4.6 (a) shows a representation of an axisymmetric horn loaded loudspeaker modelled with finite thickness walls. The resulting volume, required for the direct BEM, may contain a "thin-shape" and produce spurious results. Another disadvantage is that the direct BEM would require the entire surface of the resulting volume, both the interior and exterior of the horn, to be discretised, effectively doubling the problem size and increasing solution time. An alternative to this approach is shown in Figure 4.6 (b), where the horn geometry is embedded within a spherical volume, and does not contain any thin surfaces (see, for example,

the work of Henwood (1993) and Geaves and Henwood (1996)). An extension to this approach is shown in Figure 4.6 (c), where the horn geometry is embedded in a small cylindrical volume. This approach minimises the number of elements used compared to the approach used in Figure 4.6 (b), and is adopted in this thesis for direct BEM modelling of horn loaded loudspeakers. The most convenient approach to modelling a horn loaded loudspeaker is that of Figure 4.6 (d), where the horn geometry is represented by thin surface, where the walls are infinitesimally thin. Traditional direct BEM methods are unable to model thin surfaces, and alternative numerical methods are required for this is situation.

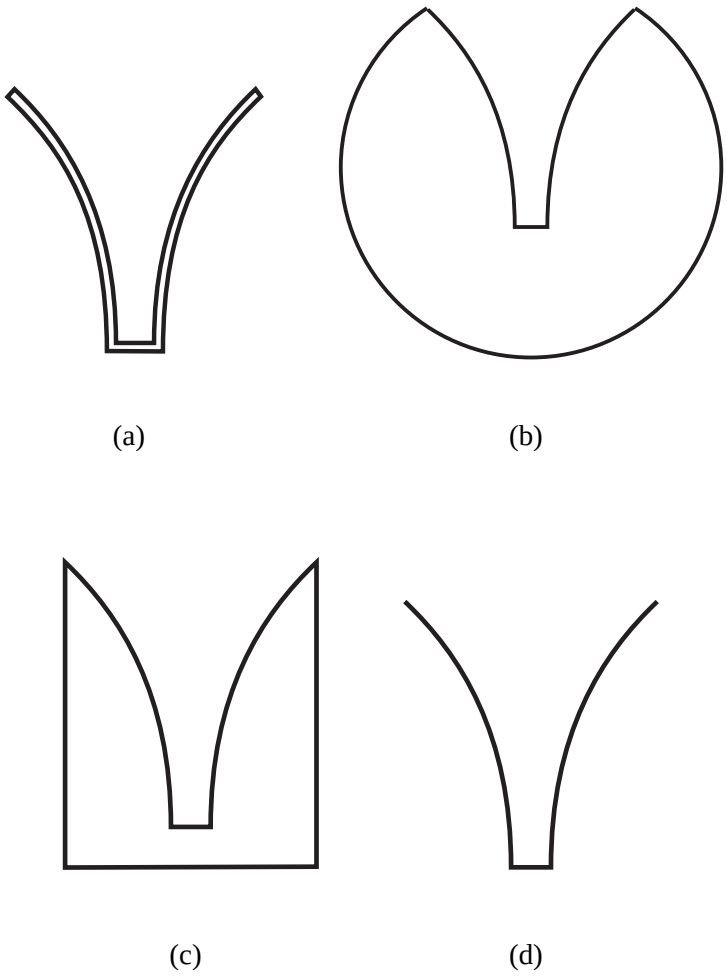

Figure 4.6: Different ways of representing horn surface geometry using the Boundary Element Method.

An alternative method to the direct BEM is the indirect formulation, and this technique is discussed briefly here for completeness. Instead of using surface velocity and pressure as primary variables, it uses the difference in normal velocity and pressure across a thin surface. These are the single and double layer potential functions described by Filippi (1977) and developed by Hamdi and Ville (1986) and Vlahopoulos and Raveendra (1998). It is capable of modelling thin surfaces directly, and when applied to a surface enclosing a volume, it can resolve the pressure both internally and externally. It does not suffer from the non-uniqueness problem of the direct BEM, but will suffer from numerical roundoff errors when the pressure difference between the interior and exterior solutions is large at these same frequencies. This is solved by the application of an impedance surface on the interior of the volume to damp out the interior resonant response.

The indirect BEM, when solved by a variational principle, will produce symmetric matrices, which reduces computational storage. However, the technique requires a double integration across the surface of each element, and the assembly time for large problems can become prohibitive (Raveendra, 1999).

This section can only touch on the different forms of Boundary Element Method. As a starting point for further reference see Wu (2000) and von Estorff (2000).

4.2.4 Source superposition technique

The source superposition technique of Koopmann and Fahnline (1997) is a numerical method that can be used to solve the acoustic pressure field generated by, and acoustic power radiated from, arbitrarily shaped surfaces. It is similar to a Boundary Element Method, but cannot be classified as such because it does not directly discretise and solve the Kirchoff-Helmholtz equation (Equation 4.30). An extensive review of the literature has not found any applications to horn modelling. This section aims to introduce the theory of the source superposition technique and to outline potential advantages of the method when it is used to model horn loaded loudspeakers.

The source superposition technique is formulated as follows. The surface is firstly divided into N surface elements, much as in a traditional boundary element technique. A combination of monopoles and dipoles are placed at the centre of each element, the dipole aligned normal to the element. The approximate solution to the pressure field can then be found by a linear combination of these N simple sources,

$$\hat{p}(\mathbf{x}) = \sum_{\nu=1}^{N} \hat{s}_\nu \left\{ \alpha_\nu \hat{g}(\mathbf{x} \mid \mathbf{x}_\nu) + \beta_\nu \left[\bigtriangledown \hat{g}(\mathbf{x} \mid \mathbf{x}_s) \cdot \mathbf{n}_s \right]_{\mathbf{x}_s = \mathbf{x}_\nu} \right\} \tag{4.37}$$

where $\hat{s}_\nu$ is the unknown source strength for source ν, and α_ν and β_ν are known constants for different source types.

Different source types can be used to describe sound radiation from different types of surfaces: a distribution of monopoles best describe sound radiation from a baffled source, such as a piston placed in an infinite baffle; dipoles best describe radiation from a thin structure, such as a disk vibrating in free space, or a horn surface such as that shown in Figure 4.6 (d); and a linear combination of a monopole and dipole, called a tripole, describes radiation from the exterior of an enclosed volume. Table 4.1 gives the different values of α_ν and β_ν for each source type.

Source type	α_ν	β_ν
monopole	1	0
dipole	0	i/k
tripole	1	i/k

Table 4.1: Constants α_ν and β_ν for monopole, dipole and tripole sources.

The constants for the tripole source are chosen to remove non-uniqueness problems that would arise at frequencies corresponding to eigenvalues of the interior volume (Copley, 1968, Schenek, 1968, Burton and Miller, 1971). For a complete discussion of the rationale behind the choice of constants for each different source type, see Koopmann and Fahnline (1997, Section 3.3). The use of dipole sources makes this technique capable of modelling thin surfaces directly, which is a significant advantage when modelling horn

loaded loudspeakers.

The aim of the numerical method is to find the source strength distribution $\hat{s}_\nu$ for a given boundary condition. Once these strengths are known, the sound pressure can be reconstructed anywhere in the field using Equation 4.37.

For most problems in acoustics, the velocity, or the ratio of pressure to velocity, is a known boundary condition. Substituting Equation 4.37 into 4.4 gives an approximate solution for the normal velocity,

$$\hat{\mathbf{v}}(\mathbf{x}) \cdot \mathbf{n} = -\frac{1}{j\omega\rho} \sum_{\nu=1}^{N} \hat{s_\nu} \bigtriangledown \left\{ \alpha_\nu \hat{g}(\mathbf{x} \mid \mathbf{x}_\nu) + \beta_\nu \left[\bigtriangledown \hat{g}(\mathbf{x} \mid \mathbf{x}_s) \cdot \mathbf{n}_s \right]_{\mathbf{x}_s = \mathbf{x}_\nu} \right\} \cdot \mathbf{n} \tag{4.38}$$

Koopmann and Fahnline (1997) apply a matching technique to find a relationship between the unknown source strengths, $\hat{s}_\nu$, and the known normal velocities, through the volume velocity,

$$\hat{u}_\mu = \int \int_{S_\mu} \hat{\mathbf{v}}(\mathbf{x}) \cdot \mathbf{n} \, dS(\mathbf{x}) \tag{4.39}$$

where S_μ is the surface associated with element μ, and $\hat{u}_\mu$ is the volume velocity of element μ. This is the average velocity over the surface of the element, multiplied by the surface area of the element. Substituting Equation 4.38 into Equation 4.39 gives

$$\hat{u}_\mu = \sum_{\nu=1}^{N} -\frac{\hat{s_\nu}}{i\omega\rho} \int \int_{S_\mu} \bigtriangledown \left\{ \alpha_\nu \hat{g}(\mathbf{x} \mid \mathbf{x}_\nu) + \beta_\nu \left[\bigtriangledown \hat{g}(\mathbf{x} \mid \mathbf{x}_s) \cdot \mathbf{n}_s \right]_{\mathbf{x}_s = \mathbf{x}_\nu} \right\} \cdot \mathbf{n} \, dS(\mathbf{x}) \tag{4.40}$$

and this equation can be calculated for each element, leading to a system of N equations for N unknowns. This can be written in matrix form

$$\mathbf{Us} = \mathbf{u} \tag{4.41}$$

where $\mathbf{s} = \{s_1, s_2, \ldots s_N\}^T$ is a column vector of source strengths, $\mathbf{u} = \{\hat{u}_1, \hat{u}_2, \ldots \hat{u}_N\}^T$ is

a column vector of volume velocities and **U** is the system matrix to be inverted, with components

$$U_{\mu\nu} = -\frac{1}{i\omega\rho}\int\int_{S_\mu} \bigtriangledown \left\{\alpha_\nu \hat{g}\left(\mathbf{x} \mid \mathbf{x}_\nu\right) + \beta_\nu \left[\bigtriangledown \hat{g}\left(\mathbf{x} \mid \mathbf{x}_s\right) \cdot \mathbf{n}_s\right]_{\mathbf{x}_s=\mathbf{x}_\nu}\right\} \cdot \mathbf{n}\, dS\left(\mathbf{x}\right) \qquad (4.42)$$

The components can be evaluated over each element by standard Gaussian integration for triangles (Cowper, 1973) or quadrilaterals (Press et al., 1992) of varying order, or by a special integration technique (Koopmann and Fahnline, 1997, Duong, 1980) when $\mu = \nu$ and the integrand is singular.

The solution of Equation 4.41 will find the source strengths required to represent the given geometry and velocity distribution. Once these strengths are found, the sound field can be reconstructed using Equation 4.37.

The source superposition code used in this research is the Fortran 77 program POWER (Koopmann and Fahnline, 1997). This program has also been modified for quarter symmetry.

This technique is likely to be efficient compared to a direct or indirect BEM for a number of reasons.

1. The number of entries to be inverted is dependent on the number of elements rather than the number of nodes. This is discussed in DeBiesme et al. (2003b) and DeBiesme et al. (2003a) and is especially relevant when the BEM uses quadratic or higher elements.

2. The technique is an approximate one that forces volume velocity of the numerical sources to match the volume velocity boundary condition, and hence the power (and consequently far field pressure) is calculated accurately, even for vary coarse meshes (Koopmann and Fahnline, 1997). A disadvantage is that the near field may not be correctly calculated.

3. The technique implicitly allows the use of thin surfaces. The direct BEM requires a surface of substantial thickness, along with an attendant doubling in the number of elements, otherwise problems associated with thin surface breakdown arise. The direct BEM has been modified to include thin surfaces (Wu, 1995), but this modification is not considered in this thesis as access to the software is not generally available. Another alternative is to use an indirect BEM method with a resulting increase in matrix assembly time.

The source superposition technique has been adopted in this thesis to model horn loaded loudspeakers mainly because of its availability, efficiency and ability to model thin surfaces directly.

4.3 Comparison to analytical results

The exact analytical results for sound radiation from a spherical cap vibrating on the surface of a sphere are compared with the results obtained using direct BEM and the source superposition technique using the same mesh. This allows the errors associated with the numerical methods to be compared directly, without the influence of mesh variation. A spherical cap vibrating on the surface is a simplistic model of a horn loaded loudspeaker (see Section 2.1.2), however the analytical solution is easily calculated (Section 4.2.1) and provides an excellent example for numerical model verification[2].

The analytical solution for a 45° vibrating spherical cap on the surface of a unit sphere has been calculated using Equations 4.21 and 4.23. The infinite sum in Equation 4.21 was truncated at 100 terms, and the pressure calculated in the far field, at a radius of $18a$. This distance compares with that used to measure horn loaded loudspeakers (see Section 5.2).

The sound field generated by a vibrating spherical cap on the surface of a sphere is quite complex, and requires many terms in Equation 4.21 to converge. It can be considered an adequate test of accuracy of the numerical methods being investigated.

Figure 4.7, reproduced from Section 2.1.2 shows a polar plot of the magnitude of the measured pressure, normalised by the maximum pressure, for a 45° vibrating spherical cap, for three different non-dimensional frequencies, $ka = \{3, 10, 20\}$.

Figure 4.7 also shows the beamwidth for each of these frequencies. The beamwidth is defined as the angle formed by the -6 dB points, with reference to the maximum reading, and the source centre (Davis and Davis, 1997) and is a measure of the distribution of sound in the specified plane. Figure 4.8 shows a plot of the beamwidth versus frequency, and is the baseline for comparison with the numerical methods. The values of beamwidth for the three frequencies shown in Figure 4.7 are also shown on Figure 4.8.

[2] For a definition of model verification refer to Babuska and Oden (2004).

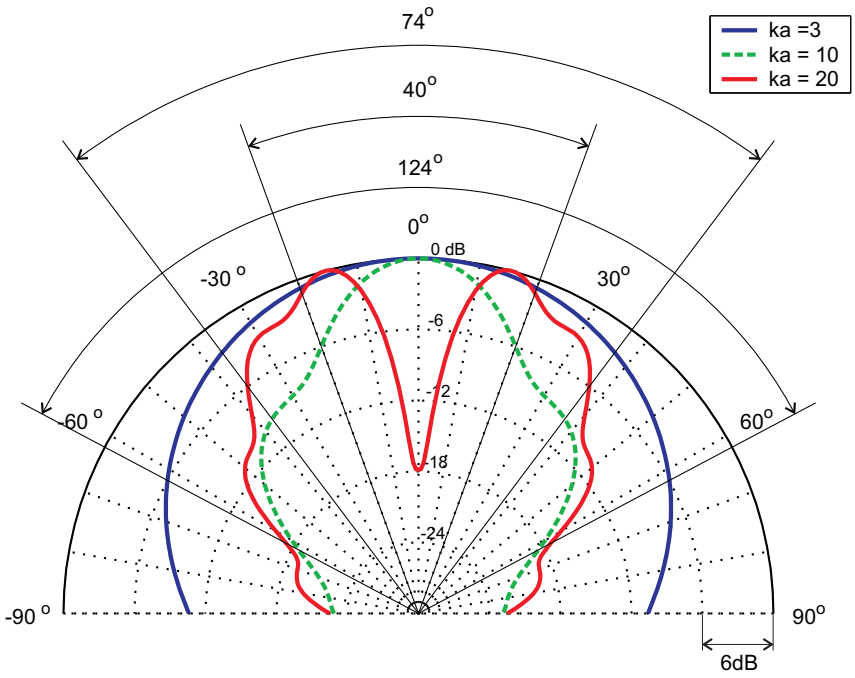

Figure 4.7: Polar plot of the magnitude of the measured pressure, normalised by the maximum pressure, for a 45° *vibrating spherical cap on the surface of a sphere. Beamwidth is also shown for each frequency.*

Simulations of a 45° vibrating spherical cap on the surface of a unit sphere have been undertaken for both the direct BEM and source superposition techniques. Figure 4.9 shows the surface mesh used to discretise the sphere. The finite element program ANSYS (Kohnke, 2001) was used to generate the mesh automatically, and the mesh size was set to be a nominal 6 elements per wavelength at the highest frequency of interest. Note the quarter symmetry of the mesh. This is critical in reducing the overall solution time of the model as the full sphere would contain four times as many nodes and elements, dramatically increasing memory usage, assembly time and solution time.

A unit normal velocity boundary condition was placed over the vibrating cap, represented by the darker area in Figure 4.9. The pressure was calculated in the far field at a radius of $18a$. In this case the number of variables to be solved is 1476 for the direct BEM and 1412 for the source superposition technique.

The beamwidth of the sphere was calculated for 135 non-dimensional frequencies (ka)

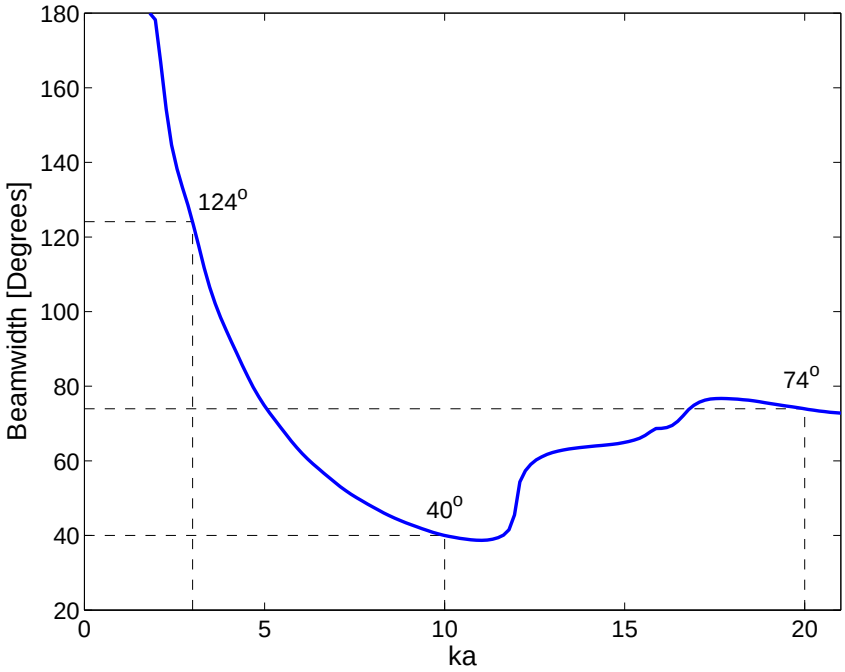

Figure 4.8: The variation of beamwidth with frequency for a 45° *vibrating spherical cap on the surface of a sphere.*

ranging linearly from 1 to 21. The upper frequency was chosen to limit the run time required for the direct BEM method. Figure 4.10 (a) shows the variation in beamwidth with frequency for the analytical, direct BEM and source superposition methods. The agreement is excellent over the entire frequency range, with the differences on this graph virtually indistinguishable.

An error criteria will show the differences in the solutions more readily. The error, ε, is defined as

$$\varepsilon = \frac{|\mathcal{B}_{\text{test}} - \mathcal{B}_{\text{ref}}|}{\mathcal{B}_{\text{ref}}} \tag{4.43}$$

where $\mathcal{B}_{\text{test}}$ is the beamwidth under test, and $\mathcal{B}_{\text{ref}}$ is the reference beamwidth. In this case $\mathcal{B}_{\text{test}}$ and $\mathcal{B}_{\text{ref}}$ are the numerical and analytical beamwidths respectively. Figure 4.10 (b) shows a comparison of the error for both the direct BEM and the source superposition methods. The agreement between both methods and the analytical solution is excellent, with errors less than 1% for the direct BEM. The source superposition technique produces a larger error of about 8% at a *ka* of 12.

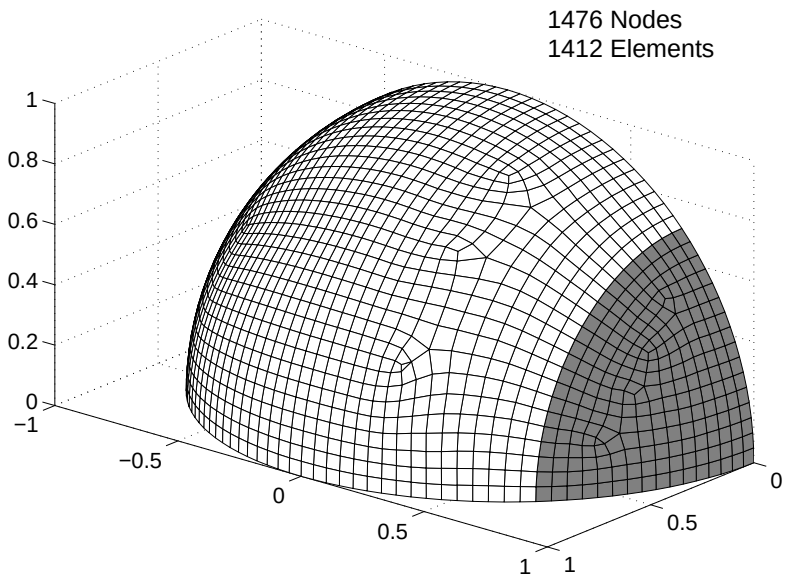

Figure 4.9: Surface mesh of the 45° *vibrating spherical cap on the surface of a sphere (*6 *elements per wavelength).*

As the speed of solution for this application is critical, a comparison of the efficiency of each technique is required. Table 4.2 compares the time taken for each solution technique. The source superposition technique was found to produce results 3.3 times faster than direct BEM. All timing calculations in this chapter were performed on the same machine, an Intel P4 1500 MHz with 512 Mb of RAM running Windows XP.

Method	Total time [seconds]	Time per frequency [seconds]	Factor
Analytical	180	1.3	0.01
Direct BEM	51165	379	3.3
Source Superposition	15525	115	1

Table 4.2: Solution times for the analytical, direct BEM and source superposition techniques.

In summary, the source superposition technique produces results for far field pressure that are almost indistinguishable from the direct BEM and analytical results. It produces these results 3.3 times faster than the direct BEM. The analytical technique is 100 times faster than the source superposition, but is not generally applicable to arbitrary geometries.

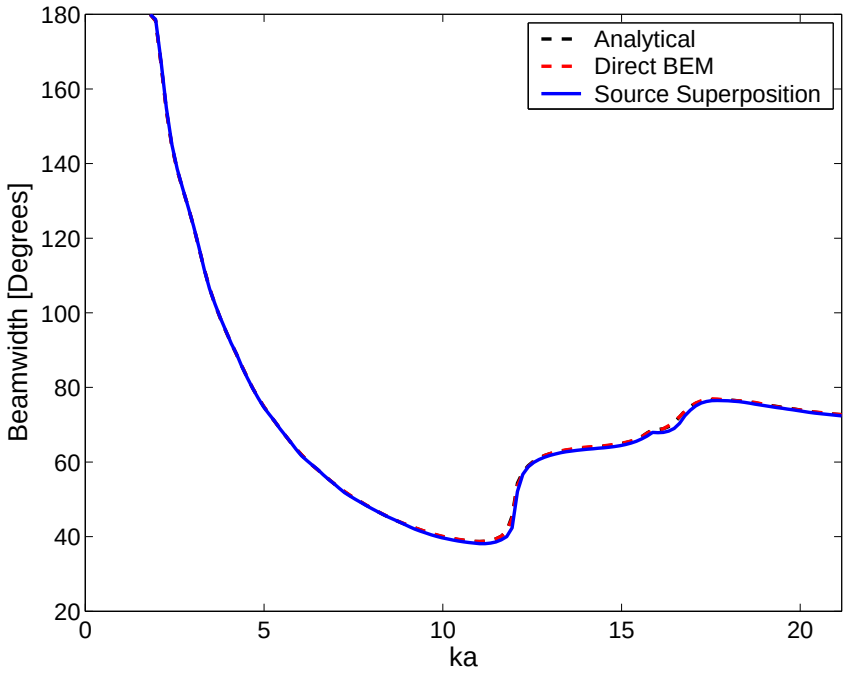

(a) Beamwidth

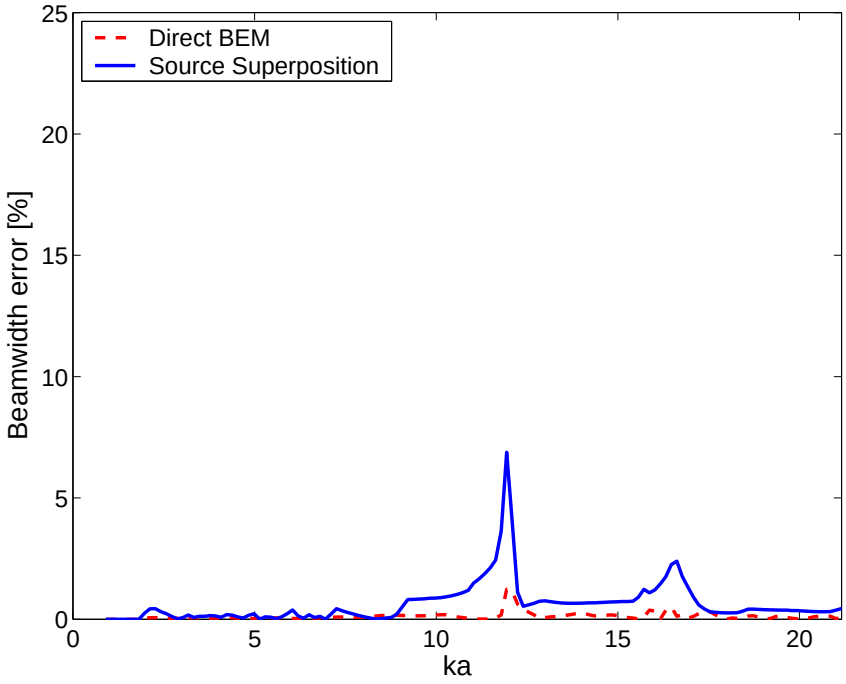

(b) Error in the beamwidth

Figure 4.10: The variation of beamwidth comparing analytical, direct BEM and source superposition results (6 elements per wavelength) for a 45° vibrating spherical cap on the surface of a sphere. Error is defined as Equation 4.43 with $\mathcal{B}_{\text{ref}}$ the analytical beamwidth.

4.4 Computational efficiency

The intended application of these numerical methods is the shape optimisation of horn loaded loudspeakers and because many hundreds (if not thousands) of calculations are needed before a suitable design is found, the computational efficiency of the technique is very important. A number of different techniques that speed up the solution time will be analysed, including: the effect on accuracy of reducing mesh density; modern iterative solution methods; the use of axisymmetry; and multi-frequency solutions.

4.4.1 Reduction in mesh density

The mesh density used in Section 4.3 was chosen using the standard finite element rule of thumb of 6 linear elements per wavelength (Marburg, 2002, Migeot et al., 2000). Figure 4.11 shows a plot of a mesh with nominally 3 elements per wavelength at the highest frequency of interest. In this case the number of variables to be solved is 436 for the direct BEM and 403 for the source superposition technique, a significant reduction from the 1476 and 1412 required for the nominal 6 element per wavelength mesh.

The beamwidth of the sphere at the reduced mesh density was calculated for 135 non-dimensional frequencies (ka) ranging linearly from 1 to 21. Figure 4.12 (a) shows the variation in beamwidth with frequency for the analytical, direct BEM and source superposition methods. Again, the agreement is excellent over the entire frequency range, with the differences on this graph virtually indistinguishable between the direct BEM and the analytical technique. There is a greater difference at higher frequencies between the source superposition technique and the analytical technique than with the full 6 elements per wavelength, but this level of error is deemed acceptable for most design purposes, especially when compared to likely errors that would occur in experimental results.

Figure 4.12 (b) shows a comparison of the error for both the direct BEM and the source

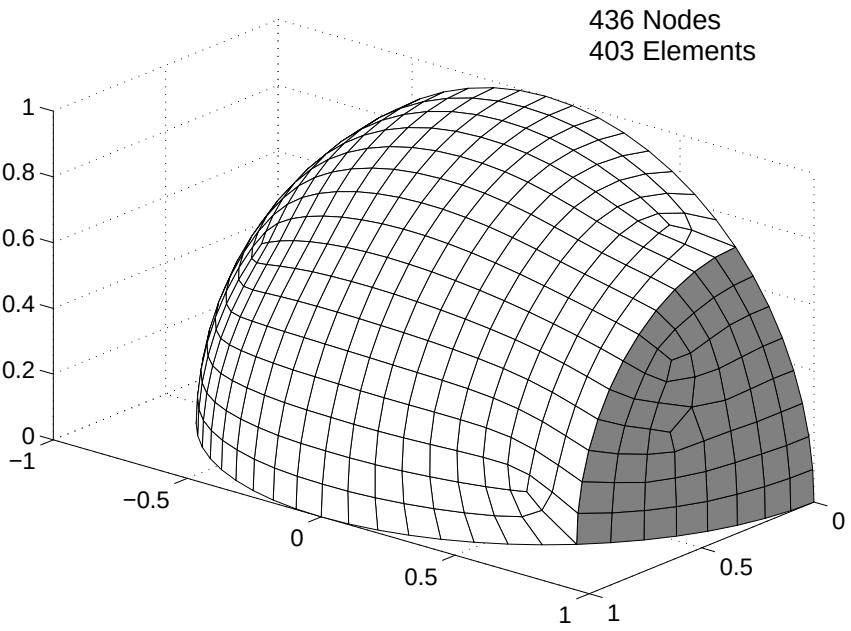

Figure 4.11: Surface mesh of the 45° *vibrating spherical cap on the surface of a sphere (*3 *elements per wavelength).*

superposition method. Again the agreement between the two methods and the analytical solution is excellent, with the error in the direct BEM less than 1% for most of the frequency range considered. The source superposition error is less than 5% for most of the frequency range, except at $ka = 12$, where it jumps to 25%. Equation 4.43 is a very sensitive measure of the sound field when the rate of change of beamwidth with frequency is large, because small changes in the beamwidth will lead to large changes in the error estimate. This quantity is perhaps not a good measure of error under these conditions. Figure 4.12 (b) shows the large errors at a *ka* of 12 are associated with the sharp jump in beamwidth at this frequency.

Table 4.3 shows the results for the solution times. The source superposition technique was found to produce results 6 times faster than the direct BEM.

More importantly, as shown in Table 4.4 the time taken to calculate the solution for the reduced mesh density compared to the full mesh density has been reduced by a factor of 11 for the direct BEM and a factor of 19 for the source superposition technique.

Method	Total time [seconds]	Time per frequency [seconds]	Factor
Analytical	180	1.3	0.2
Direct BEM	4860	36	6
Source Superposition	810	6	1

Table 4.3: Solution times for the analytical, direct BEM and source superposition techniques with reduced mesh density for calculations of sound radiation from a 45° *vibrating spherical cap on the surface of a sphere.*

Method	Time per frequency 6 EPW [seconds]	Time per frequency 3 EPW [seconds]	Factor
Direct BEM	379	36	11
Source Superposition	115	6	19

Table 4.4: Overall solution speedup with reduction in mesh density for calculations of sound radiation from a 45° *vibrating spherical cap on the surface of a sphere.*

In summary, far field solutions that calculate beamwidth for both the direct BEM and the source superposition technique, do not need as high a mesh density as has been traditionally associated with BEM. This reduces calculation time dramatically without compromising accuracy.

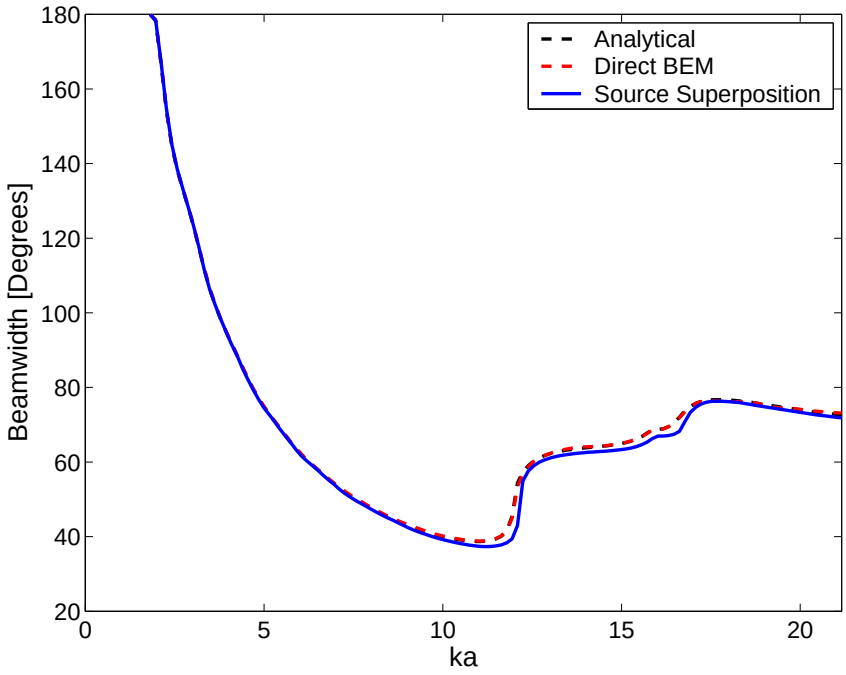

(a) Beamwidth

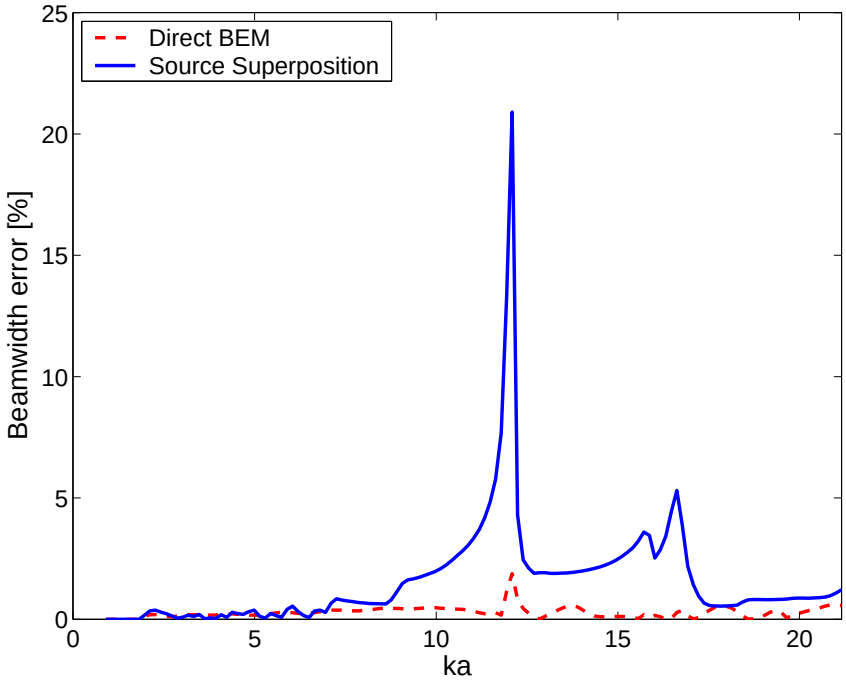

(b) Error in the beamwidth

Figure 4.12: The variation of beamwidth comparing analytical, direct BEM and source superposition results (3 elements per wavelength) for a 45° vibrating spherical cap on the surface of a sphere. Error is defined as Equation 4.43 with $\mathcal{B}_{\text{ref}}$ the analytical beamwidth.

4.4.2 Fast solvers

The solution of the system of linear equations for both the source superposition and direct BEM techniques examined in this thesis was performed with standard F77 implementations of readily available scientific software subroutine libraries; Numerical Recipes LU decomposition (Press et al., 1992, Section 2.3) and LINPACK (LINPACK, 2004) QR factorisation respectively. Details of both the LU and QR decomposition can be found in standard texts on numerical analysis (Golob and Van Loan, 1996, Press et al., 1992).

The standard implementations of these routines do not make efficient use of modern processor architecture. The routines made available by the LAPACK (LAPACK, 2004) linear algebra subroutine library make use of the BLAS library (BLAS, 2004) for basic linear algebra operations. A highly optimised version of BLAS, which is automatically tuned for maximum speed on a given processor (Whaley et al., 2001), as well as higher level LAPACK routines are used by the MATLAB (Matlab, 2002) numerical programming language. An interface between the source superposition method code (POWER) and MATLAB was developed. This allowed access to the fast direct solvers available in LAPACK, as well as a platform for rapid development of other solvers and techniques to speed up the solution times, with the ultimate aim of optimising the geometry to give a required beamwidth.

An alternative to the direct solution of the system of linear equations by decomposition techniques such as those mentioned above is available in the form of iterative solvers. These methods are motivated by the large cost associated with the direct solution of a system of linear equations (Press et al., 1992, Section 2.11).

Iterative solvers work by repeatedly improving an approximate solution to a system of linear equations, until that solution is deemed to be accurate enough (see Barrett et al. (1994) for a full description of current iterative solver technology). The rate at which iterative solutions converge is governed by the distribution of eigenvalues of the coefficient

matrix, and a preconditioned iterative technique is one that involves a second matrix that transforms the coefficient matrix to improve its spectrum. Usually the preconditioning matrix is an approximation to the original matrix that can be easily inverted.

Iterative solvers refine the solution until they reach a stop criterion. In this case, the criterion is when the norm of the residual vector has been reduced below a predefined tolerance,

$$tol = \left\| \mathbf{U}\mathbf{s}^{(i)} - \mathbf{u} \right\|_2 \tag{4.44}$$

where $\mathbf{U}$ is the coefficient matrix, $\mathbf{u}$ is the boundary condition vector, $\mathbf{s}^{(i)}$ is the ith iteration of the solution and $\|\mathbf{x}\|_2 = \left(|x_1|^2 + \ldots + |x_n|^2 \right)^{\frac{1}{2}}$ is the vector 2 norm of $\mathbf{x}$ (Golob and Van Loan, 1996, Section 2.2.1).

Iterative solvers have been used successfully to produce approximate solutions to systems of linear equations in direct BEM (Migeot et al., 2000), although they usually require some sort of preconditioning (Chen, 1999). An extensive review of the literature has not found any reference to the use of iterative solution methods with the source superposition technique.

This section reports on an investigation of the speedup in solution times obtained by applying advanced direct solvers as well as a modern iterative solution technique, the Generalised Minimal Residual (GMRES) method, to the source superposition technique. Figure 4.13 (a) shows the results of the original F77 direct solver compared to the direct solver available in MATLAB, as well as the GMRES solver with a tight (1×10^{-6}) and loose (1×10^{-3}) stopping tolerance. There is no discernible difference between the solutions, and this is confirmed by the relatively small error in the solution, defined by Equation 4.43 with $\mathcal{B}_{\text{ref}}$ the original direct solver beamwidth. Figure 4.13 (b) shows a comparison of this error for both direct BEM and the source superposition method. The error is less than 1.5% for all of the frequency range considered, and the error for the

tight (1×10^{-6}) tolerance GMRES solution and the direct MATLAB solver overlay. This implies that there is a small fundamental difference between the direct original solver and the direct MATLAB solver.

Figure 4.14 compares the error between the MATLAB direct solver and the GMRES iterative solver with varying tolerance ($\mathcal{B}_{\text{ref}}$ is now the MATLAB direct solver beamwidth). It shows that there is negligible (less than 0.5%) difference between the loose (1×10^{-3}) and tight (1×10^{-6}) tolerance GMRES solver and the MATLAB direct solver over the entire frequency range of interest.

Table 4.5 shows the solution times for each method. The MATLAB direct solver is 4 times faster than the original solver, while the iterative solvers only provide a marginal improvement in speed.

Method	Total time [seconds]	Time per frequency [seconds]	Factor
Direct Original	15525	115	3.9
Direct solver MATLAB	4018	30	1
GMRES Tol 1×10^{-6}	3457	26	0.9
GMRES Tol 1×10^{-3}	3140	23	0.8

Table 4.5: Total solution times for the original direct solver and alternative solvers for calculations of sound radiation from a 45° *vibrating spherical cap on the surface of a sphere using the source superposition technique.*

The reason for the marginal improvement in speed can be found by examining the ratio of time spent assembling the equations (70%) to the time spent solving them (30%) for the direct MATLAB solution. Comparing the solution times for each solver in Table 4.6 shows that a factor of 3 speedup can be gained by using an iterative solver with a loose tolerance, without loss of accuracy.

The GMRES technique reduces the residual of the solution to below the stopping tolerance of 1×10^{-6} in 40 iterations, and to 1×10^{-3} in 27 iterations, without preconditioning. With the application of the diagonal of matrix **U** (the matrix to be inverted to

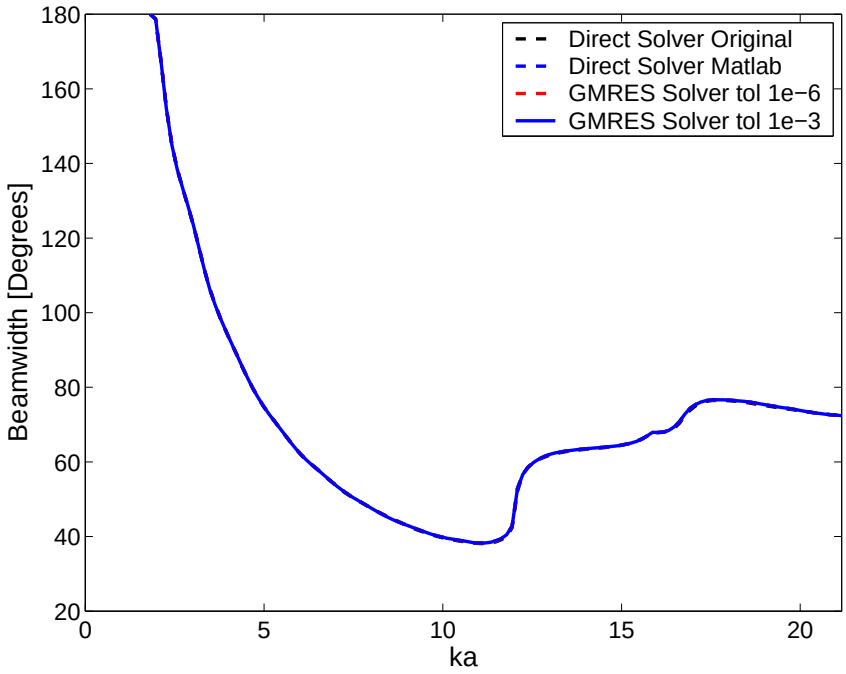

(a) Beamwidth

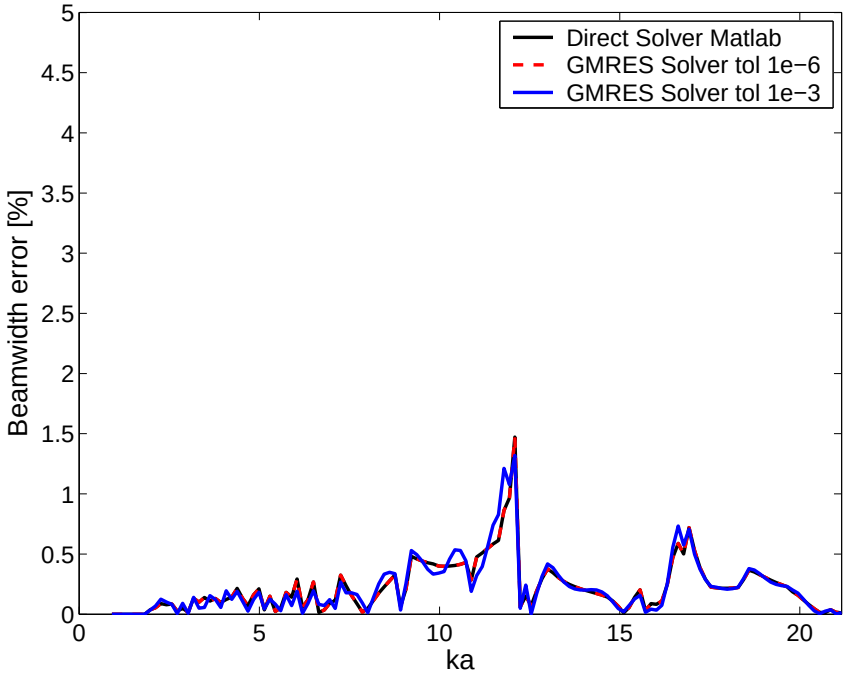

(b) Error in the beamwidth

*Figure 4.13: The variation of beamwidth with frequency with different solvers (*6 *elements per wavelength) for a* 45° *vibrating spherical cap on the surface of a sphere. Error is defined as Equation 4.43 with* $\mathcal{B}_{\text{ref}}$ *the original direct solver beamwidth.*

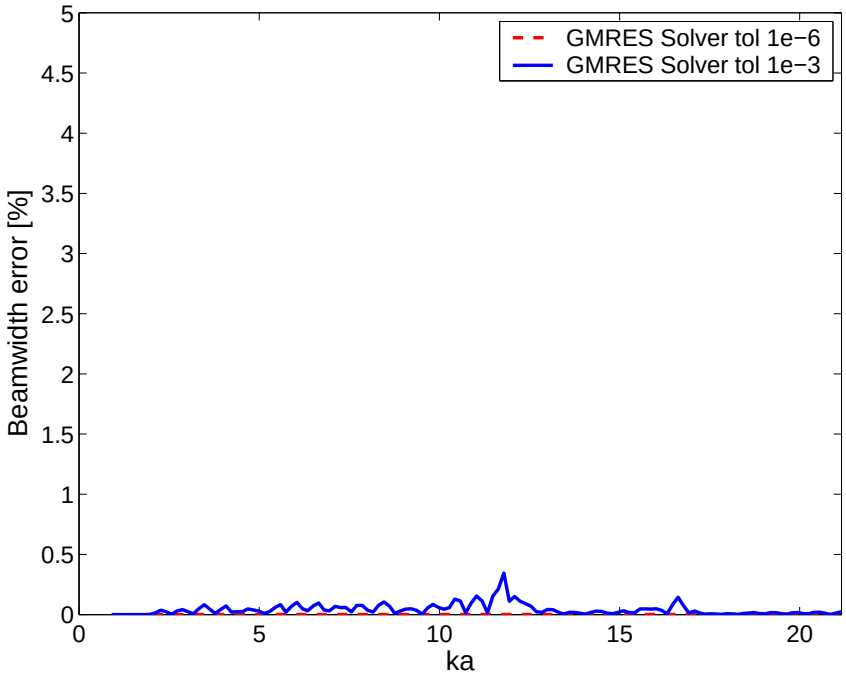

Figure 4.14: The variation of error between the MATLAB *direct solver and GMRES iterative solvers (*6 *elements per wavelength) for a* 45° *vibrating spherical cap on the surface of a sphere. Error is defined as Equation 4.43 with* $\mathcal{B}_{\text{ref}}$ *the* MATLAB *direct solver beamwidth.*

Method	Solver time [seconds]	Factor
Direct MATLAB	1210	1
GMRES Tol 1×10^{-6}	664	0.55
GMRES Tol 1×10^{-3}	350	0.29

Table 4.6: Solver solution times for the MATLAB *direct solver and GMRES iterative solvers for calculations of sound radiation from a* 45° *vibrating spherical cap on the surface of a sphere using the source superposition technique.*

find the source strength, see Equations 4.41 and4.42) as the preconditioner, the number of iterations to reduce the residual to less than 1×10^{-6} was 34, however the total time of solution increased due to the extra work required to apply the preconditioner. Figure 4.15 shows a scaled image of the absolute value of a typical $\mathbf{U}$ at $ka = 9$. The matrix is extremely diagonally dominant, with good condition number and excellent performance with iterative solvers.

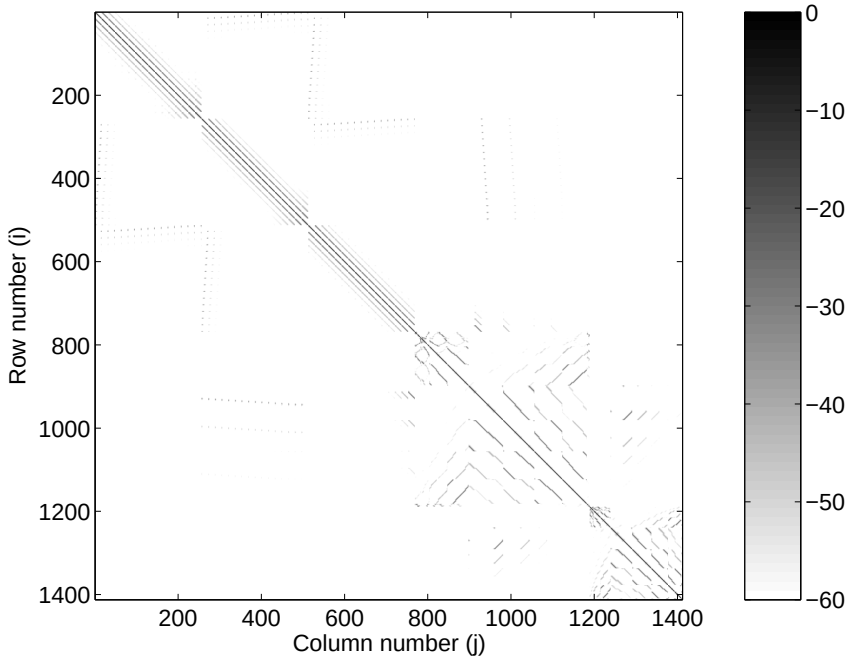

Figure 4.15: Image of $20\log 10\left(\frac{|\mathbf{U}|}{|\mathbf{U}_{\max}|}\right)$ *for* $ka = 9$ *showing the extreme diagonal dominance of the matrix produced by the source superposition method for calculations of sound radiation from a* 45° *vibrating spherical cap on the surface of a sphere.*

In conclusion, the GMRES iterative solver with a loose (1×10^{-3}) tolerance provides excellent performance in solving the linear equations produced by the source superposition technique. The difference in performance between the methods would probably be greater for larger problems where direct solver solution time is typically of the order of N^3 (Golob and Van Loan, 1996), where N is the size of the matrix, whereas the iterative solution time can be of the order of N^2 (Barrett et al., 1994). The bottleneck in solution time is the large amount of time taken to assemble the matrix $\mathbf{U}$, and methods to improve the overall speed of solution must address this issue.

4.4.3 Rotational symmetry

The implementation of the source superposition technique embodied in POWER (Koopmann and Fahnline, 1997) contains an option to speed the assembly of structures with rotational symmetry. This option reduces the number of integrations required by calculating the matrix for one sector only and copying the matrix entries for the remaining sectors.

For axisymmetric structures, an arbitrary number of sectors can be chosen. In this case, 12 sectors were chosen as seemed a reasonable compromise between the number of sectors (decreasing matrix assembly time) and the total number of elements (increasing matrix inversion time). Figure 4.16 shows the quarter symmetric (90°) mesh with 12 sectors.

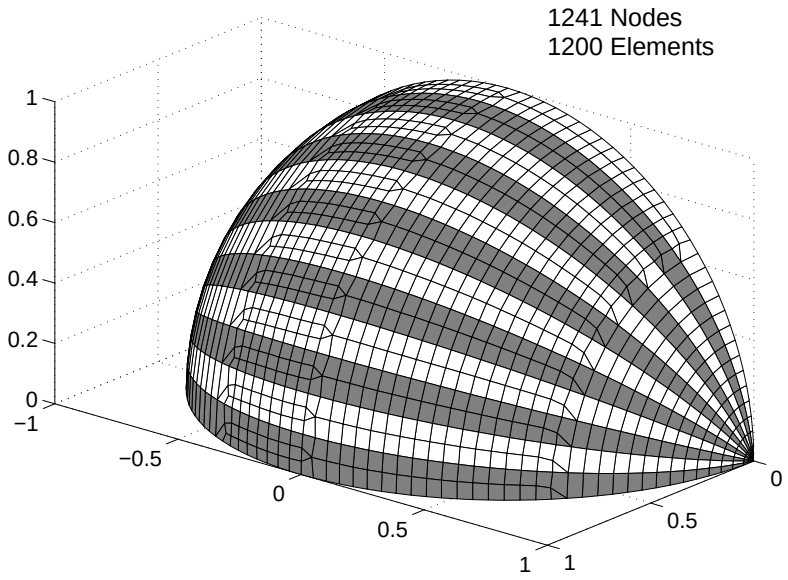

Figure 4.16: Surface mesh of the 45° *vibrating spherical cap on the surface of a sphere with* 12 *rotationally symmetric sectors (*6 *elements per wavelength).*

Figure 4.17 (a) shows a comparison of the beamwidth evaluated with both the full and rotationally symmetric mesh. This mesh, generated at a nominal density of 6 elements per wavelength, contains 1200 elements. The mesh shown in Figure 4.9, also generated at a nominal density of 6 elements per wavelength, contains 1412 elements. There should be

essentially no difference between the two solutions, which is confirmed by the error in the solution, shown in Figure 4.17 (b), defined by Equation 4.43 with $\mathcal{B}_{\text{ref}}$ the MATLAB direct solver beamwidth. The error is less than 2% for most of the frequency range considered, with a peak of 4% at $ka = 12.5$.

The time taken to assemble the full and rotationally symmetric methods is shown in Table 4.7, where the rotationally symmetric method is 5 times faster than the full method, with the change in the solution minimal, and related to the change in mesh topology rather than any error in applying rotational symmetry.

Method	Assembly time [seconds]	Factor
Full mesh assembly	3957	5.2
Rotationally symmetric mesh assembly	760	1

Table 4.7: Matrix assembly times for the the full and rotationally symmetric methods for a 45° *vibrating spherical cap on the surface of a sphere using the source superposition technique.*

In conclusion, the use of rotational symmetry allows a considerable speed up in matrix assembly time for axisymmetric structures with essentially no loss in accuracy. This method has the disadvantage that is is not applicable to shapes without rotational symmetry.

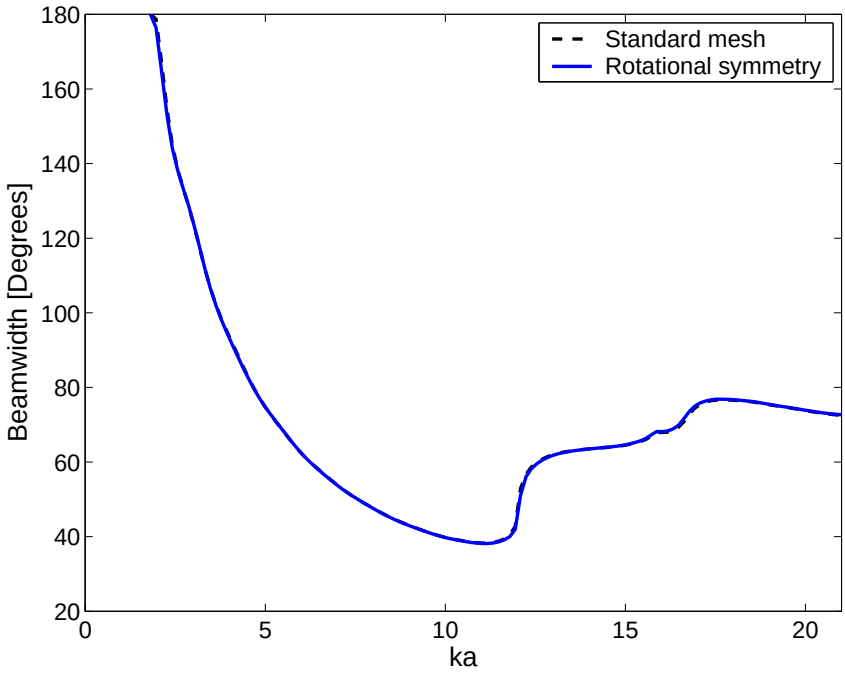

(a) Beamwidth

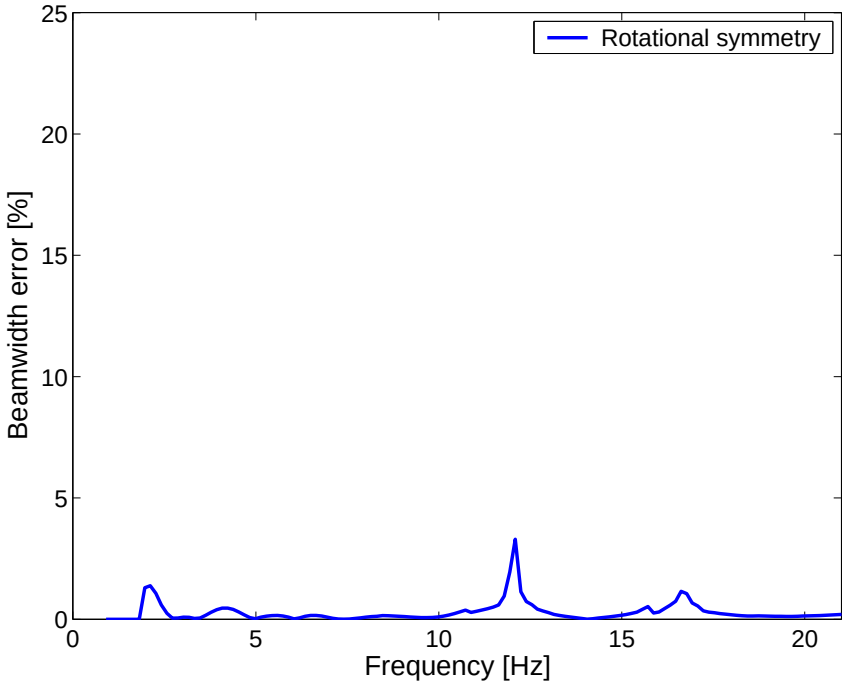

(b) Error in the beamwidth

Figure 4.17: The variation of beamwidth with frequency with full and rotationally symmetric methods (6 elements per wavelength) for a 45° vibrating spherical cap on the surface of a sphere. Error is defined as Equation 4.43 with $\mathcal{B}_{\text{ref}}$ the MATLAB *direct solver beamwidth.*

4.4.4 Multi-frequency solutions

The techniques described in previous sections aim to increase the speed of solution at a single frequency. However, most applications will require calculations over a range of frequencies. If some part of a single frequency calculation can be reused at other frequencies, then the time saved in calculating that part is saved at each frequency, and the total cost of calculation is reduced.

One such approach is frequency interpolation of the assembled matrices (Benthien and Schenck, 1991, Kirkup and Henwood, 1992, Wu et al., 1993, Raveendra, 1999, Migeot et al., 2000, von Estorff and Zaleski, 2003). If the assembly of the matrices is performed at a few key frequencies, and the matrices at frequencies in between the key frequencies efficiently interpolated, then the total cost of solution can be reduced. Such an approach could be taken for the source superposition technique; however the implementation of any one of these schemes is intricate, and beyond the scope of the current study.

Another potential approach is to use a technique that uses the solution at a key frequency to speed the subsequent solutions at the intermediate frequencies. This method, described in Kirkup and Henwood (1992) and Raveendra (1999), uses an iterative approach where the factorisation of a matrix at a key frequency is used as a preconditioner at the intermediate frequencies. The factored matrix is an approximate inverse to the solution at the new frequency. Both references appear to use simple stationary iterative solvers (Barrett et al., 1994).

For the application considered in this thesis, the solution is factorised using LU decomposition at key frequencies, and the factorisation used as a preconditioner to the GMRES technique. It has been found that the number of iterations required to reduce the solution error to below 1×10^{-3} was 27 iterations for the standard GMRES and 5 iterations for the preconditioned GMRES. This saving may be significant even with the extra cost of evaluating the preconditioner.

The times for solution of the direct, standard and preconditioned GMRES solvers are shown in Table 4.8. Preconditioning was applied between 10 evenly spaced key frequencies. The additional cost of applying the preconditioner increases the total solution time, even though the number of iterations is decreased.

Method	Solution time [seconds]	Factor
Direct MATLAB	1210	4.5
GMRES Tol 1×10^{-3}	350	1
Preconditioned GMRES Tol 1×10^{-3}	640	1.8

Table 4.8: Solution times for the preconditioned multi-frequency GMRES solver, standard GMRES solver and the direct MATLAB *solver for a* 45° *vibrating spherical cap on the surface of a sphere using the source superposition technique.*

In summary, a technique that speeds the iterative solution of the matrices formed by the source superposition technique has been developed, and its application to the problem at hand investigated. It uses the factored solution at key frequencies to precondition the iterative GMRES solver used in Section 4.4.2; however this was not found to speed up the solution time for the problem considered here.

4.5 Full model

This section describes the implementation of all of the techniques developed in Section 4.4 to speed up simulations of a 45° vibrating spherical cap on the surface of a unit sphere; The mesh shown in Figure 4.18 is used to provide a geometry with at least 3 elements per wavelength; rotational symmetry with 12 sectors is used to speed up matrix assembly; and the standard (non-preconditioned) GMRES solver with a loose (1×10^{-3}) tolerance is used to reduce the total time for the simulation.

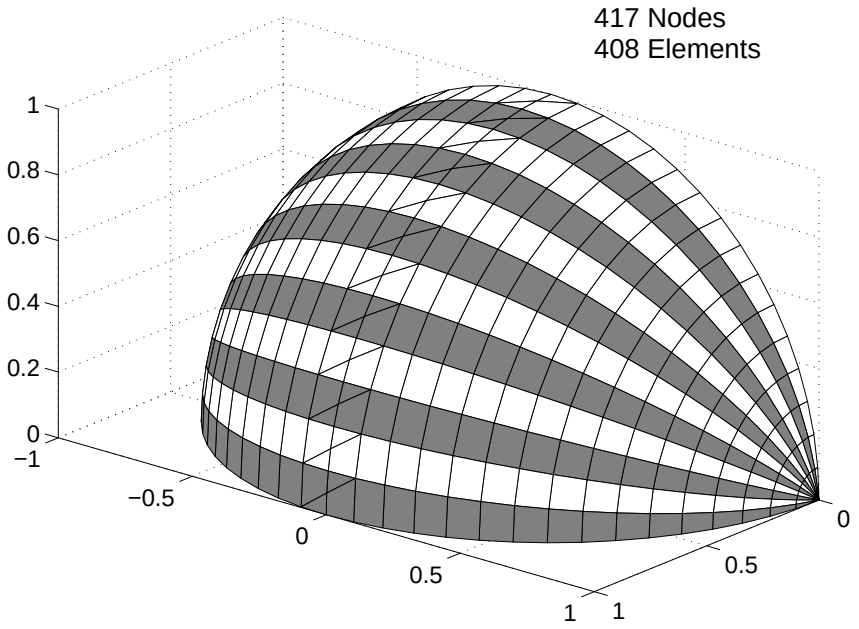

Figure 4.18: Surface mesh of the 45° *vibrating spherical cap on the surface of a sphere with* 12 *rotationally symmetric sectors (*3 *elements per wavelength).*

Figure 4.19 (a) shows the results of applying these techniques to the solution compared to a baseline MATLAB source superposition simulation. There is some error across the frequency range considered, and this is mainly due to the different mesh topology, as the GMRES solver has been shown to give very little difference between solutions for different tolerances (Figure 4.14). The error in the solution, with $\mathcal{B}_{\text{ref}}$ the MATLAB direct solver beamwidth, is shown in Figure 4.19 (b). It is less than 5% for most of the frequency range considered, with a peak of 5.5% at $ka = 17$ and 22.5% at $ka = 12$. This level of

error is deemed acceptable for most design analyses.

The solution times for the source superposition technique with reduced mesh density, iterative solver and rotational symmetry assembly (the "fast source superposition" technique) is compared to the baseline source superposition technique implemented in MATLAB, and the direct and source superposition F77 codes in Table 4.8. The fast source superposition technique is 67 times faster than the original F77 code and 220 times faster than the direct BEM method. It is now considered fast enough to be used as a component in an optimisation technique.

Method	Total [seconds]	Time / Freq [seconds]	Factor
Direct BEM	51165	379	220
Source Superposition	15525	115	67
Source superposition MATLAB	4018	30	17
Fast source superposition	233	1.7	1

Table 4.9: Solution times for the standard solvers and the fast source superposition technique for a 45° *vibrating spherical cap on the surface of a sphere.*

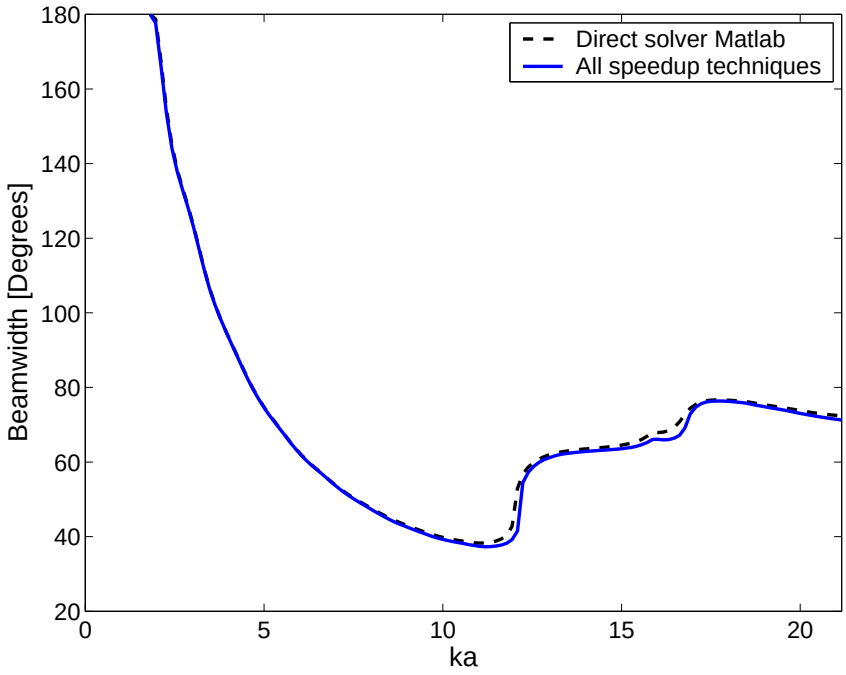

(a) Beamwidth

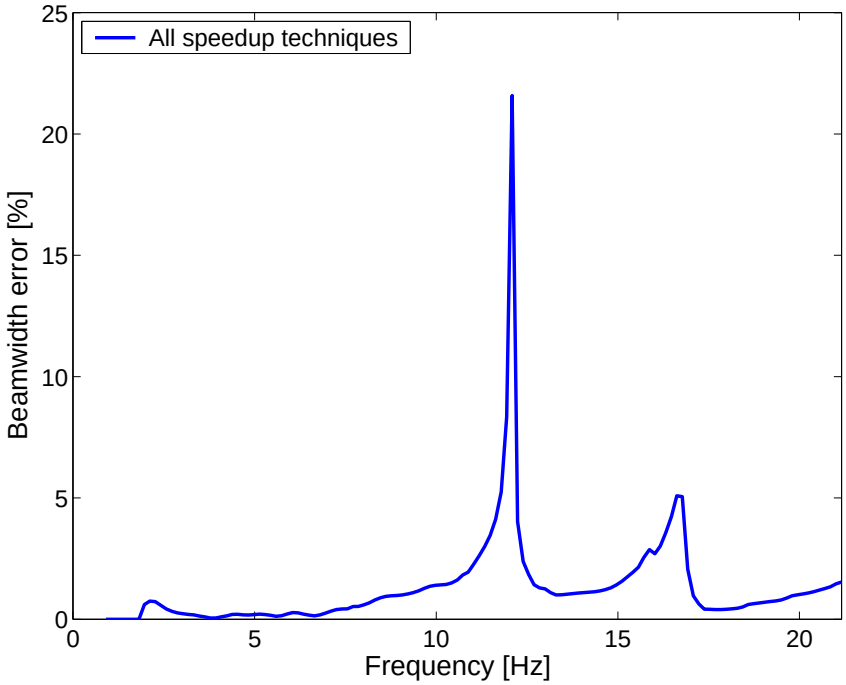

(b) Error in the beamwidth

Figure 4.19: The variation of beamwidth with frequency for the fast source superposition technique and the direct MATLAB *solver for a* 45° *vibrating spherical cap on the surface of a sphere. Error is defined as Equation 4.43 with* $\mathcal{B}_{\text{ref}}$ *the* MATLAB *direct solver beamwidth.*

4.6 Conclusions

This chapter has described the development of techniques to dramatically reduce the time required to simulate the far field acoustic response (as measured by the beamwidth) from a vibrating spherical cap on the surface of a sphere. This is a simplistic model of a horn loaded loudspeaker (see Section 2.1.2), however it provides an excellent example for numerical model verification (Babuska and Oden, 2004) because the analytical solution is easily calculated (Section 4.2.1).

Analytical solutions for a 45° vibrating spherical cap mounted on the surface of a unit sphere have been rigorously compared with those obtained from an implementation of the direct BEM (Wu, 2000) and a source superposition technique (Koopmann and Fahnline, 1997). Excellent agreement between these results was found for mesh densities of 6 elements per wavelength, the minimum recommended mesh density for BEM simulations (Migeot et al., 2000). The source superposition technique was significantly faster than the direct BEM for comparable accuracy in the far field.

There was also excellent agreement between the methods for a mesh density of 3 elements per wavelength. This is a significant finding as it allows the reduction of mesh density, and hence matrix size and solution time, for a given accuracy of far field solution. Alternatively, accurate solutions can be obtained at higher frequencies than previously expected for a given mesh density.

It has been found that the source superposition technique produces matrices that are highly diagonally dominant, are very suited to iterative solution methods such as GMRES, and do not require a preconditioning matrix. The time taken to assemble the matrix was found to be much greater than the solution time for the problems considered in this thesis, and iterative solutions to the source superposition technique may provide greater benefit for larger problems.

Because the time taken to assemble the source superposition matrix is the limiting factor,

a method that made use of rotational symmetry was investigated. It was found that the matrix assembly time was reduced by a factor of 5 with no loss in accuracy, but only for rotationally symmetric meshes.

A technique that speeds the iterative solution of the matrices formed by the source superposition technique has been developed. It uses the factored solution at key frequencies to precondition the iterative GMRES solver used in Section 4.4.2. Unfortunately it was found to increase overall solution time for this problem.

The bottleneck in solution time for the size of problem examined here was found to be the matrix assembly time. The solution time was found to be highly dependent on the number of elements, and for fast computation, every effort should be made to reduce the number of elements in the simulations.

The implementation of all of these speedup techniques, called the "fast source superposition" technique has been shown to result in solution times that are 67 times faster than the original implementation of the source superposition technique, and 220 times faster than the direct BEM, with no loss in accuracy, for predictions of the beamwidth from a vibrating spherical cap mounted on the surface of a unit sphere. This technique is now fast enough to be used as a component in an optimisation technique.

This work can be regarded as verification (see Babuska and Oden, 2004), ensuring that the correct equations are solved by the software. The next stage of the work, validation, that is comparison with experimental data to see how well the equations represent the physical system, is undertaken for the source superposition technique in Chapter 5. It should be noted, however, that the source superposition technique is well validated for calculations of acoustic power radiated from vibrating structures (Koopmann and Fahnline, 1997), and that accurate calculations of power imply that the far field is correctly modelled. The source superposition technique is also expected to perform well when calculating beamwidth for models other than a simple sphere.